

CEREBRAL AUTOREGULATION MONITORING WITH TRANSCRANIAL DOPPLER DURING NEONATAL CARDIAC SURGERY

BOYD VICTOR MARTHURUS



MASTER THESIS
TECHNICAL MEDICINE
JANUARY 2024

Cerebral Autoregulation Monitoring with Transcranial Doppler during Neonatal Cardiac Surgery

by

Boyd Victor Martherus

A master's thesis

Submitted to the Faculty of Science and Technology

University of Twente

In partial fulfilment of the requirements
for the degree of Master of Science

in

Technical Medicine

Track Medical Sensing & Stimulation

January 25th, 2024

**UNIVERSITY
OF TWENTE.**



UMC Utrecht
Wilhelmina Kinderziekenhuis

Graduation Committee

Chairman Technological Supervisor

Prof.dr.ir. P.H. (Peter) Veltink
Faculty of Electrical Engineering and Computer Science (EEMCS)
Biomedical Signals & Systems (BSS)
University of Twente

Technological Supervisor

Dr. Y. (Ying) Wang
Faculty of Electrical Engineering and Computer Science (EEMCS)
Biomedical Signals & Systems (BSS)
University of Twente

Process Supervisor

E.M. (Elyse) Walter MSc.
Faculty of Science and Technology
Technical Medicine
University of Twente

External Member

R.S.P. (Rob) Warnaar MSc.
Faculty of Science and Technology
Cardiovascular and Respiratory Physiology
University of Twente

Medical Supervisor

Dr. K. (Kim) van Loon
Department of Anesthesiology
Wilhelmina Children's Hospital, University Medical Center Utrecht

Extra Member

Dr. M.J.M. (Martine) Breteler
Department of Digital Health
University Medical Center Utrecht

Voorwoord

Deze thesis vormt mijn inhoudelijke verdediging van mijn afstudeerstage op de afdeling anesthesie in het Wilhelmina Kinderziekenhuis, te Utrecht. Met het afronden van deze afstudeerstage hoop ik mijn studie *Technical Medicine* met de specialisatie *Medical Sensing and Stimulation* succesvol af te kunnen ronden.

Na het behalen van mijn VWO diploma heb ik ervoor gekozen om in een jaar op het voortgezet algemeen volwassenenonderwijs (VAVO) het vak Wiskunde B te volgen. Met als rede om in 2016 mee te doen aan de decentrale selectie voor de bachelor Technische Geneeskunde. Na een uitdagend en langdurig traject van 7,5 jaar, sta ik op het punt om mijn Masterdiploma in ontvangst te nemen. Deze reis was gevuld met zowel hoogte- als dieptepunten, en het geeft een enorm gevoel van voldoening om te weten dat mijn doorzettingsvermogen en harde werk zich nu uitbetalen. Het is een moment van trots en reflectie, en ik kijk met veel verwachting uit naar het officieel afronden van deze belangrijke fase in mijn carrière.

Dat ik op deze bijzondere afdeling binnen het kindercentrum van het Wilhelmina Kinderziekenhuis terecht ben gekomen was met toeval, toen tijdens mijn twee TG-schap ik hier terecht kwam. Daar werd ik met open armen ontvangen en werd gelijk mijn interesse gewekt in de zorg van kinderen met een aangeboren hartafwijking. Ik wil hierbij Kim van Loon in eerste instantie van harte bedanken voor het vertrouwen wat zij in mij toonde. In de derde week van onze samenwerking gaf ik toen al aan dat ik graag terug zou willen komen om te komen afstuderen waarop ze zonder twijfel volmondig toestemde. Nu bijna 1,5 jaar later heb ik in samenwerking mijn Master thesis hier kunnen schrijven.

Dat ik uiteindelijk op deze unieke afdeling van het kindercentrum in het Wilhelmina Kinderziekenhuis ben beland, was een gelukkig toeval. Tijdens mijn tweede TG-schap kwam ik hier terecht en werd meteen warm onthaald. De zorg voor kinderen met een aangeboren hartafwijking trok direct mijn aandacht en interesse. Ik wil in het bijzonder Kim van Loon hartelijk danken voor het vertrouwen dat zij in mij stelde. Al in de derde week van onze samenwerking gaf ik aan dat ik graag terug zou keren voor mijn afstudeerproject, waarop zij zonder enige aarzeling volmondig instemde. Nu, bijna anderhalf jaar later, heb ik in samenwerking met dit haar mijn Master thesis kunnen voltooien. Daarnaast wil ik ook Martine Breteler bedanken voor het fijne contact en begeleiding binnen deze stage. Ook wil ik graag mijn dank uitspreken voor het onderzoeksteam binnen de FLOWER studie; Daniël van Vriesland, Meryem Koroglu, René van de Vosse, Thomas Alderliesten, Ilse Ceelie, Maaike Nijman, en alle andere die ik vergeet te noemen, die hun bijdrage hebben geleverd.

Deze afstudeerstage ben ik begonnen onder de technologische begeleiding van Ying Wang, waarna Peter Veltink dit heeft overgenomen. Ook wil ik heb bedanken voor hun kritische vragen en begeleiding binnen deze stage. Als laatst wil ik Rob Warnaar bedanken voor het beschikbaar zijn als buitenlid binnen de afstudeercommissie.

Verder wil ik Elyse Walter bedanken voor haar begeleiding rondom het proces en haar steun tijdens de moeilijke periodes in de TG-schappen. Ook wil ik Anouck Pilon en Laurens Corbiere bedanken voor de fijne intervisie meetings die wij hebben gehad.

Ten slotte wil ik mijn familie, vrienden, studiegenoten en huisgenoten bedanken voor hun support en onvoorwaardelijke steun tijdens deze mijn gehele studie traject. Het liefst zie het voltooiën van deze studie als teamprestatie, dank jullie wel.

Boyd Victor Martherus Utrecht, 25 januari 2024

Abstract

Background Neonates with critical congenital heart disease require life-saving cardiac surgery shortly after birth. While survival rates have improved, the challenge of improving neurological outcome, remains urgent. Evidence-based blood pressure and circulatory management strategies in congenital heart disease patients are desirable. Cerebral autoregulation monitoring offers a promising avenue for individualized blood pressure management in this vulnerable population.

Aims The objective was to evaluate the feasibility of cerebral autoregulation monitoring for blood pressure management in neonatal cardiac surgery and to investigate its clinical relevance related to neurological outcome.

Methods Cerebral autoregulation was monitored in 28 neonates during cardiac surgery with cardiopulmonary bypass between April 2022 and October 2023. Autoregulation monitoring was conducted using transcranial Doppler to measure cerebral blood flow velocity concurrently with invasive arterial blood pressure monitoring. These measurements were utilized to calculate the mean velocity index, which was determined based on their correlation with each other. A threshold value of the mean velocity index of 0.45 is used to distinguish intact from impaired autoregulation. The mean velocity index is used to determine each individual's optimal blood pressure and limits of autoregulation. The clinical relevance was assessed by examining the association with new white matter injury, as identified through pre- and post-operative MRI scans. Additionally, for comparative purposes, we also employed near-infrared spectroscopy, the modality most commonly reported in the literature for autoregulation monitoring, despite its inherent limitations.

Results Mean gestational age was 38.5 ± 1.0 weeks, and all patients received cardiac surgery within 16 days of life. Cerebral autoregulation monitoring with Transcranial doppler was superior to near infrared spectroscopy. The lower limit of autoregulation was 29.4 ± 6.4 mmHg (range: 19.0 - 41.5), optimal mean arterial blood pressure was 42.0 ± 7.0 mmHg (range: 34.4 - 56.2), and the upper limit of autoregulation was 49.5 ± 4.9 mmHg (range: 44.3 - 58.4). No significant association between patient characteristics and the ability to delineate the cerebral autoregulation curve was found. Additionally, the time spent outside the range for intact autoregulation was not significantly associated with new white matter injury.

Conclusions The study established the feasibility of using Transcranial Doppler for personalized blood pressure management in neonatal cardiac surgery, highlighting significant individual variations in blood pressure thresholds. However, it found no significant link between autoregulation limits during surgery and brain lesion size. Despite its limitations, the study paves the way for future research to refine blood pressure management strategies and improve outcomes in neonatal cardiac care.

Table of Contents

1	General Introduction	10
2	Clinical Background	12
2.1	Congenital Heart Disease	12
2.2	Cerebral Autoregulation in the Neonate	14
3	Technical Background	17
3.1	Cerebral Autoregulation Monitoring	17
4	Objectives	22
4.1	Research Aim	22
4.2	Thesis Outline	22
5	Delineation of the Cerebral Autoregulation Range	24
5.1	Introduction	24
5.2	Materials & Methods	25
5.3	Results	32
5.4	Discussion	37
5.5	Conclusion	40
6	Perioperative Brain Damage	41
6.1	Introduction	41
6.2	Materials & Methods	41
6.3	Results	45
6.4	Discussion	48
6.5	Conclusion	50
7	General Discussion	51
7.1	Limitations	51
7.2	Clinical Implications	52
7.3	Future Recommendations	53
7.4	Conclusion	54
8	Eindverantwoording	60
8.1	Persoonlijke Ontwikkeling	60
8.2	Klinische Ontwikkeling	62
8.3	Waardevolle Leermomenten	68
8.4	Ontwikkelingen Buiten Het Afstuderen Om	69
8.5	Conclusie	70
	Appendix A TCD Protocol	71

Appendix B	Stepwise Delineation CA Curve	78
Appendix C	Overview Per Patient Baseline Characteristics	81
Appendix D	Results CA Delineation	83
Appendix E	Results T1CR and MRI	84
Appendix F	Results Imputation CA Characteristics	85
Appendix G	All plots	86
Appendix H	MatLab Code	101
Appendix I	WCPCCS Poster	126

List of Figures

1	Original Lassen curve	14
2	Regulatory mechanisms of cerebral autoregulation	15
3	Schematic plot of cerebral blood flow versus arterial blood pressure	16
4	Schematic U-shaped curve of an cerebral autoregulation index	17
5	Transcranial Doppler probe positioning for insonating the middle cerebral artery	18
6	Schematic of near-infrared spectroscopy of the brain	20
7	Intraoperative measurement setup with bilateral TCD probe fixation.	27
8	Example Lassen plots of two patients	34
9	Example cerebral autoregulation curve plots of two patients	35

List of Tables

1	Summary of Baseline Characteristics	33
2	Odds ratios for predicting ability to delineate the LLA, MAPopt and ULA.	37
3	Summary of Baseline Characteristics	45
4	Model performances TICR	47
5	Estimated Coefficients TICR	47
6	Model performance CA characteristic	48
7	Estimated Coefficients CA Characteristic	49
8	Patient characteristics	82
9	Per patient identified characteristics of cerebral blood flow autoregulation from Transcranial Doppler monitoring.	83
10	TICR and MRI	84
11	Imputed CA characteristics	85

List of Abbreviations

- ABP – Arterial blood pressure
- AUC – Area under the curve
- CA – Cerebral autoregulation
- CB – Cerebral blood flow
- CBFV – Cerebral blood flow velocity
- CHD – Congenital heart disease
- COx – Cerebral oximetry index
- CPB – Cardiopulmonary bypass
- CPP – Cerebral perfusion pressure
- HLHS – Hypoplastic left heart syndrome
- LLA – Lower limit of autoregulation
- MAPopt – Optimal mean arterial blood pressure
- MCA – Middle cerebral artery
- MRI – Magnetic resonance imaging
- Mx – Mean velocity index
- NIRS – Near-infrared spectroscopy
- PA – Pulmonary atresia
- PDA – Patent ductus arteriosus
- rSO₂ – Regional oxygen saturation
- TCD – Transcranial Doppler
- TGA – Transposition of the great arteries
- TICR – Time in critical region
- ULA – Upper limit of autoregulation
- UMCU – University Medical Centre Utrecht
- VSD – Ventricle septum defect
- WMI – White matter injury

1 General Introduction

Neonates with congenital heart disease (CHD) requiring expert cardiological care constitute a significant portion of live births, with an incidence of approximately 6 per 1000 births [1]. Medical and surgical advancements have significantly improved survival rates, now reaching approximately 90% [2, 3]. However, long-term neurodevelopmental outcomes remain a concern, as nearly 50% of school-age survivors exhibit neurobehavioral symptoms such as inattention, cognitive problems, and hyperactivity [4]. Consequently, there has been a shift towards improving neurodevelopmental outcomes in CHD patients. Although the exact causes of neurodevelopmental delay are not known, studies have found a combined pattern of neurodevelopment delay and acquired brain injury [5]. A recent study identified new postoperative magnetic resonance imaging (MRI) lesions in 43% of neonates with CHD, of which new white matter injury (WMI) is the most prevalent [6]. WMI is defined as damage to the white matter of the brain, i.e. the axons, and may cause neurological symptoms.

Currently, evidence-based blood pressure goals to maintain sufficient cerebral blood flow (CBF) are nonexistent. Hypotension in neonates is commonly based on their gestational age in weeks [7]. However, uncertainty remains if these goals for blood pressure management are adequate for maintaining sufficient CBF in all neonates [8]. Furthermore, it is hypothesized that neonates have an individualized blood pressure range for optimal cerebral perfusion which calls for the need for individualized blood pressure management to optimize cerebral perfusion while myocardial demand is limited [9].

Cerebral autoregulation (CA) is the ability of the brain to keep the blood flow in the brain relatively constant over a range of perfusion pressures. Intraoperative monitoring of CA can define the blood pressure range that best supports cerebral perfusion in neonates and may aid in preventing neurological injury and improving long-term outcomes for neonates with CHD [9]. Near-infrared spectroscopy (NIRS) has been widely used to monitor CA because of its availability and ease of use but has several limitations, such as poor spatial resolution and limited penetration depth [9]. Transcranial Doppler (TCD) is an alternative technique that can provide real-time information on CBF and offers advantages over NIRS for CA monitoring, including a higher temporal resolution and the ability to directly measure blood flow velocity in the middle cerebral artery.

A high incidence of neurological injury remains in neonates with CHD after cardiac surgery, presumably caused by insufficient perfusion of the brain. Delineation of the autoregulation curve for personalized blood pressure management was possible in adults during cardiopulmonary bypass (CPB) [10, 11], it is unknown if this is also possible and beneficial for neonates with CHD.

The aim of this thesis is to assess the feasibility of employing CA monitoring as a tool for individualized blood pressure management during neonatal cardiac surgery. The hypothesis is that continuous monitoring of CA using TCD can effectively guide intraoperative blood pres-

sure management, ultimately enhancing cerebral perfusion and potentially improving neurological outcomes in neonates with CHD. The significance of this thesis outcome lies in refining intraoperative management, possibly impacting neurodevelopmental outcomes, and paving the way for tailored neonatal critical care. As neonatal cardiac surgery advances, this research marks a crucial step toward integrating autoregulation monitoring into standard practices for enhanced precision.

2 Clinical Background

2.1 Congenital Heart Disease

CHD represents a diverse group of structural abnormalities in the heart or the blood vessels surrounding it, which are present at birth. These conditions can range from mild, often asymptomatic defects to complex, life-threatening malformations. CHD is the most common congenital anomaly globally, with a substantial impact on public health. Its prevalence varies depending on the region, but, on average, approximately 1% of newborns are affected by some form of CHD. This prevalence translates to a significant number of individuals and families grappling with the challenges posed by CHD. Advances in medical care and surgical interventions have greatly improved the outlook for those born with CHD, leading to increased survival rates and improved quality of life for affected individuals. However, CHD remains a critical area of medical research and clinical care to further enhance the management and long-term outcomes for those living with these conditions.

2.1.1 Diagnosis

Ultrasound during pregnancy, also known as prenatal ultrasound or fetal ultrasound, is a medical imaging technique widely employed to monitor the development and well-being of the fetus in the womb. It is a non-invasive and safe tool used to create real-time images of the developing fetus. Prenatal ultrasounds are conducted at different stages of pregnancy to achieve various objectives, such as confirming pregnancy, estimating gestational age, assessing fetal growth, and identifying any potential abnormalities or congenital anomalies.

Since 2021, the Dutch prenatal screening program for severe congenital anomalies has included a first-trimester prenatal echography at 13 weeks of pregnancy, often referred to as the "13-weeks echo". A recent publication from the Netherlands reported a 70% detection rate of severe CHDs when combining the 13-weeks echo with the 20-weeks echography [12]. Following a diagnosis of a severe CHD, expectant parents are offered genetic testing and counseling to discuss prognosis and perinatal management options. Throughout the remaining pregnancy, fetuses with a severe CHD diagnosis receive close monitoring, including assessments of brain growth, maturation, and potential damage. Fetal MRI is primarily utilized for tracking brain development within the scope of research studies and is not yet integrated into routine clinical care.

2.1.2 Treatment

Patient with duct-dependent cardiac lesions follows a structured path. Initially, regular echography is conducted during pregnancy to monitor fetal development and identify any potential cardiac anomalies. After delivery, which usually takes place at the WKZ and often involves planned or induced labor or cesarean section, echocardiography is performed postnatally to assess the newborn's cardiac condition.

If a duct-dependent cardiac lesion is identified, it necessitates the maintenance of an open patent ductus arteriosus (PDA) to ensure adequate blood flow either to the pulmonary or systemic circulation. To prevent the closure of the PDA, Alprostadil, a prostaglandin E1 analogue, is administered intravenously. This is a critical step as it stabilizes the newborn's condition by maintaining necessary blood flow.

Subsequently, the infant is admitted to the intensive care unit for further monitoring and care. Depending on the specific cardiac condition and its severity, cardiac surgery may be planned as part of the treatment process often in the first weeks of life, especially in neonates with severe CHD.

The various types of cardiac malformations may require different surgical interventions. Without delving into extensive details, surgeries can generally be categorized into two groups: those aimed at repairing the malformation itself and procedures designed to enhance the neonate's circulatory system, enabling them to develop until a reparation procedure can be performed.

2.1.3 The burden of neurological injury after surgery

Neurological challenges after heart surgery in newborns are a significant concern. These surgeries, essential for congenital heart defects, can lead to developmental issues. Factors influencing these outcomes include genetic conditions like trisomy 21 and Williams syndrome, and socioeconomic elements highlighted the impact of family background on post-surgery cognitive development [13–15].

Intraoperative practices, especially CPB and deep hypothermic circulatory arrest (DHCA), crucially influence brain health. Extended periods of circulatory arrest during surgery are linked to heightened neurological risks [16–18]. Post-surgery, factors like low cardiac output syndrome and systemic inflammation response due to CPB can exacerbate neurological issues [19, 20]. Effective management in this phase is vital for minimizing brain-related risks.

Follow-up assessments reveal impacts on cognitive, motor, and language skills, with socioeconomic status playing a role in recovery [16]. The long-term outlook involves risks of behavioral and learning difficulties, necessitating ongoing support [21, 22].

2.2 Cerebral Autoregulation in the Neonate

2.2.1 Cerebral Physiology

The brain's high metabolic demands, along with its limited energy storage, requires precise control for the delivery of nutrients and oxygen and the removal of waste products. The mechanisms that performs this function are highly intricate and collectively referred to as cerebral autoregulation. LASSEN [23] first used the collective term 'cerebral autoregulation' in a 1959 review. In this study, the results produced a curve showing that cerebral blood flow remained relatively constant across a broad range of mean arterial blood pressures, as illustrated in **Figure 1**. This method of graphing CBF versus arterial blood pressure (ABP) results in a curve which since has been named Lassen curve.

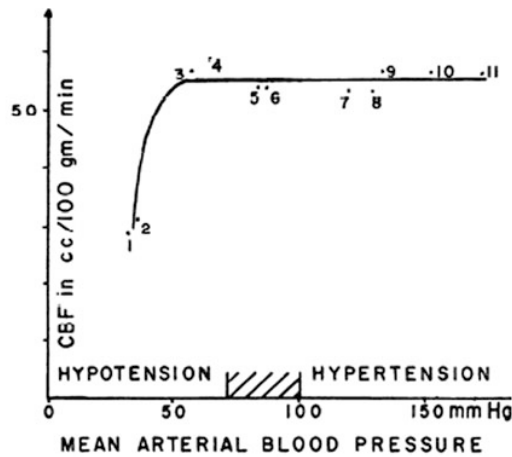


FIG. 1. Cerebral blood flow and blood pressure. Mean values of 11 groups of subjects reported in 7 studies have been plotted. Various acute and chronic conditions have been selected, characterized by a change in blood pressure. In all, this figure is based on 376 individual determinations.

1 and 2, Drug-induced severe hypotension (81). 3 and 4, Drug-induced moderate hypotension (206). 5 and 6, Normal pregnant women and normal young men (206, 173). 7, Drug-induced hypertension (230). 8, Hypertensive toxemic pregnancy (206). 9, 10, 11, Essential hypertension (229, 131, 228).

Figure 1: Original Lassen curve. Reprinted from [23].

CA protects the brain from hypotension induced hypoperfusion and from hypertension induced hyperemia [24]. The term CA comprises of four mechanisms which regulate the cerebral blood flow; myogenic, neurogenic, endothelial, and metabolic. The myogenic mechanism alters vascular smooth muscle activation, changing the arterial vessel diameter in response to changes in transmural pressures. The metabolic responses is mediated by PaCO₂. ABP outside the limits of CA may lead to inadequate CBF causing a regional accumulation of CO₂ causing local vasodilation. In turn, ABP above the ULA results in hyperperfusion and a decrease in local PaCO₂. An increase or decrease of 1-mmHg PaCO₂ causes an 4% change in cerebral blood flow [25]. The neurogenic mechanism involves the dynamic regulation of vasodilation and vasoconstriction in small to medium-sized arterial vessels, mediated by sev-

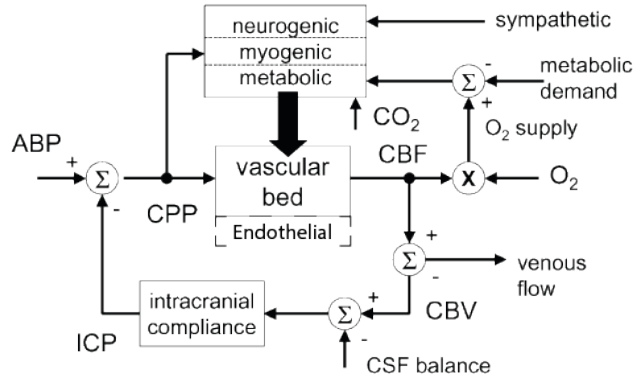


Figure 2: Schematic of primary regulatory mechanisms involved in cerebral autoregulation. Adapted from [27, 28].

eral neurotransmitters secreted by neurons. Serotonin and neuropeptide Y are associated with vasoconstriction, while acetylcholine and nitric oxide play roles in vasodilation. In turn, the endothelial mechanism affects vascular tone and thus CBF in response to neurotransmitters, hemodynamic stimuli, metabolic stimuli, and pharmaceuticals [26]. It is mediated through substances secreted by the endothelium, both during normal physiological states and pathological conditions. Notably, nitric oxide is an important vasodilator, while endothelin-1 and thromboxane A2 cause vasodilatory effects. The conceptual model shown in **Figure 2** visualizes the pathways of the myogenic, neurogenic, and metabolic regulatory mechanism of cerebral autoregulation. The model also illustrates how changes in cerebral blood volume (CBV) and cerebrospinal fluid (CSF) balance can impact intracranial pressure and blood flow. Feedback loops are indicated by positive and negative signs, denoting how different factors in the system enhance or inhibit each other to maintain CA.

The CA response has limits to its range, due to maximal dilatation and maximal constriction. The two values of ABP between cerebral blood flow is maintained constant are termed the lower limit of autoregulation (LLA) and the upper limit of autoregulation (ULA), where maximal vasodilation and vasoconstriction are achieved respectively, as displayed in **Figure 3**. Conceptually, the optimal mean arterial blood pressure (MAP_{opt}) lies at the midpoint between the LLA and ULA, where the margin for deviations of blood pressure staying within the limits is largest.

2.2.2 Development

The neonatal brain differs significantly from the adult brain. While the neonatal brain constitutes about 17% of body mass and receives 17% of the cardiac output, the adult brain, comprising only 2% of body mass, receives 20% of the cardiac output. More so, the cerebral physiology of the term infant differs from the pre-term infant.

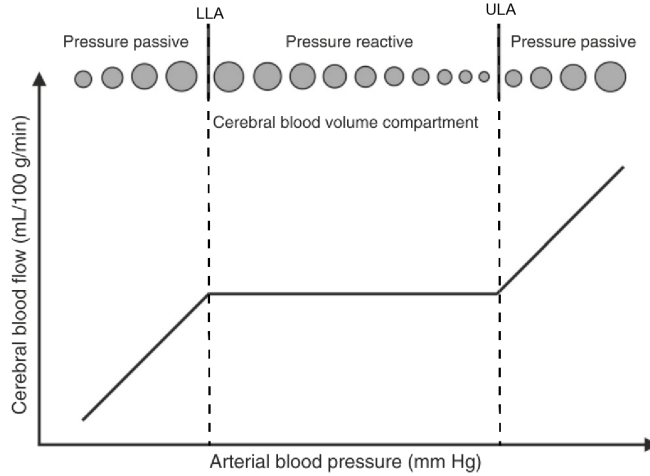


Figure 3: Schematic of the arterial blood pressure range where cerebral blood flow is pressure reactivity and pressure passive. LLA = lower limit of cerebral autoregulation, ULA = upper limit of autoregulation. Adapted from [9].

To understand physiological differences and vulnerability of the neonatal brain, we need to review the speed and complexity of early brain development. During fetal and neonatal life neurogenesis and neural network formation takes place, after 32 weeks of gestation myelination starts and this is followed around birth by a controlled process of pruning and cell death. Healthy brain development can already be disrupted by the effects of severe CHD with consequences for oxygenation, perfusion and nutrient distribution to the brain. In normal fetal development, the oxygenated blood coming from the placenta is transferred directly through the foramen ovale, into the left side of the heart, to the coronaries and carotid arteries. In neonates with transposition of the great arteries (TGA) the oxygenated blood is predominantly redistributed to the gut. This explains why neonates with severe CHD display findings of brain dysmaturation as well as vulnerability to brain injury, assessed by MRI [5, 29].

2.2.3 Association of cerebral autoregulation with patient outcome

Studies have shown that maintaining ABP within the optimal ABP determined by CA monitoring is associated with improved survival and neurological recovery in adult traumatic brain injury, neonatal hypoxic-ischemic encephalopathy, pediatric cardiac arrest, and pediatric traumatic brain injury [30–36]. Continuous monitoring of CA can help identify the MAPopt during CPB in adult patients [10, 11]. In neonates undergoing surgery involving CPB, maintaining MAP within the autoregulatory limits may play a crucial role in preventing or minimizing the occurrence of new cerebral lesions [37]. To the best of our knowledge, there is a lack of studies showing that monitoring CA during neonatal cardiac surgery leads to improved outcomes.

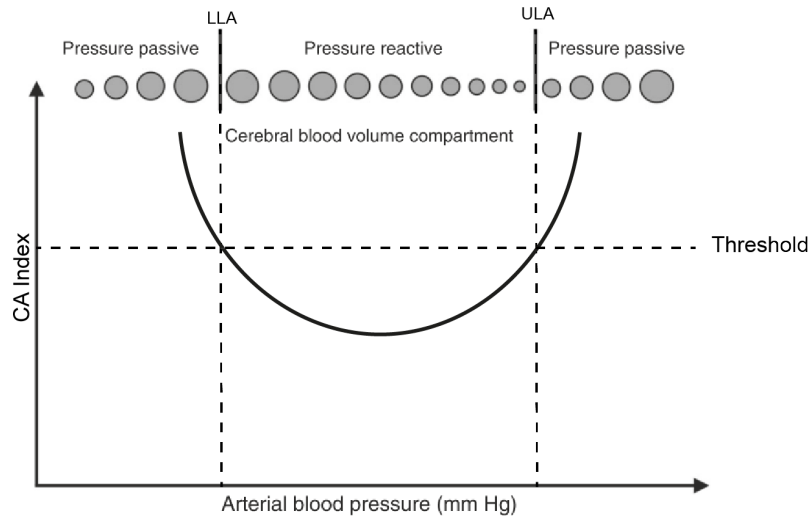


Figure 4: Schematic curve of a cerebral autoregulation index plotted versus the arterial blood pressure, displaying an U-shaped curve. Pressure reactive cerebral blood flow is achieved when the index is below the set threshold. The crossover points of the U-shaped curve with the threshold indicates the LLA and ULA. LLA = Lower limit of autoregulation, ULA = upper limit of autoregulation.

3 Technical Background

3.1 Cerebral Autoregulation Monitoring

The objective of monitoring CA is to investigate the conditions under which CBF becomes pressure passive, indicating impaired CA, and when it remains pressure reactive, signifying intact autoregulation. Calculating a CA index and creating a plot against ABP allows for the visualisation of the ABP range that supports intact CA. In **Figure 4**, a conceptual U-shaped curve of the CA index versus ABP is depicted.

A multitude of indices exist for assessing CA, all theoretically requiring the measurement of both CBF and cerebral perfusion pressure (CPP). However, direct measurement of CBF during neonatal surgery is not feasible with current technology, as this requires either invasive flow probes or continuous measurement of vessel diameter. Therefore, proxy measures for CBF are necessary in the context of neonatal cardiac surgery. These challenges regarding direct measurements of CBF have driven the usage of different modalities, metrics and corresponding CA indices. The two main modalities are TCD and NIRS, which will be discussed later.

Similarly, monitoring CPP involves invasive intracranial pressure monitoring, mostly reserved for patients with traumatic brain injury. However, because CPP is calculated as the difference between MAP and ICP, it is common to use MAP as a substitute for CPP, assuming that ICP

remains constant. Hlatky *et al.* [38] demonstrated that changes in MAP and CPP are nearly identical, providing strong support for the use of MAP as a proxy for CPP. This practical approach simplifies monitoring and assessment in clinical settings, as it allows for a more accessible and less invasive estimation of CPP. As a result, MAP is commonly utilized as a proxy for CPP in situations where direct ICP measurements are not accessible.

3.1.1 Transcranial Doppler

TCD is a non-invasive imaging technique used to assess blood flow within the arteries of the brain. TCD works based on the principles of Doppler ultrasound, a technology that uses sound waves to measure the speed and direction of moving objects, such as blood flow. TCD employs high-frequency sound waves, beyond the range of human hearing, typically in the 2 to 5 MHz frequency range. These sound waves are emitted by a small, handheld device called a transducer. The transducer is placed on the patient's scalp over specific locations where major cerebral arteries can be insonated. These locations are known as 'acoustic windows' and offer a direct path for ultrasound waves to penetrate the skull and access the cerebral arteries, which is displayed in **Figure 5**.

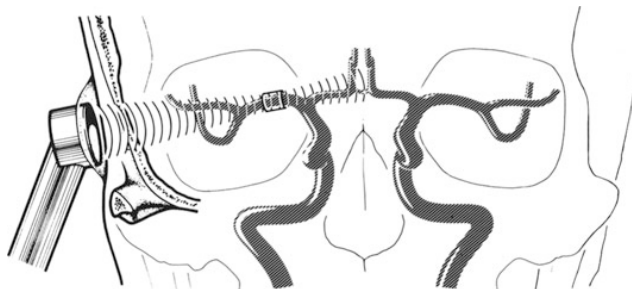


Figure 5: Transcranial Doppler probe positioning for insonating the middle cerebral artery. Adapted from [39].

As the emitted sound waves encounter moving red blood cells within the arteries, they bounce off these cells and return to the transducer. When blood cells move toward the transducer, the sound waves are compressed, leading to a higher frequency of the returning sound waves. Conversely, when blood cells move away from the transducer, the sound waves are stretched, resulting in a lower frequency. The TCD device detects these frequency shifts in the returning sound waves. By analyzing the frequency shifts, TCD can determine the speed and direction of blood flow in the cerebral arteries, calculated as

$$V = \frac{\Delta f * c}{2 * f_0 * \cos \theta} \quad (1)$$

where V is the speed of the red blood cell in cm/s, Δf is the observed frequency shift in

Hz, c is the speed of sound in the medium, f_0 is the emitted frequency, and θ is the angle of insonation in radians.

TCD provides quantitative measurements of cerebral blood flow velocity (CBFV) (in centimeters per second) and can be used to calculate various hemodynamic parameters, such as pulsatility index and resistive index. These measurements offer valuable insights into CBF and can be used to assess conditions like vasospasms, stenosis, emboli.

While CBFV is not the same as CBF, as one is measured in cm/seconds and the other in ml/seconds, studies have shown that they reflect similar transient changes under the assumption that the diameter of the measured vessel remains unchanged [40]. This substantiates the use of using CBFV as measured with TCD as an approximation for CBF, which is considered an accepted and well-validated tool to assess CA [24].

3.1.2 Near Infrared Spectroscopy

Besides TCD, NIRS has been widely used for CA monitoring [33, 41, 42]. NIRS is non-invasive light based technology used to monitor regional tissue oxygenation first explained by Jöbsis [43]. The relative transparency of biological tissue allows infrared light to penetrate. At the wavelength of the near-infrared spectrum, 700 to 1000 nm, light absorption is very low. Light that has traveled up to 8 centimeters into the tissue can be detected. In contrast, visible light, at the wavelength of 450 to 700 nm, penetrates less than 1 cm of biological tissue. After penetrating the target tissue, it interacts with the hemoglobin in the blood. Due to different absorption spectra for oxygenated and deoxygenated hemoglobin, measuring the amount of light absorbed by the hemoglobin allows for quantifying the levels of oxygenated and deoxygenated hemoglobin. The NIRS device then calculates the tissue saturation levels based on the absorption patterns.

NIRS is used and adapted for different tissues including muscles, kidneys, or the brain. In the context of neonatal cardiac surgery, NIRS is applied to monitor brain oxygenation saturation, of which the adhesive NIRS probe is applied to the forehead. A NIRS probe consist of near-infrared light emitting diodes, detecting photodiodes, and a dispersive element allowing the selective measurements of multiple wavelengths. The emitting diodes fire photons into the target tissue which interact with the oxygenated and deoxygenated hemoglobin. The detecting photodiodes, located at a distance of around 3 centimeters from the emitting diode, measure the absorption patterns of the reflecting light. The NIRS device then calculates the oxygen saturation levels in the tissue based on the absorption patterns, which is defined as the regional oxygenation (rSO_2) of the brain tissue of the frontal lobe. It is important to keep in mind that measured rSO_2 can be affected by other physiological variables including cardiac output, hemoglobin levels, $PaCO_2$, pulmonary function, acid-base status, and hypoxemia, which all not only affect partial oxygen pressure but also CBF [44].

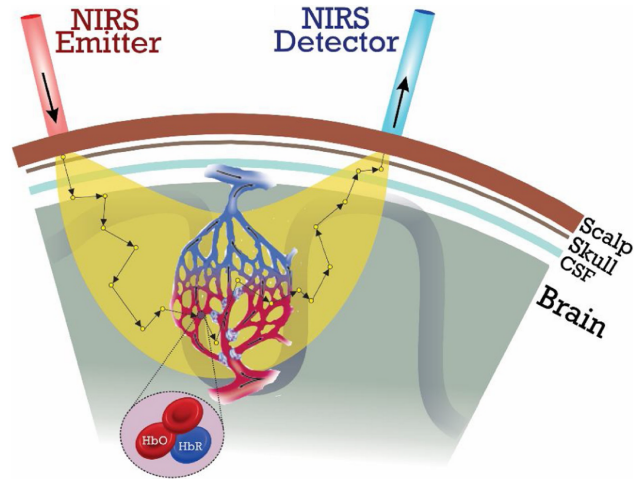


Figure 6: Schematic of near-infrared spectroscopy of the brain. Adapted from [45].

The rationale for utilizing NIRS to monitor CA is based on the assumption that the brain’s oxygen content reflects the arterial oxygen saturation, CBF, and oxygen-tissue diffusivity, while inversely associated with the cerebral metabolic rate for oxygen. Analysing short periods of time (3 to 6 minutes) that occur in response to MAP fluctuations with stable arterial saturation, metabolism, and diffusivity, is assumed to reflect similar information to the comparison of CBF and MAP [46].

3.1.3 Invasive arterial blood pressure monitoring

Invasive ABP monitoring is the gold standard for accurate blood pressure measurement in high-risk procedures like neonatal cardiac surgery. It entails inserting a catheter into an artery, often the right radial or ulnar artery in neonates, to measure blood pressure directly. This method provides real-time, precise readings of systemic perfusion, crucial for patient management.

The Mean Arterial Pressure, or MAP in short, calculated using the formula $MAP = DP + \frac{1}{3}(SP - DP)$, where DP is Diastolic Pressure and SP is Systolic Pressure, is a key metric derived from ABP monitoring. MAP is vital as it indicates the average blood pressure in the arteries, reflecting the blood flow to organs and tissues. Although this formula is an approximation, it’s widely used in clinical settings for its simplicity and reasonable accuracy.

3.1.4 Static and dynamic monitoring

The regulatory ability of the brain's vascular system to maintain relatively constant CBF can be assessed by static and dynamic autoregulation [47]. Static autoregulation refers to the ability for further vasoconstriction or vasodilation during a change in CPP [40, 48]. LUNDBERG [49] was the first to describe naturally occurring fluctuations in ABP which were termed 'slow waves'. These 'slow waves' have a period of 30 to 300 seconds [42, 50], and are most commonly used for measuring the autoregulation. 'Slow waves' are ideal for assessing CA since they occur at a frequency that engage the autoregulatory mechanism, approximately 0.003 to 0.030 Hz. More rapid fluctuations caused by the cardiac cycle or respiration are not moderated by CA. Thus, 'slow wave' oscillations in ABP have emerged as the preferred method for real-time autoregulation monitoring. CA monitoring and the delineation of the individuals MAPopt, LLA, and ULA are dependent on the occurrence of 'slow wave' oscillations over the range of blood pressure exceeding the individuals range of intact autoregulation [41]. When the presented blood pressures during monitoring remain within autoregulatory limits (i.e., the LLA and ULA), pinpointing the crossover point is not feasible. Similarly, solely presenting blood pressure values below or above these limits does not enable the delineation of an individual's CA curve.

4 Objectives

4.1 Research Aim

The central research question of this thesis is:

"What is the feasibility of cerebral autoregulation monitoring as a tool for blood pressure management during cardiac surgery that requires cardiopulmonary bypass in neonates with congenital heart disease?"

The aim of this thesis is to explore the feasibility and potential of CA monitoring as a tool for individualized blood pressure management and pave the way for improving neurological outcomes in this vulnerable patient population.

4.2 Thesis Outline

4.2.1 Phase 1

The goal of phase 1 is to develop a method for identifying and delineating the CA range. The limits of the CA range may serve as blood pressure goals during surgery, providing an additional tool for blood pressure management. The objective of phase one is to explore the feasibility of the actual delineation of the CA curves in the patient population of neonatal cardiac surgery with transcranial Doppler monitoring. In **Chapter 5**, the clinical study is presented which aimed to answer the research question:

1. How can the cerebral autoregulation range be delineated with combined transcranial Doppler and invasive arterial blood pressure monitoring?

However, before delineated CA curve characteristics may be used for blood pressure targets, additional evidence supporting the idea that maintaining blood pressure within the limits of intact CA will lead to improved neurological outcomes is required. Specifically, the neurological outcome under consideration is the incidence of new white matter injury (WMI) as observed in postoperative MRI brain scans, compared to preoperative MRI brain scans. The main objective of phase 2 is to explore the validity of using the delineated CA curve as blood pressure targets. A second clinical study is conducted and discussed in **Chapter 6**.

4.2.2 Phase 2

The first sub-question assesses whether blood pressure levels outside the determined limits of autoregulation during surgery are associated with worsened outcomes, as indicated by the potential occurrence of new WMI. If such an association is observed, it would provide evidence supporting the idea that maintaining blood pressure within the limits of CA can lead to improved outcomes. The second sub-question aims to determine the feasibility of using CA monitoring to establish blood pressure goals for all neonates with CHD, considering potential variations based on factors such as the type of surgery or specific medical conditions. The sub-questions for Phase 2 are as follows:

1. What is the association between blood pressure levels during surgery outside the delineated limits of cerebral autoregulation and the occurrence of new postoperative MRI lesions?
2. To what extent can intraoperative cerebral autoregulation monitoring be used for individualized blood pressure management in all neonates with congenital heart disease?

In conclusion, the results from both phases will be discussed in **Chapter 7**. This chapter will provide an overview of the findings in the conducted clinical studies and offer insights into the potential clinical implications of using cerebral autoregulation monitoring during neonatal cardiac surgery in relation to individualized blood pressure management.

5 Delineation of the Cerebral Autoregulation Range

5.1 Introduction

To our knowledge, there is no prior research on CA monitoring specifically in neonatal cardiac surgery. However, recent studies in comparable patient populations have successfully demonstrated the feasibility and significance of CA monitoring. Zipfel *et al.* [51], have demonstrated the feasibility and reliability of NIRS-based CA monitoring in 36 pediatric patients (range: 3 - 190 days) *after* pediatric CHD surgery. They concluded that CA monitoring with their method can be used to identify individual blood pressure goals to optimize cerebral perfusion. In the study they identified individualized blood pressure targets to optimize cerebral perfusion, which differed from traditional targets. Notably, only 7 patients that were included were in their first month of life. Iller *et al.* [41], have taken the next step and have demonstrated that NIRS-based CA monitoring in 20 pediatric patients (range: 0 - 39 months) *during* major elective surgery, excluding cardiac surgery, is feasible.

Additionally, the two discussed studies used NIRS for CA monitoring, a common modality for monitoring cerebral perfusion because of its ease of use and availability. However, recently NIRS has become is a disputed modality for evaluating the cerebral perfusion. [52], have stated that NIRS-derived oximetry is sub-optimal for clinical decision making from there study in 36 pediatric patients (range: 30 - 94 months) undergoing cardiac catheterization based on moderate concordance of NIRS-derived tissue oximetry with venous oximetry from two monitors. Despite these concerns, the application of NIRS in CA monitoring may be more forgiving, as consistent trend traces could be sufficient compared to the necessity for precise absolute values of tissue oxygenation in clinical decision making. This assumes that maintaining consistency in measuring fluctuations in tissue oxygenation is more crucial than achieving accurate absolute values for calculating correlation based CA indices. TCD monitoring is an alternative modality that can provide real-time information on CBF and offers advantages over NIRS for CA monitoring, including a higher temporal resolution and the ability to directly measure blood flow velocity in the middle cerebral artery.

ICM+ software (Cambridge Enterprises, Cambridge, UK) is used in nearly all published CA research, as well as in the two discussed studies [41, 51], facilitating simultaneous recording of signals at the bed-side, calculation of CA indices, and delineation of the CA curve. This software has to be purchased, which reduces availability and hinders additional evidence-based data from randomized control trials which are critical in substantiating the use of individualizing blood pressure targets for improves patient outcome. Additionally, studies using the software lack clarity about the fitting procedure of the U-shaped curve which can heavily influence the result of the delineated CA curve. Moreover, the commonly used U-shaped parabola, using a second-order polynomial, does not take the percentage of time for each bin recorded into account, making the fitting process vulnerable to outliers [24].

It remains, that no published research substantiating the feasibility of CA monitoring during surgery of neonates with CHD. Possibly, the population with most to benefit from individualized blood pressure management. Coincidentally, also a population very suited for CA monitoring as large MAP fluctuations are common in neonatal cardiac surgery with cardiopulmonary bypass. A methodology has been developed in the current study to be able delineate the CA curve from TCD- and NIRS-derived indices. The methodology developed for the current study incorporates a weighting function reducing the effect of outliers.

This pilot study aims to assess the feasibility of both TCD- and NIRS-based CA monitoring during neonatal cardiac surgery, using the developed methodology, with the objective of delineating the CA curve as a means for guiding individualized blood pressure management. The primary objective of this study is to descriptively analyze the feasibility of CA monitoring to delineate the individuals CA curve. Additionally, the study aims to identify individual and mean population CA curves, which are compared to currently used traditional blood pressure goals. Lastly, a secondary objective is to compare NIRS- and TCD-based CA monitoring results, aiming to assess the validity of NIRS-based CA monitoring.

5.2 Materials & Methods

5.2.1 Study design

The current study is a component of the FLOWER project (METC 21-823). The FLOWER project employs an observational design in which TCD measurements are obtained during major elective surgeries. It's important to note that flow velocity measurements from TCD are not used for routine clinical decision-making except for specific situations, such as detecting air or thrombotic emboli, assessing large left-to-right differences during improper positioning of the aortic cannula, or in cases of absent flow. Two groups are included into the study. The first group aims to include a total of 40 neonates diagnosed with CHD, and the second group is a control group that aims to include 40 neonates with non-cardiac conditions. This study makes use of a subset of prospectively collected data from the FLOWER project to assess the feasibility of CA monitoring with TCD in neonates with severe CHD.

5.2.2 Study population

Eligible patients are term infants within 42 days (6 weeks) after birth, or infants born prematurely (with a gestational age >32 weeks) at a corrected age of <42 days, who are scheduled for cardiac surgery. Eligible patients are approached to be included in the FLOWER (METC 21-823) project at the University Medical Center Utrecht (UMCU). All measurements are made at the Wilhelmina Children's Hospital which is part of the UMCU. Inclusion and exclusion criteria of the FLOWER project are as stated below with the addition of one exclusion

criteria specifically for this study.

Inclusion criteria:

- Elective and semi-elective cardiac surgery requiring cardiopulmonary bypass
- Age < 42 days for term neonates
- Gestational age of > 32 weeks with an corrected age of < 42 days for preterm neonates

Exclusion criteria:

- Gestational age < 32 weeks
- III - IV degree intracranial hemorrhage
- No signed informed consent form
- Incomplete CA monitoring data acquisition during surgery*

5.2.3 Data Acquisition

CA monitoring in neonatal cardiac surgery requires a proxy for the CPP and a proxy for CBF. The two modalities used in this study to approximate the CBF for CA monitoring are TCD and NIRS. Data acquisition with both modalities will be explained further. Lastly, the modality for measuring MAP as an approximation for CPP will be explained.

5.2.4 Surgery Event Times

During surgery, events such as time of incision, time of aortic cannulation, start of cooling, end of procedure are noted at the digital surgery following software. Event labels and event times are used to determine the relevant time period of surgery for data analysis. The selected period of surgery was taken after the sternum was opened until closure.

5.2.4.1 Transcranial Doppler

The CBFV of the left and right middle cerebral artery (MCA) is measured with the *Doppler BoxTMX* (DWL, Compumedics Germany GmbH, Singen, Germany) using two *2MHz PW Probes, Screw Topped* (DWL, Compumedics Germany GmbH, Singen, Germany). The probes

are positioned and fixated on the temporal window on either side of the head, as shown in **Figure 7**. The TCD operator who positioned the probes adjusted the insonation depth and gain required to get a satisfactory signal. The CBFV as measured by TCD, is stored with a sampling rate of 100Hz.



(a) Application of fixation ring



(b) Mounted TCD probe

Figure 7: Intraoperative measurement setup with bilateral TCD probe fixation.

5.2.4.2 Near Infrared Spectroscopy

Two NIRS sensors are placed on the forehead on the left and right side of the midline. Regional oxygen saturation (rSO₂) is measured during the whole surgery with a sampling period of 60 second. NIRS monitoring is routine clinical care in neonatal cardiac surgery. The NIRS monitor used was the *Hamamatsu Niro 200NX* (Hamamatsu Photonics Deutschland GmbH, Herrsching, Germany).

5.2.4.3 Mean Arterial Blood Pressure

Invasive ABP is measured with an arterial pressure catheter as a routine clinical procedure for neonatal cardiac surgery. The catheter is inserted into the right radial artery. In cases where this placement is unsuccessful or not feasible, alternative sites such as the left arm or the legs is attempted for catheter insertion to ensure accurate and continuous monitoring of blood pressure during the surgical procedure. The MAP is derived from the ABP trace by the central monitoring system, and stored with a frequency of 1Hz. Invasive ABP monitoring

is routine clinical care in neonatal cardiac surgery. The patient monitoring system used was the *Philips IntelliVue Patient Monitor M8010A* (Koninklijke Philips N.V., Amsterdam, The Netherlands).

5.2.5 Data Analysis

All data analysis is performed with MatLab version R2023a (version R2023a, MathWorks, Natick, MA). The MatLab code used for data analysis in this study can be found in **Appendix H**.

5.2.5.1 Artefact Cleaning

Artefacts in the MAP signal caused arterial line flushing are detected automatically. This was done by excluding periods of 10 seconds before and 10 seconds after the MAP signal exceeded a value of three times the mean MAP of the entire observed period. Arterial line flushing causes transient abnormally high MAP values, the rationale of the set threshold for detecting these artefacts is that physiologically viable values of MAP do not exceed 120 mmHg in neonatal cardiac surgery, and this such high spikes can be considered artefacts. The 20 second window is implemented to catch any abnormal MAP trace around the detected artefact, which may not exceed the threshold but is still caused by arterial line flushing.

Artefacts due to electrocautery were almost entirely excluded from the relevant time period during surgery used for data analysis. This was possible due to the fact that electrocautery is almost always only used at the very start of the surgery.

5.2.5.2 Lassen Curves

Lassen plots are the gold-standard for delineating an individual's CA curve [23]. However, the identification of classic S-shaped Lassen curves may be heavily hindered by signal noise, physiological fluctuations, or a limited range of observed MAP values. A multitude of CA indices have been developed over the years as an alternative to the classic Lassen curves. However, Lassen plots remain critical to determine threshold values of these CA indices [53, 54]. This often requires a large study population as recent study was able to identify classical S-shaped Lassen curves in only 59 out of 226 (26%) adult patients undergoing cardiac surgery [54].

In the current study, Lassen plots for both left and right MCA CBFV tracings are created for each patient to assess the presence and characteristics of classic S-shaped curves within this population. The Lassen plot are constructed as 2 mmHg mean (SD) binned values of consecutive 120 second paired means of CBFV in cm/s and MAP in mmHg all patients. A

fifth-degree polynomial is fitted on the averaged binned values of CBFV for visualization of the data trend, as is in line with a recent study [54]. The ideal Lassen curve shows an S-shaped curve, with first a rising slope, then a plateau, and lastly, a rising slope again. The LLA is defined as the MAP at the transition between the first slope and the plateau. The ULA is defined as the MAP at the transition between the plateau and the second slope. The optimal MAP is often defined as the center of the slope, between LLA and ULA.

Lassen plots for all patients are examined to identify the presence of a classic S-shaped curve. An S-shaped curve is characterized primarily by the existence of a distinct plateau, aligning with the range of intact CA. Additionally, the curve is assessed for the S-shape by determining if a rising slope is observable at both the beginning and end of the plateau. If at least one of a patient's Lassen plots (left and right MCA) exhibited a clearly distinguishable S-shape, it was scored 'good' If one or both Lassen plots showed a moderately distinguishable S-shape, they were scored 'moderate' if no S-shaped curve was evident, and they were categorized as 'none' if the evaluation of Lassen plots was solely conducted by the author.

5.2.5.3 Descriptive Analysis: Determining CA Index Threshold from Lassen Curves

A descriptive analysis is conducted to assess the feasibility of establishing CA index thresholds in this population. Given the relatively small size of the FLOWER project population (eventually 40 neonates) compared to the 229 adult patients undergoing cardiac surgery which were used in a recent study to determine the threshold values of three CA indices [54], it is improbable to derive CA index thresholds from this dataset. As a result, threshold values for CA indices in the current study were adopted from previously published studies.

5.2.5.4 Cerebral Autoregulation Monitoring - Delineation of the CA curve

In the current study two CA indices are implemented, the TCD-derived mean velocity index (Mx) and the NIRS-derived regional cerebral oximetry index (COx), and are used to delineate the per patient CA curve [24].

Mx is determined through a continuous Pearson correlation coefficient between MAP and CBFV. This computation involves consecutive paired 10-second averaged values of MAP and CBFV over a 5-minute duration. Additionally, a 5-minute average value of the 10-second MAP means is calculated, parallel to Mx for the entire 5-minute period. The Mx for a 5-minute period is calculated once every minute, resulting in a 80% overlap. The COx is calculated using the same methodology, as a continuous Pearson correlation coefficient between MAP and the rSO2. However, due to a sampling period of 60 second for rSO2, the computation of COx involves consecutive paired 60-second averaged values of MAP and rSO2 over a 10 minute period. Where the COx is calculated once every two minutes, resulting in an equal 80% overlap. A step wise explanation with figures can be found in **Appendix B**.

Studies have shown that indices of CA, such as the Mx and COx as presented in the current

study, commonly follow a U-shaped curve [34, 55–57]. Thus fitting a U-shaped curve on the binned index values is thus done in this study in line with similar studies previously published. The exact method for fitting this U-shaped curve is not mentioned in studies and thus a method to emulate this has been developed. The reasoning behind the currently used method is to model an upside-down Gaussian distribution, and then fit this on the data, which is the binned mean Mx or COx. This was achieved with the following formula

$$f(x) = 1 - a * e^{-\frac{(x-b)^2}{c^2}} \quad (2)$$

where a , b , and c are parameters to be fitted to the data, and x represents the input variable, which is the MAP in this context. This function is fitted on the binned mean values of the CA index with the MatLab function `'fit'`. The parameters all control a certain aspect of the U-shaped curve, namely a determines the depth of the curve minimum, b determines the MAP value of the minimum, and c determines the width of the curve.

The initial values for the fit are set to $[1, 40, 1]$ for $[a, b, c]$ respectively. This provides a starting point for the fitting process, and results in a very narrow distribution around the center of 40 mmHg, which is equal to the blood pressure goal of a neonate with a full 40 week gestation. This is done in order to battle fitting errors.

The lower and upper boundary values for the fit are set to $[0, -\infty, 0]$ and $[2, \infty, \infty]$, respectively. These boundaries constrain the to be fitted parameters during the optimization process. The lower and upper boundary of $a(0)$ and $a(2)$ constrain $f(x)$ to values of -1 to 1. This is substantiated by the fact that the Pearson's correlation coefficient results in a possible range of -1 to 1, reflecting a strong negative and strong positive linear correlation respectively. The lower boundary of c is set to 0 to prevent negative curve widths. In this way, $f(x)$ is fitted to the data while respecting the boundaries, without inducing any preconceived constraints about finding an expected best fit. This approach is expected to help tackle potential false positives, especially when dealing with a U-shaped curve that is fitted at the predefined boundaries, like the upper limit for width. If the data supports fitting a U-shaped curve, it provides insights into the feasibility of cerebral autoregulation monitoring in this population.

To battle outliers in the calculated binned mean CA indices, a weight function is used in the fitting process. The weight (W) of the bin in question (k) is calculated bt the following equation:

$$W(k) = 2 \times \frac{n(k)}{n_l} + 1 \times \frac{CI^{-1}(k)}{CI_m^{-1}} \quad (3)$$

Which shows that the computation of $W(k)$ is based on two components. The first term, $2 \times \frac{n(k)}{n_l}$, serves as a weighting factor proportional to the ratio of the number of indices ($n(k)$)

used to calculate the mean of the current bin to the number of indices (n_i) used for the bin with the highest entry count among all bins. The second term, $1 \times \frac{CI^{-1}(k)}{CI_m^{-1}}$, involves the inverse values of the 95% confidence intervals ($CI^{-1}(k)$ and CI_m^{-1}) for the current bin and the bin with the lowest confidence interval, respectively. This formulation aims to assign weights considering both the data size and confidence interval information, with the weight factor for the The reasoning is that bins with a larger number of CA index values, along with smaller confidence intervals, provide a more accurate representation of an individual's true CA curve. As a result, these bins are assigned greater weight in the fitting process, emphasizing their importance in accurately capturing the CA curve.

After the U-shaped curve is fitted on the binned mean CA index with help of the weighting function, the autoregulation curve is delineated. The threshold values of Mx and COx above which they are indicating of impaired autoregulation above are considered are 0.45 and 0.35 respectively, as reported in [54]. This means that the crossover points of the fitted U-shaped curve over the threshold determines the value of LLA and ULA respectively. The MAPopt is located at the minimum of the curve. It is important to note that CA curve characteristics, including LLA, MAPopt, and ULA, are deemed valid only if the curve crosses the threshold value within the observed MAP range. While U-shaped curves are extrapolated beyond the observed MAP values, this is not done for the purpose of determining CA characteristics.

Two CA curves are computed for each patient, corresponding to the left and right MCA or rSO2. Only one of the CA curves is selected for further analysis based on several criteria; A CA curve with three delineated characteristics is prioritized over the other if the latter displays only two delineated characteristics. Likewise, CA curves with two characteristics are favored over the other side if it exhibits only one delineated CA characteristic. In cases where both the left and right CA curves display an equal number of delineated CA characteristics, the side with the smallest range of CA is chosen.

5.2.5.5 Comparison of NIRS and TCD based CA monitoring

The comparison between NIRS-derived COx and TCD-derived Mx is based on their respective success rates, expressed as percentages, in delineating the LLA, MAPopt, ULA, and the range of CA. This analysis aims to assess the additional benefits of TCD-based CA monitoring compared to the more prevalent use of NIRS-based monitoring. It's important to note that the sampling periods differ; 0.01 seconds for CBFV measured with TCD and 60 seconds for rSO2 measured with NIRS. Comparison of average CA characteristic values are outside the scope of this study.

5.2.5.6 Statistical Analysis: Characteristics Predictive of Successful CA Delineation

Analyses were performed with MatLab version R2023a (version R2023a, MathWorks, Natick, MA). The aim of the statistical analysis is to investigate whether the ability to delineate the LLA, MAPopt, and ULA (success = 1 or failure = 0) is influenced by patient CHD diagnosis.

For the statistical analysis, logistic regression models were used to examine the association between CHD diagnosis and the capacity to delineate the LLA, MAPopt, and ULA.

Models were adjusted for patient sex, gestational age, birth weight, CPB time, total time measured, average Vmean, spO2 (pre-/postductal). The total time measured in minutes is the time span of the selected relevant time period used for calculation of CA indices. The average of the left and right Vmean is calculated for each person as a measure for baseline for CBFV (post induction, pre surgical intervention). In patients with a missing preductal spO2, the postductal spO2 is included, as the measure for systemic oxygenation.

Model performance is evaluated through accuracy, sensitivity, specificity and precision of predicting whether delineating of LLA, MAPopt, or ULA possible. Possible delineation of the LLA for example, was considered successful if the fitted U-shaped curve crossed the CA index threshold within the observed range of MAP. The Chi-squared goodness-of-fit test is performed to assess the predicted and observed outcome distributions, with h-value of 1 and a corresponding p-value less than 0.05 indicate a significant discrepancy, indicating model performance. Nagelkerke R2 is then calculated to measure the proportion of variance in the outcome captured by the model, where a higher value indicates a better ability to explain variability in the response variable. Lastly, odds ratios are computed along with their 95% confidence intervals to assess predictor influence.

5.3 Results

5.3.1 Patient Data

29 patients were recruited into the FLOWER project from April 2022 until October 2023. For the current study, one patient was excluded due to a connection error between the recording computer and the central monitoring system, leading to the absence of a synchronous recorded MAP signal during surgery — a requirement for CA monitoring. Consequently, patient 17 is excluded from further analysis.

Twenty-eight patients (21 male/7 female) undergoing cardiac surgery were successfully monitored. Mean gestational age was 38.5 with a range of 36 to 40 weeks. All patients had surgery within 16 days after birth. Baseline characteristics are summarized in **Table 1**. A per patient overview of baseline characteristics can be found in **Appendix C**.

CHD diagnosis are clustered into 4 groups, based on varying distinct physiology's. **(1)** The 'TGA' group comprises patients diagnosed with TGA with and without ventricular septum defect (VSD). In TGA, oxygenated and deoxygenated blood circulate parallel to each other, leading to inadequate oxygenation of the body. **(2)** The 'SVP' group includes patients diagnosed with single ventricle pathologies such as Hypoplastic Left Heart Syndrome (HLHS)

or other univentricular heart conditions. Individuals in this group have a single functional ventricle tasked with pumping blood to both the pulmonary and systemic circulations, often resulting in mixed blood flow. **(3)** 'AoAO' group comprises patients diagnosed with aortic arch obstructions such as coarctation of the aorta and hypoplastic aortic arch. This restricts flow and increasing workload for the left ventricle. **(4)** The 'Other' group includes patients with pulmonary atresia (PA). In PA, the pulmonary valve is either absent or significantly narrowed, obstructing blood flow to the pulmonary system and hindering the postnatal oxygenation process. Additionally, this group includes patients with truncus arteriosus, where a single vessel emerges from the heart carrying mixed blood, resulting in reduced overall oxygenation of the systemic circulation.

Table 1: Summary of Baseline Characteristics

Characteristic	Overall, N = 28
Birth Weight [gr], mean (SD)	3396.7 (515.9)
Weight @ Surgery [gr], mean (SD)	3398.2 (528.9)
Gestational Age [weeks], mean (SD)	38.5 (1.0)
Age @ Surgery [days], mean (SD)	6.9 (3.3)
Male, n / N (%)	21 (75.0%)
CHD Diagnosis Group	
TGA, n / N (%)	10 (35.7%)
SVP, n / N (%)	6 (21.4%)
AoAO, n / N (%)	8 (28.6%)
Other, n / N (%)	4 (14.3%)
Surgery Group	
Arterial Switch, n/N (%)	10 (35.7%)
Aortic Arch Repair, n/N (%)	7 (25.0%)
Central Shunt +/- Atrial Septectomy, n/N (%)	4 (14.3%)
Norwood I, n/N (%)	3 (10.7%)
Other, n/N (%)	3 (10.7%)
Coarctation of Aortic Arch Repair, n/N (%)	1 (3.6%)
Surgery Characteristics	
CPB Time [min], mean (SD)	142.8 (42.0)
Aristotle Score, mean (SD)	9.8 (2.4)
Aortic Clamping Time [min], n / N (%)	25 (89.3%)
mean (SD)	95.6 (24.7)
(S-)ACP Time [min], n / N (%)	11 (39.3%)
mean (SD)	56.7 (22.9)
Arrest Time [min], n / N (%)	3 (10.7%)
mean (SD)	6.0 (1.0)
Cooling Temperature [°C] - mean (SD)	26.1 (5.0)

5.3.2 Lassen Curves

Important to note that the scoring of Lassen plots is highly subjective and may even vary within one observer upon reevaluation. Visual evaluation by the author resulted in the scoring of 4 (14.3%) 'good', 4 (14.3%) 'moderate', and 20 (71.4%) 'non' Lassen plots. A notably difference between the left and right MCA derived Lassen plots was only noticed in one case (patient 14).

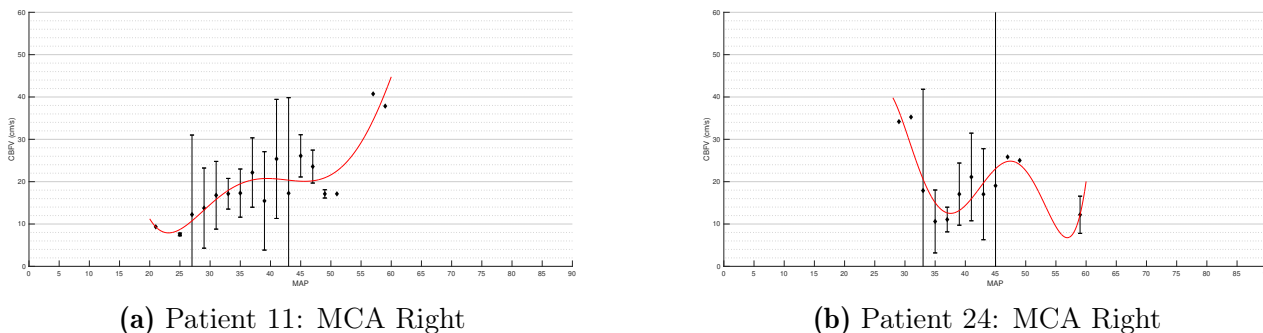


Figure 8: Example Lassen plots of two patients scored 'good' (a) and 'none' (b).

Two examples of Lassen plots are displayed in **Figure 8**. Limits of CA from **Figure 8 (a)** were estimated at 38 mmHg and 48 mmHg for the LLA and ULA respectively. To be noted that very limited amount of data points are present above a MAP of 45 mmHg. **Figure 8 (b)** displayed no clear plateau and rising slopes.

5.3.3 Cerebral Autoregulation Monitoring: Delineating MAPopt, LLA, and ULA

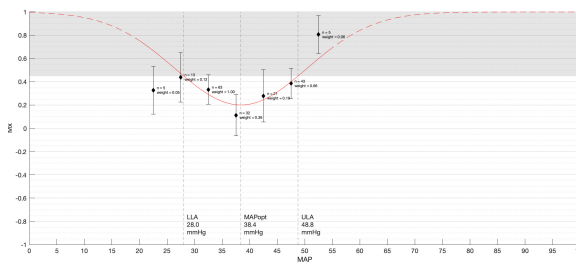
Satisfactory bilateral insonation of the MCA's was achieved in all 28 patients. No notable difference between the left and right trace was reported during monitoring. The rSO2 was successfully recorded in 23 patients. Missing recordings were due to connection error between the NIRS system and the central monitoring system. The CA curve plots of every patient can be found in **Appendix G**.

It should be noted that two CA curves are computed for each patient, corresponding to the left and right MCA. The selection of the CA curve for further analysis is based on several criteria. A CA curve with three delineated characteristics is prioritized over the other if the latter displays only two delineated characteristics. Likewise, CA curves with two characteristics are favored over the other side if it exhibits only one delineated CA characteristic. In cases where both the left and right MCA-derived CA curves display an equal number of delineated CA characteristics, the side with the smallest range of CA is chosen.

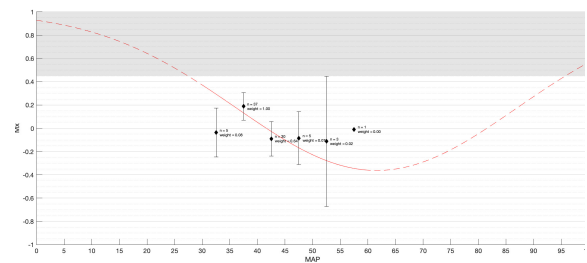
Among the 28 patients, the LLA could be determined in 10 (35.7%) and 14 (50.0%) patients with NIRS and TCD respectively. The MAPopt could be determined for 15 (53.6%) patients

with NIRS and 16 (57%) patients with TCD. Lastly, the ULA could be determined in 10 (35.7%) versus 11 (39.3%) patients. Interestingly, the complete CA curve could be delineated in 10 (36%) patients with NIRS and 10 (36%) with TCD, of which 6 are overlapping. Notably, for both modalities, if any characteristic of the CA curve could be delineated, MAPopt is always determined. Given these results, further data and statistical analysis focuses on the TCD-derived CA curves. Comparing the means of the NIRS- versus TCD-derived CA characteristics are outside the scope of this study.

The CA delineation using Mx revealed mean values for CA characteristics: LLA at 29.4 ± 6.4 mmHg (range: 19.0 - 41.5), MAPopt at 42.0 ± 7.0 mmHg (range: 34.4 - 56.2), and ULA at 49.5 ± 4.9 mmHg (range: 44.3 - 58.4). The overall range of the complete CA curve averaged 20.9 ± 6.1 mmHg (range: 12.3 - 32.0). The delineated CA curve characteristics of every patient are summarized in **Appendix D**.



(a) Patient 11: MCA Right



(b) Patient 24: MCA Right

Figure 9: Example of Mx plots with (a) and without (b) a delineated cerebral autoregulation curve. Mx = mean velocity index, MAP = mean arterial pressure.

Two examples of delineated CA curves of patient 11 and 24 with Lassen plots scored 'good' and 'none' respectively, are displayed in **Figure 9**. The binned mean Mx values in **Figure 9 (a)** span both above and below the threshold of 0.45, distributed across a bin width from 20 to 55 mmHg. The U-shaped curve appears to fit closely with the data, yielding a well-defined CA curve with LLA = 28.0, MAPopt = 38.4, and ULA = 48.8 mmHg. These delineated values of MAPopt and ULA are in close proximity to the Lassen plot based estimates of LLA = 38, and ULA = 48 respectively, to note that at 38 mmHg the Lassen plot yielded an estimate for LLA, and Mx plots delineated the MAPopt at that MAP.

The binned mean Mx values in **Figure 9 (b)** exclusively fall below the threshold of 0.45. Nevertheless, they cover a similarly large bin width of 30 to 60 mmHg. Apparently, the U-shaped curve demonstrated an optimal fit to the data, where the descending slope of the U-shaped curve best matched the observed data. The crossover points and the minimum of the fitted curve were all outside the observed range of MAP, preventing delineation of any cerebral CA curve characteristics. It remains that all values of the binned mean Mx are below the threshold, indicating intact CA from a theoretical standpoint.

5.3.3.1 Incomplete Delineated CA Curves

The 18 (64%) patients without a fully delineated CA curve appeared to exhibit similar patterns. In cases with an incomplete CA curve, displaying only two characteristics ($n = 5$, 17.9%), 4 (14.3%) patients were missing an ULA, and 1 (3.6%) patient was missing an LLA. The remaining CA curve characteristics of these patients were outside the range of observed MAP, as indicated by the extrapolated fitted U-shaped curve.

For patients where either only one or none of the CA characteristics are delineated ($n = 13$, 46.4%), the majority of the binned mean values of Mx were below the threshold of 0.45 in 10 (35.7%) patients, while no patient exhibited a majority above the threshold. The remaining 3 (10.7%) patients Mx values were distributed indistinctly both above and below the threshold.

5.3.3.2 Optimal MAP and Current Blood Pressure Targets

The delineated MAPopt exceeds the patient's GA for all patients. The mean difference between GA and the delineated MAPopt was 5.3 ± 5.6 (range: 0.1 - 17.2) mmHg. Otherwise, all of the delineated MAPopt values were greater than the corresponding patients GA. Emphasizing the currently routine use of a patient's GA as a MAP goal due to a lack of evidence-based blood pressure goals in this population.

5.3.3.3 Predictive Patient Characteristics for Delineating CA Curve

This study employed logistic regression models to investigate the association between CHD diagnosis and the ability to delineate the CA curve, including the LLA, MAPopt, and ULA. Calculated Odds Ratios with corresponding p-values are summarized in **Table 2**.

For the LLA prediction model, the accuracy was 64.3%, sensitivity was 64.3%, specificity was 64.3%, and precision was 64.3%. The Chi-Squared Goodness-of-Fit Test indicated a significant dissimilarity between predicted and observed LLA delineation ability ($h = 1$, $p < 0.05$). Nagelkerke's R-squared was 0.034, implying minimal variability capture.

The second model, focused on predicting MAPopt, achieved an accuracy of 67.8%, sensitivity of 81.3%, specificity of 50.0%, and precision of 68.4%. The Chi-Squared Goodness-of-Fit Test revealed a significant difference between predicted and observed MAPopt delineation ability ($h = 1$, $p < 0.05$). However, Nagelkerke's R-squared of 0.023 suggested a limited ability to capture variability.

In the last model predicting ULA, the accuracy reached 64.3%, sensitivity was 45.5%, specificity was 76.5%, and precision was 55.6%. The Chi-Squared Goodness-of-Fit Test highlighted a significant difference between predicted and observed ULA delineation ability ($h = 1$, $p < 0.05$). Nagelkerke's R-squared was 0.030, indicating a marginal ability to capture variability.

Table 2: Odds ratios for predicting ability to delineate the LLA, MAPopt and ULA.

Variables	LLA				MAPopt				ULA			
	OR	CI lower	CI upper	P-value	OR	CI lower	CI upper	P-value	OR	CI lower	CI upper	P-value
Sex (male)	0.39	0.02	6.92	0.487	0.31	0.01	6.67	0.421	2.86	0.13	58.69	0.462
Birth Weight	1.00	1.00	1.00	0.398	1.00	1.00	1.00	0.869	1.00	1.00	1.00	0.380
CPB min	1.01	0.95	1.07	0.863	0.97	0.91	1.05	0.420	1.00	0.93	1.07	0.996
CHD group Other	2.82	0.05	170.35	0.593	5.20	0.06	425.62	1.000	0.17	0.00	17.33	0.416
CHD group SVP	1.04	0.04	28.87	0.983	0.30	0.01	11.49	0.483	1.44	0.03	81.98	0.849
CHD group TGA	1.58	0.06	42.78	0.769	2.59	0.08	80.32	0.560	1.87	0.06	58.03	0.700
Gestational Age	1.22	0.43	3.44	0.687	0.55	0.15	2.06	0.341	0.88	0.28	2.74	0.810
Total Time Measured	1.22	0.96	1.06	0.688	1.03	0.98	1.09	0.219	0.99	0.94	1.05	0.745
Vmean	1.00	0.87	1.16	0.951	0.97	0.83	1.14	0.707	1.07	0.91	1.26	0.383
spO2	0.94	0.77	1.13	0.455	0.94	0.78	1.15	0.532	0.94	0.78	1.14	0.501

CHD group reference is the AoAO group.

5.4 Discussion

The main aim of this study was to assess the feasibility of CA monitoring during neonatal cardiac surgery. We successfully performed non-invasive CA monitoring in 28 neonates with CHD, during cardiac surgery in the first weeks of life, and demonstrated that CA monitoring provides robust data and can be performed reliably and safely in clinical practice.

Two modalities for CA monitoring were compared in this study. Our data suggest that TCD outperforms NIRS for CA monitoring, based on the number of delineated CA characteristics in this population. However, the sampling rate of TCD was significantly higher than that of the NIRS, which likely is an important factor in the data analysis. No definitive comparison can be made based on our data. Analysis of delineated LLA, MAPopt, and ULA was based on the results generated from the TCD based monitoring.

The key observation of this study are as follows. Firstly, CA monitoring in this vulnerable population to delineate the LLA, MAPopt, and ULA is feasible and offers new information about the range of MAP for optimal CA functionality. Comparing our results to those of Iller *et al.* [41], who successfully delineated the entire CA range in 11 out of 20 (55.0%) infants during non-cardiac surgery, our success rate in delineating the complete CA curve for 10 out of 28 (36.0%) patients is lower. While cardiac surgery is well-suited for CA monitoring due to the high incidence of blood pressure fluctuations, it may be that additional unforeseen factors may negatively impact the ability to delineate the CA curve. Furthermore, the younger age of our population may introduce complications in CA monitoring.

Secondly, the variance in CA range highlights the need to transition from a one-size-fits-all approach to individualized blood pressure management in this population. The mean LLA and MAPopt were 29.4 ± 6.4 mmHg (range: 19.0 - 41.5) and 42.0 ± 7.0 mmHg (range: 34.4 - 56.2), respectively, which demonstrates the significant variability within our patient population. Additionally, our data suggest that current guidelines on blood pressure management might be too low, which is in accordance with recent studies [41, 51]. The patients gestational age in weeks is often utilized as the blood pressure target in mmHg which is always lower than

the delineated MAPopt in our study.

An important secondary observation of this study is that the ability to delineate the patients CA curve relies on having a sufficiently broad range of blood pressure managements, which is necessary to assess the whole CA curve. Namely, in the 18 patients with an incomplete delineated CA curve, all had Mx values below the threshold, suggesting that the observed range of MAP did not stray outside the patient range for intact CA. This suggest that the inability to delineate the patients CA range does not necessarily imply the absence of an intact CA range in the patient.

We also explored whether patient characteristics, specifically the CHD diagnosis, influenced the ability to delineate the CA curve. The aim was to determine whether CA monitoring is feasible in all neonates with CHD. However, our data do not suggest that the ability to delineate the CA curve differs across CHD diagnosis. It's worth noting that our relatively small sample size for certain CHD groups might have influenced these findings.

The mean MAPopt in this population is considerably lower than those reported in a study in infants with a mean age of 4.1 ± 2.8 months after cardiac surgery [51]. This underscores the continued development of the autoregulatory function of the cerebral vasculature in the first months after birth. This necessitates the research in CA specifically in these neonates, as new WMI after surgery is still a problem.

In addition to CA monitoring, we also generated Lassen curves for each patient. Lassen curves are traditionally used to delineate the limits of CA but are susceptible to signal noise and physiological fluctuations, which can reduce their ability to accurately delineate the CA curve. However, it is important to note that the threshold values used to distinguish between intact and impaired autoregulation for the CA indices (Mx and COx) are still based on these Lassen curves. In this study, we utilized threshold values of 0.35 for COx and 0.45 for Mx, which were determined from a large cohort of 226 adult patients after cardiac surgery with respect to developing acute kidney injury [54]. It remains unclear whether these thresholds are optimal for identifying the CA curve in relation to the occurrence of new brain lesions in neonates with CHD.

Clinical implications

The findings in this study offer valuable novel information about the range of MAP which supports intact CA, which is associated with improved outcome [30–36]. In neonatal cardiac surgery it is necessary to maintain adequate cerebral perfusion while protecting the myocardium. This data presented in this study paves the way for clinicians to answer the question 'How low can we go?'. Although the high variance in average LLA and MAPopt do not allow for setting a new blood pressure target for all neonates with CHD, it does offer clinicians more context to take into account which they can base their approach on,

While less relevant during cardiac surgery, the calculated mean ULA of 49.5 ± 4.9 mmHg (range: 44.3 - 58.4) provides valuable novel insights. This is because both hypo- and hyper-

perfusion of the brain can result in significant neurological injury. The ULA helps elucidate the upper limit beyond which hyperperfusion may occur. While not directly relevant during cardiac surgery, as blood pressure is typically maintained well below this limit to reduce myocardial demand and prevent hemorrhages, this threshold was previously unknown, and is relatively low for some patients.

Limitations

First of all, the observational design and relative small sample size impair the power of the study findings. As there is no universally accepted 'gold standard' for defining the CA curve, the limits of autoregulation determined in studies, including this one, are inherently approximate. The specific method employed to fit the U-shaped curve plays a crucial role in delineating the CA curve. Due to the absence of a benchmark methodology, the validity of this approach can be challenging to ascertain. Nonetheless, in this study, the methodology adopted for fitting the U-shaped curve demonstrated a consistency in aligning with the CA indices resembling the consistency of the fitting process in similar studies [54, 58]. This consistency lends support to the credibility of the methodology used in our analysis. Future studies are needed to determine which methodology is best suited to delineate the CA curve when the validity of the delineated CA curve is based on the patients neurological outcome.

Furthermore, our monitoring approach involved both the left and right MCA during surgery, leading to the generation of two CA curves for each patient. While in most cases, these curves were similar, the decision to select one over the other could potentially introduce bias. Future studies should aim to explore the underlying reasons for any differences between the left and right MCA readings. Identifying these variances is essential as it could inform the choice of the most representative CA curve, thereby more accurately reflecting the physiological state of the patient.

Potential artefacts in the collected data were removed with an automatic algorithm. This algorithm has not been validated and may have caused under or over detection of artefacts influencing results. Additional research in automatic detection of artefacts caused by the patient moving or by electrocautery may be validated with manual detection of artefacts. This was outside the scope of this study. We also suggest that to increase the signal-to-noise ratio of the CA curves, epochs with no or little variance are excluded for the fitting of the U-shaped curve.

Lastly, an important limitation of this study is the inability to objectively validate the fitted S-shaped Lassen curves and U-shaped CA-curves. Although the confidence intervals of the calculated Lassen and CA plots appear high, they appear of similar scale of those displayed in previous studies. This may have affected the accuracy of the delineated CA characteristics. Increasing the measurement time can enhance the accuracy of Lassen and CA curves. However, this improvement is limited by the duration of the procedure and necessitates alternative solutions. In this study, we attempted to correct the fitting process by taking CA index bin confidence interval and amount of values included into the bin to improve the fitting

process. The use of slow waves dictates the refresh rate of autoregulation monitoring, and is the rate-limiter for time to delineate the CA curve. More advanced analysis techniques such as wavelet analysis may prove useful in improving the minimal time needed to delineate the CA curve [57].

5.5 Conclusion

In this study, we successfully demonstrated the feasibility of delineating each patient's CA curve using TCD. This approach provided new insights into the optimal MAP range that best supports CBF. The results of this study offer valuable information to clinicians as the high variance in specifically the LLA, show that current blood pressure targets are not adequate for all neonates with CHD. Given the multifactorial nature of new brain lesions post-surgery, understanding the relationship between maintaining blood pressures within the individualized CA curve and the potential reduction in brain lesions is essential. This knowledge is key to determining whether adherence to these individualized CA parameters can indeed diminish the incidence of brain lesions in this vulnerable population.

6 Perioperative Brain Damage

6.1 Introduction

The development of new WMI after neonatal cardiac surgery is likely multifactorial. Studies have identified several risk factors, including aspects related to birth history, the clinical course of the neonate, catheterization and surgical procedures, as well as the specific cardiac diagnosis [6]. Furthermore, deviations in MAP below or above the LLA and ULA can result in both hypo- and hyperperfusion, which in turn increase the risk of brain injury and neurological disability [9].

In the study presented in Chapter 5, it was demonstrated that it is feasible to delineate the CA curve using TCD-based monitoring during neonatal cardiac surgery. This study also revealed that the delineated optimal MAP values differ from those commonly used as clinical blood pressure targets. This suggests that the blood pressure targets typically employed in clinical care may be set too low. However, it remains uncertain whether these delineated autoregulation limits hold practical clinical relevance as blood pressure targets in the context of neonatal cardiac surgery. The beneficial effects of maintaining blood pressures within the autoregulation limits have been demonstrated in other patient populations, as evidenced by various studies [30–36]. However, it is yet to be established whether this holds true for neonatal cardiac surgery.

In this study we assess the association of the delineated CA characteristics and the time during surgery spent outside these limits, with the occurrence and size of new WMI lesions. The primary objective of this study is to determine whether there is an association between the time spent outside a patient’s CA curve and the development of new WMI lesions. This finding could potentially support the use of CA monitoring as a valuable tool for blood pressure management during neonatal cardiac surgery. Additionally, as a secondary objective, we aim to evaluate whether the CA characteristics can serve as indicators of a patient’s overall susceptibility to acquiring new WMI.

6.2 Materials & Methods

6.2.1 Study Design

The current study is part of the FLOWER study (METC 21-823). The FLOWER study follows an observational design, where measurements are obtained during major elective surgery from two distinct groups. The first group aims to include a total of 40 neonates diagnosed with CHD, and the second group is a control group that aims to include 40 neonates with non-cardiac conditions. This pilot study utilizes a subset of prospectively collected data from

the FLOWER study to assess the clinical relevance of the delineated CA characteristics as reported in **Chapter 5**.

6.2.2 Study Population

Eligible patients are term infants within 42 days (6 weeks) after birth, or infants born prematurely (with a gestational age >32 weeks) at a corrected age of <42 days, who are scheduled for cardiac surgery. Eligible patients are approached to be included in the FLOWER (METC 21-823) project at the UMCU. All measurements are made at the Wilhelmina Children's Hospital which is part of the UMCU. Inclusion and exclusion criteria of the FLOWER study are as stated below with the addition of two exclusion criteria specifically for this study.

Inclusion criteria:

- Elective and semi-elective cardiac surgery requiring cardiopulmonary bypass
- Age < 42 days for term neonates
- Gestational age of > 32 weeks with an corrected age of < 42 days for preterm neonates

Exclusion criteria:

- Gestational age < 32 weeks
- III - IV degree intracranial hemorrhage
- No signed informed consent form
- Incomplete CA monitoring data acquisition during surgery*
- Missing pre- or postoperative cerebral MRI scoring**

6.2.3 Data Acquisition

6.2.3.1 Perioperative Magnetic Resonance Imaging

The main outcome of this study is new WMI lesion size in millimeters measured as the largest lesions diameter in 2D, as detected by MRI. A brain MRI is made pre- and postoperative and is scored by radiologists according to the scoring system determined by the European Association Brain in Congenital Heart Disease Consortium, as used in Stegeman *et al.* [6]. The metric used to reflect the occurrence and severity of new WMI injury is the cumulative 2D size of new WMI lesions. WMI was identified as one or more white matter lesions, without

a maximum size limit, characterized by high signal intensity on T1 images and typically low signal intensity on T2 images. The size of the lesions was measured on T1 images at the plane showing the largest diameter, with the measurement of the largest lesion being reported. Please refer to [6] for the MRI scanning protocol.

6.2.4 Data Analysis

All data analysis and statistical analysis is performed with MatLab version R2023a (version R2023a, MathWorks, Natick, MA).

6.2.5 Statistical Analysis: TICR and Outcome

In this statistical analysis the association between four calculated surgical variables and outcome is assessed. The Outcome is new WMI 2D size [mm], which is calculated from the sum of length of WMI lesions measured in 2D. The aim of this analysis was to assess the clinical relevance during surgery of the calculated limits of CA. The variables include; time in critical region (TICR), area under the curve (AUC) of TICR, AUC of TICR < LLA, and AUC of TICR > ULA. TICR is calculated as the time during surgery spent outside the calculated limits of CA. If no CA limits could be delineated in **Chapter 5**, TICR is set to 0 under the assumption that the observed range of MAP was within the CA range. The AUC of TICR is calculated as the magnitude of time spent outside the limits of CA in [$\Delta mmHg \times seconds$]. The AUC of TICR < LLA represents the magnitude of time spent below the LLA, similarly the AUC of TICR > ULA is the magnitude of time spent above the ULA.

Separate models are constructed for the predictors TICR, AUC of TICR, AUC of TICR < LLA, and AUC of TICR > ULA.. These models were adjusted for patient sex (male/female), birth weight, CPB time, (S-)ACP + CA time, CHD group, and gestational age. An additional dichotomous variable ('TICR_NaN') was added which described whether the CA characteristics are delineated which enabled the calculation for TICR. The rationale for this was to capture the possible effect of added predictor influence of imputed CA characteristics with respect to delineated CA characteristics.

Model performance is evaluated using metrics including root-mean squared error (RMSE), R-squared, and the F-statistic. Individual predictor estimates with corresponding p-values are analyzed to assess the influence of individual predictors on the outcome.

6.2.5.1 Data Imputation

In **chapter 5** it was determined that all patient with an incomplete delineated CA curve had Mx values below the threshold of 0.45, indicating the presence of intact CA in all these patients. Therefore, in this clinical study the assumption is made that the missing CA characteristics are not due to the absence of an CA curve in these patients, but because the observed range of MAP was within the CA limits.

In order to maximize the study population used in this study, the missing CA characteristics are imputed. For imputing the CA characteristics, all 28 patients included in **Chapter 5** are utilized to maximize model input. In the case where two delineated characteristics, i.e. MAPopt and LLA or LLA, the missing CA limit is extrapolated. This is possible due to the fact that the distance in MAP from MAPopt to LLA is equal to MAPopt to ULA. This fact is implied by the delineation using an U-shaped curve, where MAPopt is exactly in the middle of the upper and lower limit. After extrapolation, a linear regression model is used to impute missing MAPopt values. The model uses the patient characteristics; birth weight, weight at surgery, gestational age, age at surgery, sex, and CHD diagnosis group, as can be found in table C. Missing ULA's are then imputed with an similar linear regression model with the addition of MAPopt as a predictor. After imputation of the missing ULA's, the missing LLA's are extrapolated as explained before, resulting in complete CA curves for every patient.

6.2.6 Statistical Analysis: CA characteristics and Outcome

In this statistical analysis, the association between the delineated CA characteristics from Chapter 5, along with the addition of imputed CA characteristics as explained earlier, and the outcome of new WMI 2D size (measured in mm) is examined. The analysis aims to determine whether patients' CA characteristics reflect their general vulnerability to acquiring new WMI.

Separate models are constructed for the predictors LLA, MAPopt, ULA, and CA Range. These models were adjusted for patient sex (male/female), birth weight, CPB time, (S-)ACP + CA time, CHD group, and gestational age. Additionally, a binary variable labeled 'imputed_true' was introduced to account for the potential influence of imputed CA characteristics on the outcome. This variable was included based on the rationale that it could capture any potential effects of imputed CA characteristics in relation to the outcome.

Model performance is evaluated using metrics including RMSE, R-squared, and the F-statistic. Individual predictor estimates with corresponding p-values are analyzed to assess the influence of individual predictors on the outcome.

6.3 Results

6.3.1 Patient Data

The CA curve was delineated for 28 patients in **Chapter 5** which are considered for this study. An overview of the delineated CA curve characteristics for each patient is provided in **Appendix D**. To reiterate, the determined CA curves of patient 5, 16, and 24, are treated as missing due to a fitting error. The outcomes measures; TICR, TICR < LLA, and TICR > ULA are set to zero for these patients under the assumption that the observed range of MAP was inside the limit of CA, causing the inability to delineate the CA characteristics.

CA delineation of patient 17 was not possible due to missing CA data acquisition and is thus excluded. Furthermore, because MRI scoring was outsourced to an independent radiologist which was not able to score all patient, the last six consecutive patients (patient 24 - 29) did not have an outcome measure. These patients are excluded in this study due to missing outcome measures. Resulting in a total of 19 patients included for this study, a summary of patient characteristics is shown in **table 3**.

Of the 19 patients with an pre- and postoperative MRI scoring, 6 (31.6%) had new WMI on the postoperative MRI with a range of 2.4 to 73.1 mm size measured on 2D slices. The CHD group TGA consisted of 3 patients with new WMI, while CHD group AoAO included 2 patients. The Other group had 1 patient with new WMI, and the SVP group had 0 patients with new WMI. An overview of the per patient intraoperative predictors and MRI scores can be found in **Appendix E**.

Table 3: Summary of Baseline Characteristics

Patient Characteristics	Overall, N = 19
Birth Weight [gr], mean (SD)	3409.5 (348.6)
Weight @ Surgery [gr], mean (SD)	3423.7 (352.1)
Gestational Age [weeks], mean (SD)	38.6 (1.0)
Age @ Surgery [days], mean (SD)	6.7 (3.2)
Male, n / N (%)	16 (78.9%)
CHD Diagnosis Group	
TGA, n / N (%)	6 (31.6%)
SVP, n / N (%)	2 (10.5%)
AoAO, n / N (%)	8 (42.1%)
Other, n / N (%)	3 (15.8%)
Surgery Group	
Arterial Switch, n/N (%)	7 (36.8%)
Aortic Arch Repair, n/N (%)	6 (31.6%)
Central Shunt +/- Atrial Septectomy, n/N (%)	2 (10.5%)

Table 3 continued from previous page

Characteristic	Overall, N = 28
Norwood I, n/N (%)	1 (5.3%)
Other, n/N (%)	2 (10.5%)
Coarctation of Aortic Arch Repair, n/N (%)	1 (5.3%)
Surgery Characteristics	
CPB Time [min], mean (SD)	148.9 (40.9)
Aristotle Score, mean (SD)	9.8 (2.4)
Aortic Clamping Time [min], n / N (%) - mean (SD)	18 (94.7%) - 94.7 (28.0)
(S-)ACP [min], n / N (%) - mean (SD)	9 (47.4.3%) - 59.3 (17.5)
Arrest Time [min], n / N (%) - mean (SD)	2 (10.5%) - 5.5 (0.7)
Cooling Temperature [°C] - mean (SD)	25.3 (4.7)
Outcome	
New WMI 2D Size [mm], mean (SD)	9.1 (19.5)

6.3.2 Association TICR with outcome

The relationship between TICR, AUC of TICR, AUC of TICR < LLA, and AUC of TICR > ULA with the 2D size of new WMI lesions was evaluated using four distinct linear regression models. The summarized model performance is presented in **Table 4**. The performance metrics suggest that these models exhibit moderate explanatory capacity, explaining approximately 75% of the variance in the outcome, albeit with results that are nearly statistically significant.

The estimated coefficients for the models can be found in **Table 5**. Notably, there is a significant negative association between the TGA group and the outcome when compared to the AoAO group. However, it's important to note that this result may be influenced by the fact that the two patients with the large 2D size of new WMI lesions (73.1 and 35.3 mm) are both in the AoAO group, which are much higher than most other patients with new WMI lesions.

Among the calculated predictors, including TICR, AUC of TICR, AUC of TICR < LLA, and AUC of TICR > ULA, none demonstrated significant predictive capability. This lack of significance may potentially be influenced by the presence of the AoAO group. Additionally, the inclusion of the variable "TICR_NaN_true", which signifies cases where TICR could not be determined due to an undelineated CA curve, also did not yield a significant effect.

6.3.3 Extrapolation and Imputation of CA characteristics

The LLA and ULA of patients with 2 delineated CA characteristics were extrapolated for 1 and 4 patients respectively. The MAPopt was imputed for 12 patients using a linear regression

Table 4: Model performances TICR

Model	RMSE	R-squared	Adj R-Squared	F-statistic	p-value
TICR	15.4	0.723	0.377	2.09	0.155
AUC TICR	15.1	0.733	0.399	2.20	0.139
AUC TICR <LLA	15.1	0.733	0.399	2.19	0.139
AUC TICR >ULA	15.4	0.723	0.376	2.08	0.155

Table 5: Estimated Coefficients TICR

TICR					AUC of TICR				
Predictor	Estimate	SE	tStat	pValue	Predictor	Estimate	SE	tStat	pValue
pat_sex (male)	11.188	10.198	1.097	0.305	pat_sex (male)	12.186	10.121	1.204	0.263
pat_birth_weight	0.005	0.011	0.420	0.686	pat_birth_weight	0.007	0.011	0.650	0.534
CPB_min	0.079	0.180	0.442	0.670	CPB_min	-0.002	0.199	-0.012	0.991
acp_ca	-0.331	0.245	-1.352	0.213	acp_ca	-0.296	0.248	-1.192	0.267
CHD_group_Other	-27.248	15.162	-1.797	0.110	CHD_group_Other	-26.543	14.912	-1.780	0.113
CHD_group_SVP	22.011	15.147	-1.453	0.184	CHD_group_SVP	-17.604	15.222	-1.157	0.281
CHD_group_TGA	-36.771	17.071	-2.154	0.063	CHD_group_TGA	-34.440	17.210	-2.001	0.080
gestational_age	-14.612	4.356	-3.355	0.010	gestational_age	-13.762	4.350	-3.164	0.013
TICR_NaN_true	-1.336	13.814	-0.097	0.925	TICR_NaN_true	-8.244	12.601	-0.654	0.531
TICR	0.036	0.296	0.123	0.905	AUCofTICR	-0.001	0.001	-0.565	0.587
AUC of TICR <LLA					AUC of TICR >ULA				
Predictor	Estimate	SE	tStat	pValue	Predictor	Estimate	SE	tStat	pValue
pat_sex (male)	17.557	15.097	1.163	0.278	pat_sex (male)	11.395	10.345	1.102	0.303
pat_birth_weight	0.001	0.012	0.112	0.914	pat_birth_weight	0.005	0.012	0.373	0.719
CPB_min	-0.005	0.203	-0.026	0.980	CPB_min	0.072	0.166	0.435	0.675
acp_ca	-0.307	0.244	-1.260	0.243	acp_ca	-0.334	0.247	-1.353	0.213
CHD_group_Other	-28.206	14.916	-1.891	0.095	CHD_group_Other	-27.496	15.190	-1.810	0.108
CHD_group_SVP	-13.828	19.230	-0.720	0.493	CHD_group_SVP	-21.246	14.035	-1.514	0.169
CHD_group_TGA	-35.574	16.874	-2.108	0.068	CHD_group_TGA	-36.978	17.548	-2.107	0.068
gestational_age	-11.827	6.339	-1.866	0.099	gestational_age	-14.452	4.266	-3.388	0.010
TICR_NaN_true	-9.616	14.740	-0.653	0.532	TICR_NaN_true	-2.271	10.268	-0.221	0.831
AUCofLLA	-0.001	0.002	-0.556	0.593	AUCofULA	0.000	0.001	0.071	0.945

model, which demonstrated a statistically significant fit (F-statistic = 7.85, $p = 0.007$), explaining a substantial portion of the variance in MAPopt ($R^2 = 0.900$). The model exhibited good accuracy, reflected by an RMSE of 3.24. Among the predictors, three showed statistical significance, ordered by increasing p-values: birth weight ($p = 0.002$), gestational age ($p = 0.004$), and weight at surgery ($p = 0.005$). Number of observations was 16 with 7 error degrees of freedom. The ULA was imputed for 13 patients using a linear regression model, presenting a statistically significant fit (F-statistic = 8.62, $p = 0.014$) that accounted for a substantial portion of the variance in ULA ($R^2 = 0.939$). The model demonstrated good accuracy, as indicated by an RMSE of 4.52. Among the predictors, MAPopt showed the highest statistical significance ($p = 0.118$), other predictors did not reach statistical significance. The model was based on 15 observations with 5 degrees of freedom for error. Lastly, the remaining 13 missing LLA's were extrapolated from corresponding MAPopt and ULA values.

Extrapolation and imputation of missing CA characteristics resulted in a mean LLA of 28.8 ± 5.5 mmHg, MAP_{opt} of 42.6 ± 8.2 mmHg, ULA of 56.3 ± 14.0 mmHg, and a Range of 27.5 ± 13 mmHg. An overview of the resulting CA characteristics can be found in **Appendix F**.

6.3.4 Association CA characteristics with outcome

The association between LLA, MAP_{opt}, ULA, and CA Range with the 2D size of new WMI lesions was examined using four distinct linear regression models. The performance of these models is summarized in **Table 6**. All four models exhibited moderate predictive capability, accounting for approximately 75% of the variance in the outcome. However, it's important to note that while the results were not statistically significant, they approached significance.

The estimated coefficients for the models are provided in **Table 7**. Similar to the TICR and AUC of TICR models, both the TGA group and gestational age exhibited a significant negative association. However, it's worth noting that this observed association could potentially be influenced by the over representation of the AoAO group concerning the outcome.

Remarkably, the variables MAP_{opt}, ULA, and Range demonstrated a nearly significant negative association with the outcome, as indicated by p-values of 0.145, 0.140, and 0.140, respectively. The estimated coefficients for these variables were -0.984, -0.529, and -0.558, respectively. The additional variable 'imputed_true' was included to account for the potential impact of CA characteristics being imputed. However, it's worth noting that this variable did not demonstrate a significant association with the outcome.

Table 6: Model performance CA characteristic

Model	RMSE	R-squared	Adj R-squared	F-statistic	p-value
LLA	15.2	0.732	0.397	2.190	0.140
MAP _{opt}	13.4	0.791	0.529	3.020	0.065
ULA	13.4	0.792	0.533	3.050	0.064
Range	13.4	0.792	0.533	3.050	0.064

6.4 Discussion

For this study, 19 patients were included, all of whom underwent both pre- and postoperative MRI scoring. Among these patients, 6 exhibited new WMI lesions after surgery. The duration of time spent outside the delineated limits of autoregulation did not emerge as a significant predictor of the size of these new WMI lesions.

In Chapter 5, our conclusion was that the inability to delineate the CA curve was due to the limited range of observed MAP values across all CHD diagnosis groups. Assuming that these

Table 7: Estimated Coefficients CA Characteristic

LLA					MAPopt				
Predictor	Estimate	SE	tStat	pValue	Predictor	Estimate	SE	tStat	pValue
pat_sex (male)	12.292	10.183	1.207	0.262	pat_sex (male)	8.198	9.049	0.906	0.391
pat_birth_weight	-0.004	0.019	-0.193	0.852	pat_birth_weight	-0.004	0.011	-0.417	0.688
CPB_min	0.089	0.159	0.559	0.592	CPB_min	0.116	0.140	0.830	0.430
acp_ca	-0.569	0.500	-1.138	0.288	acp_ca	-0.383	0.215	-1.780	0.113
CHD_group_Other	-32.444	17.539	-1.850	0.102	CHD_group_Other	-29.777	13.222	-2.252	0.054
CHD_group_SVP	-22.078	13.844	-1.595	0.150	CHD_group_SVP	-26.700	12.626	-2.115	0.067
CHD_group_TGA	-49.650	29.220	-1.699	0.128	CHD_group_TGA	-48.360	16.497	-2.932	0.019
gestational_age	-9.792	9.616	-1.018	0.338	gestational_age	-12.710	3.843	-3.307	0.011
imputed_true	-3.227	8.020	-0.402	0.698	imputed_true	-1.173	7.107	-0.165	0.873
LLA	-1.480	2.732	-0.542	0.603	MAPopt	-0.984	0.609	-1.615	0.145
ULA					Range				
Predictor	Estimate	SE	tStat	pValue	Predictor	Estimate	SE	tStat	pValue
pat_sex (male)	7.585	9.095	0.834	0.429	pat_sex (male)	7.000	9.188	0.762	0.468
pat_birth_weight	-0.002	0.010	-0.208	0.840	pat_birth_weight	0.001	0.009	0.091	0.930
CPB_min	0.113	0.139	0.812	0.440	CPB_min	0.107	0.138	0.777	0.459
acp_ca	-0.301	0.213	-1.417	0.194	acp_ca	-0.210	0.224	-0.936	0.377
CHD_group_Other	-28.138	13.097	-2.148	0.064	CHD_group_Other	-26.274	13.105	-2.005	0.080
CHD_group_SVP	-26.853	12.593	-2.132	0.065	CHD_group_SVP	-26.858	12.592	-2.133	0.065
CHD_group_TGA	-44.600	15.540	-2.870	0.021	CHD_group_TGA	-40.139	14.919	-2.690	0.027
gestational_age	-14.260	3.670	-3.885	0.005	gestational_age	-16.019	3.784	-4.233	0.003
imputed_true	-0.870	7.106	-0.122	0.906	imputed_true	-0.578	7.135	-0.081	0.937
ULA	-0.529	0.323	-1.639	0.140	Range	-0.558	0.340	-1.640	0.140

patients did possess a CA curve, we successfully imputed these missing CA characteristics. This approach maximized the available sample size for evaluating the general vulnerability to acquiring new WMI.

Despite our models demonstrating moderate predictive power for new WMI lesion size, the CA characteristics did not significantly contribute to this predictive ability. Among the significant predictors, in models including MAPopt, ULA, and Range, were gestational age and CHD group, with TGA relative to AoAO within the CHD groups. Theoretically, we expected the LLA to show the most significant predictive power for new WMI lesion size, as hyperperfusion (MAP below the LLA) is a conceivable cause of WMI. However, our results did not support this assumption. It's important to note that these results might be influenced by the relatively high impact of the CHD group, which can be attributed to the inclusion of two patients with notably higher WMI lesion size scores in the CHD AoAO group compared to the other groups. Alternatively, multicollinearity between gestational age and LLA values might be present, potentially downplaying the influence of these two predictors. However, we did not specifically analyze this, so no definitive multicollinearity can be concluded.

Bonthrone *et al.* [59] identified risk factors for the development of new WMI, with a single ventricle pathology being a notable risk in neonates with CHD. Contrasting with these findings, our results showed an association between increased WMI size and diagnoses of coarctation of the aorta and hypoplastic aortic arch. However, it is important to consider that these results

might be influenced by the small sample size of patients ($n = 6$, 31.6%) with new WMI in our study cohort.

6.5 Conclusion

In this study, we examined the possible relationship between the duration of time spent outside the delineated limits of autoregulation during surgery and new WMI lesion size. However, our results did not uncover any significant association between these variables. Furthermore, the imputed limits of autoregulation did also not exhibit substantial predictive power. To draw more definitive conclusions about the potential significance of limits of autoregulation and time spent outside these limits, we implore that further research with a larger study population is needed. Expanding the study size could provide a clearer understanding of whether there is a meaningful association between these factors and the study outcome.

7 General Discussion

This thesis presents an examination of individualized blood pressure management during neonatal cardiac surgery based on cerebral autoregulation monitoring. Our findings suggest that TCD monitoring is safe and feasible to determine personalized blood pressure goals during surgery. In **Chapter 5** we successfully demonstrated the delineation of the LLA and MAP_{opt} in 14 (50%) and 16 patients (57%) respectively. The notable variability observed in LLA and MAP_{opt} underscores the necessity of adopting an individualized approach to blood pressure management. Additionally, the data on the range of intact CA and the ULA offer new insights to clinicians, potentially enhancing their understanding and approach towards patient care.

In **Chapter 6**, we could not show a significant association between MAP outside the limits of CA and worsened outcomes. Additionally, the values of the CA characteristics did also not show general vulnerability with respect to acquiring new WMI lesions. The results of this study may be affected by the small sample size of patient who displayed new WMI lesion post surgery, only 6 out of 19 patients who had pre- and postoperative scoring, had new WMI lesions.

7.1 Limitations

In this research, the delineation of the CA curve for patients undergoing cardiac surgery with CPB was primarily based on the correlation between ABP and CBFV or rSO₂. However, it's important to acknowledge a limitation in our methodology, as we did not account for the potential influences of cooling during hypothermia and variations in PaCO₂ levels on this delineation process. Recognizing these factors as unaddressed variables underscores the need for further investigation to refine our understanding of CA in the context of neonatal cardiac surgery with CPB.

Smith *et al.* [60] conducted a research into whether hypothermia leads to impaired autoregulation. However, they were unable to provide a definitive conclusion due to the collinearity between ABP, temperature, and CA. They do emphasize the importance of obtaining a conclusive answer to the question of whether hypothermia affects CA before implementing clinical monitoring of CA. This is essential to prevent the determination of an optimal blood pressure range that does not accurately reflect the normothermic physiological state. In the studies conducted for this thesis we did not account for temperature on the delineation process which is a limitation and may have influenced results. A more recent study by Finnigan *et al.* [61], the impact of cooling during aortic arch repairs with cardiopulmonary bypass was examined, revealing a significant increase of 10 cm/s in CBFV compared to normothermia. This finding underscores the need to further explore how hypothermia affects CA and influences the delineation of CA curves used to establish optimal blood pressure ranges. Moving forward,

future research should continue to investigate the complex interplay between hypothermia and CA, aiming to enhance our understanding of this relationship and pave the way for clinical applications.

Additionally, PaCO₂ is the most potent regulator of CBF where even small variation can result in large changes in CBF. Although this vasodilatory effect is well established, the translation to CA and delineation of the CA curve is not well established. A review from 2015 Meng & Gelb [62] investigated the effect of PaCO₂ and perfusion pressures on CA from based on published large animal and human data studies with some speculation. This review showed that during hypercapnia, the CBF is increased and the range of intact CA is shortened, which means a rightward shift of the LLA and a leftward shift of the ULA. During hypocapnia the CBF is reduced and the LLA remains unchanged. The impact of PaCO₂ on the ULA remains unknown. It's crucial to investigate whether these findings are applicable to the developing brains of neonates with CHD. Future studies should focus on understanding how arterial CO₂ levels influences not only CBF but especially the CA curve within this specific population.

7.2 Clinical Implications

Although we were not able to demonstrate significance of using delineated CA characteristics for blood pressure management related to new WMI lesions after surgery, the high variance of LLA and MAPopt already offer valuable information for clinicians. Clinicians should be alerted about the variance in MAP ranges best supporting CA, and thus the use of gestational age as a one-size-fits-all approach to blood pressure managing. Off course clinicians also use additional monitors to monitor cerebral perfusion such as the commonly used NIRS monitors, which is standard clinical care in the WKZ as well as in 80% of European hospitals [63]. However, while NIRS is a valuable tool to monitor intraoperative changes, current publications raised concerns about the reliability of NIRS monitoring. Zaleski & Kussman [64] underlined the limitations regarding NIRS with regard to the normative and critical values related to outcome. Moreover, in a recent study by Iliopoulos *et al.* [52], it was found that two advanced NIRS monitors exhibited only moderate agreement with each other. This finding raises significant concerns regarding the applicability of normative and critical rSO₂ values across different medical centers.

A multi-modal approach, which better reflects the patient's physiological state, can be achieved by incorporating TCD monitoring during high-risk procedures for neonates with CHD. In addition to its use in CA monitoring, TCD monitoring offers additional functionality. It offers a non-invasive bedside approach for air emboli detection [65], and may also be valuable for emboli detection during cannulation for CPB in neonatal cardiac surgery. Moreover, during (S-)ACP, TCD provides real-time insights into CBF when the arterial cannula is inserted into the carotid artery, aiding in achieving optimal cannula placement.

7.3 Future Recommendations

This research has provided starting evidence that individualized pressure management may be beneficial in neonates with CHD, and may ultimately aid in preventing brain damage acquired during surgery. Some hurdles have to be overcome before clinical implementation, which I will discuss my view on this shortly.

First of all, we have shown that delineation of the CA curve in neonatal cardiac surgery is feasible, whether the limits of CA may be used to prevent new brain lesions has still to be determined. Future studies should evaluate with larger study population if the association between time spent outside the limits of autoregulation are associated with worsened outcome. If so, this provides evidence that the delineated limits of autoregulation are clinically relevant and may be used as a substitution for traditional blood pressure goals.

However, assuming that personalized delineated LLA or MAPopt are preferred over gestational age, we run into a technical problem. As currently, data is collected during the whole surgery, and is analysed after the fact. Future studies should be performed researching how long it takes to delineate a first LLA or MAPopt and whether this is reliable. Iller *et al.* [41] showed in their study in infant during major non-cardiac surgery that the time to first reliable MAPopt was 18 ± 3 minutes, and was influenced by the amount of fluctuations in MAP. Similar studies in neonatal cardiac surgery are needed to point out if an LLA or MAPopt can be determined in a manner that is clinically usable for the remaining of the procedure.

However, if we consider that personalized delineated LLA or Mean Arterial Pressure at MAPopt as preferable blood pressure target over gestational age, a technical challenge arises. Currently, data is collected throughout the entire surgery and analyzed retrospectively. To address this, future studies should investigate how long it takes to delineate the first reliable LLA or MAPopt. An example provided by Iller *et al.* [41] in infants undergoing major non-cardiac surgery revealed that the time required to establish the first reliable MAPopt was 18 ± 3 minutes. They point out that the duration for first delineation was influenced by fluctuations in MAP. Similar investigations in neonatal cardiac surgery are essential to determine whether LLA or MAPopt can be reliably determined and applied in a clinically practical manner for the remainder of the procedure.

Only after addressing these challenges can we progress toward a non-blinded randomized control trial that will provide insights into the effectiveness of personalized blood pressure targets based on TCD-based CA monitoring. In this proposed randomized control trial, one group of neonates would receive care based on their gestational age, while the other group would be guided by personalized blood pressure targets determined through TCD-based CA monitoring. This pivotal trial will not only help establish the clinical relevance and superiority of personalized targets over gestational age but also pave the way for broader clinical implementation.

7.4 Conclusion

This thesis aimed to explore the feasibility and potential of individualized blood pressure management in neonatal cardiac surgery, utilizing CA monitoring. The results revealed significant variability in LLA and MAPopt, suggesting that currently used blood pressure targets are not adequate for all neonates with CHD.

Despite the study's limitations, such as the small sample size and the absence of accounting for factors like hypothermia and PaCO₂ levels, the research has laid the groundwork for future studies. These studies should focus on the interaction between these variables and CA, refining the understanding of CA in neonatal cardiac surgery with CPB.

To conclude, it is evident that while the direct association of CA parameters with neurological outcomes like new WMI lesions post-surgery is not definitively established, the study's insights into the variability of delineated CA characteristics are valuable. They provide a new perspective on managing blood pressure in neonates undergoing cardiac surgery, advocating for a personalized approach based on individual CA characteristics.

Future research should aim to overcome the current study's limitations, expand the sample size, and incorporate a broader range of variables to validate the clinical relevance of CA monitoring in this vulnerable patient population. The ultimate goal remains to enhance the care and outcomes of these vulnerable neonates, steering towards a future where precision medicine plays a pivotal role in pediatric cardiac surgery.

References

1. Hoffman, J. I. & Kaplan, S. The incidence of congenital heart disease. *Journal of the American College of Cardiology* **39**, 1890–1900. ISSN: 07351097 (June 2002).
2. Moons, P., Bovijn, L., Budts, W., Belmans, A. & Gewillig, M. Temporal trends in survival to adulthood among patients born with congenital heart disease from 1970 to 1992 in Belgium. *Circulation* **122**, 2264–2272. ISSN: 1524-4539 (Nov. 2010).
3. Mandalenakis, Z. *et al.* Survivorship in Children and Young Adults With Congenital Heart Disease in Sweden. *JAMA internal medicine* **177**, 224–230. ISSN: 2168-6114 (Feb. 2017).
4. Lynch, J. M. *et al.* Time to surgery and preoperative cerebral hemodynamics predict postoperative white matter injury in neonates with hypoplastic left heart syndrome. *The Journal of thoracic and cardiovascular surgery* **148**, 2181–2188. ISSN: 1097-685X (Nov. 2014).
5. Miller, S. P. *et al.* Abnormal brain development in newborns with congenital heart disease. *The New England journal of medicine* **357**, 1928–1938. ISSN: 1533-4406 (Nov. 2007).
6. Stegeman, R. *et al.* A Uniform Description of Perioperative Brain MRI Findings in Infants with Severe Congenital Heart Disease: Results of a European Collaboration. *AJNR. American journal of neuroradiology* **42**. ISSN: 1936-959X (Nov. 2021).
7. Levene, M. I. Development of audit measures and guidelines for good practice in the management of neonatal respiratory distress syndrome. Report of a Joint Working Group of the British Association of Perinatal Medicine and the Research Unit of the Royal College of Physicians. *Archives of disease in childhood* **67**, 1221–1227. ISSN: 1468-2044 (1992).
8. Dempsey, E. M. & Barrington, K. J. Diagnostic criteria and therapeutic interventions for the hypotensive very low birth weight infant. *Journal of perinatology : official journal of the California Perinatal Association* **26**, 677–681. ISSN: 0743-8346 (Nov. 2006).
9. Rhee, C. J. *et al.* Neonatal cerebrovascular autoregulation. *Pediatric research* **84**, 602. ISSN: 15300447 (Nov. 2018).
10. Brown, C. H. *et al.* Effect of Targeting Mean Arterial Pressure During Cardiopulmonary Bypass by Monitoring Cerebral Autoregulation on Postsurgical Delirium Among Older Patients: A Nested Randomized Clinical Trial. *JAMA surgery* **154**, 819–826. ISSN: 2168-6262 (Sept. 2019).
11. Hogue, C. W. *et al.* Personalized Blood Pressure Management During Cardiac Surgery With Cerebral Autoregulation Monitoring: A Randomized Trial. *Seminars in Thoracic and Cardiovascular Surgery* **33**, 429–438. ISSN: 1043-0679 (June 2021).
12. Lugthart, M. A. *et al.* Early Detection of Isolated Severe Congenital Heart Defects Is Associated with a Lower Threshold to Terminate the Pregnancy. *Fetal diagnosis and therapy* **50**, 248–258. ISSN: 1421-9964 (Oct. 2023).

13. Gaynor, J. W. *et al.* Apolipoprotein E genotype and neurodevelopmental sequelae of infant cardiac surgery. *The Journal of thoracic and cardiovascular surgery* **126**, 1736–1745. ISSN: 0022-5223 (2003).
14. Mahle, W. T., Clancy, R. R., McGaurn, S. P., Goin, J. E. & Clark, B. J. Impact of prenatal diagnosis on survival and early neurologic morbidity in neonates with the hypoplastic left heart syndrome. *Pediatrics* **107**, 1277–1282. ISSN: 1098-4275 (2001).
15. Forbess, J. M. *et al.* Neurodevelopmental Outcome After Congenital Heart Surgery: Results From an Institutional Registry. *Circulation* **106**. ISSN: 00097322 (Sept. 2002).
16. Bellinger, D. C. *et al.* Developmental and neurological status of children at 4 years of age after heart surgery with hypothermic circulatory arrest or low-flow cardiopulmonary bypass. *Circulation* **100**, 526–532. ISSN: 1524-4539 (Aug. 1999).
17. Bellinger, D. C. *et al.* Neurodevelopmental status at eight years in children with dextro-transposition of the great arteries: The Boston Circulatory Arrest Trial. *The Journal of Thoracic and Cardiovascular Surgery* **126**, 1385–1396. ISSN: 0022-5223 (Nov. 2003).
18. Gaynor, J. W. *et al.* Increasing duration of deep hypothermic circulatory arrest is associated with an increased incidence of postoperative electroencephalographic seizures. *The Journal of thoracic and cardiovascular surgery* **130**, 1278–1286. ISSN: 1097-685X (Nov. 2005).
19. Hoffman, T. M. *et al.* Efficacy and safety of milrinone in preventing low cardiac output syndrome in infants and children after corrective surgery for congenital heart disease. *Circulation* **107**, 996–1002. ISSN: 1524-4539 (Feb. 2003).
20. Licht, D. J. *et al.* Preoperative cerebral blood flow is diminished in neonates with severe congenital heart defects. *The Journal of thoracic and cardiovascular surgery* **128**, 841–849. ISSN: 0022-5223 (Dec. 2004).
21. Newburger, J. W. *et al.* Length of stay after infant heart surgery is related to cognitive outcome at age 8 years. *The Journal of pediatrics* **143**, 67–73. ISSN: 0022-3476 (July 2003).
22. Wernovsky, G. *et al.* Cognitive development after the Fontan operation. *Circulation* **102**, 883–889. ISSN: 1524-4539 (Aug. 2000).
23. LASSEN, N. A. Cerebral blood flow and oxygen consumption in man. *Physiological reviews* **39**, 183–238. ISSN: 0031-9333 (Apr. 1959).
24. Rivera-Lara, L. *et al.* Cerebral Autoregulation-oriented Therapy at the Bedside: A Comprehensive Review. *Anesthesiology* **126**, 1187–1199. ISSN: 1528-1175 (2017).
25. Rangel-Castilla, L., Gasco, J., Nauta, H. J., Okonkwo, D. O. & Robertson, C. S. Cerebral pressure autoregulation in traumatic brain injury. *Neurosurgical focus* **25**. ISSN: 1092-0684 (2008).
26. Claassen, J. A., Thijssen, D. H., Panerai, R. B. & Faraci, F. M. Regulation of cerebral blood flow in humans: physiology and clinical implications of autoregulation. *Physiological Reviews* **101**, 1487. ISSN: 15221210 (Oct. 2021).

27. Panerai, R. B. The critical closing pressure of the cerebral circulation. *Medical Engineering and Physics* **25**, 621–632. ISSN: 13504533 (2003).
28. Ainslie, P. N., Wilson, M. H. & Imray, C. H. Cerebral circulation and brain. *High Altitude: Human Adaptation to Hypoxia*, 141–170 (July 2013).
29. Licht, D. J. *et al.* Brain maturation is delayed in infants with complex congenital heart defects. *The Journal of thoracic and cardiovascular surgery* **137**, 529. ISSN: 00225223 (Mar. 2009).
30. Howlett, J. A. *et al.* Cerebrovascular autoregulation and neurologic injury in neonatal hypoxic-ischemic encephalopathy. *Pediatric research* **74**, 525–535. ISSN: 1530-0447 (Nov. 2013).
31. Lee, J. K. *et al.* Optimizing Cerebral Autoregulation May Decrease Neonatal Regional Hypoxic-Ischemic Brain Injury. *Developmental neuroscience* **39**, 248–256. ISSN: 1421-9859 (July 2017).
32. Carrasco, M. *et al.* Cerebral Autoregulation and Conventional and Diffusion Tensor Imaging Magnetic Resonance Imaging in Neonatal Hypoxic-Ischemic Encephalopathy. *Pediatric neurology* **82**, 36–43. ISSN: 1873-5150 (May 2018).
33. Brady, K. M. *et al.* Continuous time-domain analysis of cerebrovascular autoregulation using near-infrared spectroscopy. *Stroke* **38**, 2818–2825. ISSN: 1524-4628 (Oct. 2007).
34. Steiner, L. A. *et al.* Continuous monitoring of cerebrovascular pressure reactivity allows determination of optimal cerebral perfusion pressure in patients with traumatic brain injury. *Critical care medicine* **30**, 733–738. ISSN: 0090-3493 (2002).
35. Lee, J. K. *et al.* A pilot study of cerebrovascular reactivity autoregulation after pediatric cardiac arrest. *Resuscitation* **85**, 1387–1393. ISSN: 1873-1570 (Oct. 2014).
36. Lewis, P. M. *et al.* Cerebrovascular Pressure Reactivity in Children With Traumatic Brain Injury. *Pediatric critical care medicine : a journal of the Society of Critical Care Medicine and the World Federation of Pediatric Intensive and Critical Care Societies* **16**, 739–745. ISSN: 1529-7535 (Nov. 2015).
37. Spilka, J. M., O’Halloran, C. P., Marino, B. S. & Brady, K. M. Perspective on Cerebral Autoregulation Monitoring in Neonatal Cardiac Surgery Requiring Cardiopulmonary Bypass. *Frontiers in Neurology* **12**, 1788. ISSN: 16642295 (Oct. 2021).
38. Hlatky, R., Valadka, A. B. & Robertson, C. S. Analysis of dynamic autoregulation assessed by the cuff deflation method. *Neurocritical care* **4**, 127–132. ISSN: 1541-6933 (2006).
39. Aaslid, R., Markwalder, T. M. & Nornes, H. Noninvasive transcranial Doppler ultrasound recording of flow velocity in basal cerebral arteries. *Journal of neurosurgery* **57**, 769–774. ISSN: 0022-3085 (1982).
40. Czosnyka, M., Smielewski, P., Kirkpatrick, P., Menon, D. K. & Pickard, J. D. Monitoring of cerebral autoregulation in head-injured patients. *Stroke* **27**, 1829–1834. ISSN: 0039-2499 (1996).

41. Iller, M. *et al.* Intraoperative monitoring of cerebrovascular autoregulation in infants and toddlers receiving major elective surgery to determine the individually optimal blood pressure – a pilot study. *Frontiers in Pediatrics* **11**. ISSN: 2296-2360 (Feb. 2023).
42. Lee, J. K. *et al.* Cerebrovascular reactivity measured by near-infrared spectroscopy. *Stroke* **40**, 1820–1826. ISSN: 1524-4628 (May 2009).
43. Jöbsis, F. F. *Noninvasive, Infrared Monitoring of Cerebral and Myocardial Oxygen Sufficiency and Circulatory Parameters* tech. rep. (1977), 1264–1267.
44. Vretzakis, G. *et al.* *Cerebral oximetry in cardiac anesthesia* 2014.
45. Mohammadi-Nejad, A. R. *et al.* *Neonatal brain resting-state functional connectivity imaging modalities* June 2018.
46. Steiner, L. A. *et al.* Near-infrared spectroscopy can monitor dynamic cerebral autoregulation in adults. *Neurocritical Care* **10**, 122–128. ISSN: 15416933 (Feb. 2009).
47. Czosnyka, M., Brady, K., Reinhard, M., Smielewski, P. & Steiner, L. A. Monitoring of cerebrovascular autoregulation: facts, myths, and missing links. *Neurocritical care* **10**, 373–386. ISSN: 1541-6933 (June 2009).
48. Czosnyka, M. *et al.* Continuous assessment of the cerebral vasomotor reactivity in head injury. *Neurosurgery* **41**, 11–19. ISSN: 0148-396X (July 1997).
49. LUNDBERG, N. Continuous recording and control of ventricular fluid pressure in neurosurgical practice. *Volume 36, Issue 149, Pages 1 - 193* **36**, 1–193. ISSN: 00651591 (1960).
50. Steinmeier, R. *et al.* Slow rhythmic oscillations of blood pressure, intracranial pressure, microcirculation, and cerebral oxygenation. Dynamic interrelation and time course in humans. *Stroke* **27**, 2236–2243. ISSN: 0039-2499 (1996).
51. Zipfel, J. *et al.* Identifying the optimal blood pressure for cerebral autoregulation in infants after cardiac surgery by monitoring cerebrovascular reactivity—A pilot study. *Paediatric Anaesthesia* **32**, 1320–1329. ISSN: 14609592 (Dec. 2022).
52. Iliopoulos, I. *et al.* Absolute Versus Relative Near-Infrared Spectroscopy in Pediatric Cardiac Patients. *Pediatric Critical Care Medicine* **24**, 204–212. ISSN: 19473893 (Mar. 2023).
53. Rivera-Lara, L. *et al.* Determining the upper and lower limits of cerebral autoregulation with cerebral oximetry autoregulation curves: A case series. *Critical Care Medicine* **46**, e473–e477. ISSN: 15300293 (May 2018).
54. Liu, X. *et al.* Determining Thresholds for Three Indices of Autoregulation to Identify the Lower Limit of Autoregulation during Cardiac Surgery. *Critical Care Medicine*, 650–660. ISSN: 15300293 (2021).
55. Donnelly, J. *et al.* Individualising thresholds of cerebral perfusion pressure using estimated limits of autoregulation. *Critical care medicine* **45**, 1464. ISSN: 15300293 (Sept. 2017).

56. Aries, M. J. *et al.* Continuous determination of optimal cerebral perfusion pressure in traumatic brain injury. *Critical care medicine* **40**, 2456–2463. ISSN: 1530-0293 (Aug. 2012).
57. Liu, X. *et al.* Comparison of different metrics of cerebral autoregulation in association with major morbidity and mortality after cardiac surgery. *British Journal of Anaesthesia* **129**, 22–32. ISSN: 14716771 (July 2022).
58. Liu, X. *et al.* Comparison of wavelet and correlation indices of cerebral autoregulation in a pediatric swine model of cardiac arrest. *Scientific Reports 2021 10:1* **10**, 1–9. ISSN: 2045-2322 (Apr. 2020).
59. Bonthron, A. F. *et al.* Risk Factors for Perioperative Brain Lesions in Infants With Congenital Heart Disease: A European Collaboration. *Stroke* **53**, 3652–3661. ISSN: 15244628 (Dec. 2022).
60. Smith, B. *et al.* Does hypothermia impair cerebrovascular autoregulation in neonates during cardiopulmonary bypass? *Paediatric Anaesthesia* **27**, 905–910. ISSN: 14609592 (Sept. 2017).
61. Finnigan, L. E., Lotto, R., Jones, H. & Lotto, A. Cerebral blood flow velocity and oxygenation in neonatal aortic arch repair at two perfusion temperatures. *European Journal of Cardio-thoracic Surgery* **63**. ISSN: 1873734X (June 2023).
62. Meng, L. & Gelb, A. W. Regulation of cerebral autoregulation by carbon dioxide. *Anesthesiology* **122**, 196–205. ISSN: 1528-1175 (2015).
63. Feldmann, M. *et al.* Neuromonitoring, neuroimaging, and neurodevelopmental follow-up practices in neonatal congenital heart disease: a European survey. *Pediatric Research 2022 93:1* **93**, 168–175. ISSN: 1530-0447 (Apr. 2022).
64. Zaleski, K. L. & Kussman, B. D. Near-Infrared Spectroscopy in Pediatric Congenital Heart Disease. *Journal of Cardiothoracic and Vascular Anesthesia* **34**, 489–500. ISSN: 1053-0770 (Feb. 2020).
65. Kussman, B. D., Imaduddin, S. M., Gharedaghi, M. H., Heldt, T. & Larovere, K. Cerebral Emboli Monitoring Using Transcranial Doppler Ultrasonography in Adults and Children: A Review of the Current Technology and Clinical Applications in the Perioperative and Intensive Care Setting. *Anesthesia and Analgesia* **133**, 379–392. ISSN: 15267598 (Aug. 2021).

Appendix A TCD Protocol

Concept

SOP

Neonatal monitoring with Transcranial Doppler WKZ

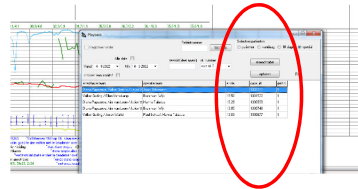
TCD meetprotocol FLOWER studie

Auteurs: K. (Kim) van Loon [kinderanesthesioloog], D. (Daniël) van Vriesland [PA Klinische neurofysiologie], E. (Ella) Fonteyn [neuroloog, klinisch neurofysioloog], A. (Anja) Ezendam [KNF laborant TCD]



Divisie Vitale Functies

2. Meetschema



Dag -1

MRI &/ echo cerebrum (CUS)
NIRS, EEG volgens LifeSpan protocol.

Dag 0 (operatie)

- 7:20-7:45 uur Openen BedBase file met BESTANDSNAAM: [Anstat case_id] .flower.bed
Pre-TCD meting bdz [duur 10 min] Openen DopplerBox file met BESTANDSNAAM: [Anstat case_id] .flower.box
Positioneren van zwarte fixatie ring
Notitie: intubatie ja/nee, reactief ja/nee, vitale parameters: iabp? nibd? spO2 preductaal? EtCO2? Hartfreq? Nirs L/R?
Afkoppelen probes
- 7:45-8:15 uur Installeren Doppler op OK 6, aansluiting Philips monitor en opstarten Bedbase
- 8:05 uur Transport naar OK door anesthesieteam
- 8:20 uur Start monitoring anesthesie OK 6. Aansluiten TCD. Start TCD Metingen
Check schrijven data naar BedBase (IABP vanuit Philips, flow velocity TCD)
- ±9:20 uur Start chirurgie / Openen Sternum
- ±9:50 uur Canulatie Aorta
- ±10:00 uur Start Bypass. Start koelen naar 'xx' graden Celcius.
- ±10:10 uur Sluiten ductus arteriosus
- ±10:30 uur Snugger vena cava superior
Plaatsen Aortacanule
Start cardioplegie. Totale bypass
- ±10:40 Start antegrade cerebrale perfusie (ACP) met "xx" % totale flow op de Tr. Brachiocephalica
In uitzonderlijke gevallen: Totaal circulatoir arrest ("stil staan bij 20 gr°C") [tijdelijke stop TCD metingen]
- ± 11:10 Stop ACP, start opwarmen naar "xx" gradenCelcius
- ± 12:00 Volledig opwarmen
- ± 12:30 uur Aortaklem los. Partiele bypass.
- ± 13:00 uur Afkomen van de bypass. Openen van eventuele shunt naar longen.

- ± 14:00 uur Einde ingreep. Transport naar PICU. Losmaken probes inclusief zwarte ring.
Controleer op drukplekken en evt. roodheid
- ± 15:30 uur Nameting TCD. Aanbrengen probes. [duur 10 min]
Notitie: intubatie ja/nee, reactief ja/nee, vitale parameters: iabp? nibd? spO2? EtCO2?
Hartfreq? Nirs L/R?

Dag +1 (eerste postoperatieve dag)

- 8:00- 16:00 Nameting eerste postoperatieve dag. TCD [duur 10 min]
Notitie: intubatie ja/nee, reactief ja/nee, vitale parameters: iabp? nibd? spO2? EtCO2?
Hartfreq? Nirs L/R?

3. Aanbrengen adhesive pads en probe positioneren

Positionering 2 MHz TCD probes temporaal

2 MHz GROEN – probe wordt gepositioneerd aan **LINKER** zijde

2 MHz ROOD – probe voor **RECHTER** zijde

1. Haal de probe door de kleine zwarte ring, de witte fixeer-ring en draai-dop.
 2. Zoek met de probe naar het juiste temporale venster. Gebruik evt. een huidstift om de positie op de huid te markeren.
 3. Reinig de huid rondom met alcohol en laat drogen.
 4. Fixeer de grote zwarte ring op de huid met de grote ronde kleefpleister (Art-No 3319) **Foto 1**
 5. Breng een hoeveelheid gel aan in de ring op de probe/huid.
 6. Fixeer de kleine zwarte ring over de probe met de witte fixeer-ring. **Foto 2**
 7. Draai de draai-dop gedeeltelijk aan en ga op zoek naar het venster en fixeer.
- Herhaal bovenstaande stappen voor de andere zijde. **(Foto 3)**
 - Tijdens transport en manipulatie van het hoofd, worden de probes verwijderd door de kleine zwarte fixeer ring los te maken. De grote fixeerring en pleisters blijven op de huid aanwezig.

Foto 1



Foto 2



4. Gebruik DopplerBox

Voor gebruik DopplerBox: Nederlandse gebruiksaanwijzing Doppler-Box X

Verwachte range van instellingen voor verkrijgen van een optimaal signaal. **Foto 4**

PW- (pulse wave) modus (de dopplershift informatie komt alleen uit het gebied van het meetvolume op de ingestelde diepte)

DEPTH 25-35 mm

POWER 50-90 mW/cm²

Volg het ALARA principe – Zorg voor een zo laag mogelijke ultrasonische belasting.

Hanteer een maximale intensiteit van 94 mW/cm²

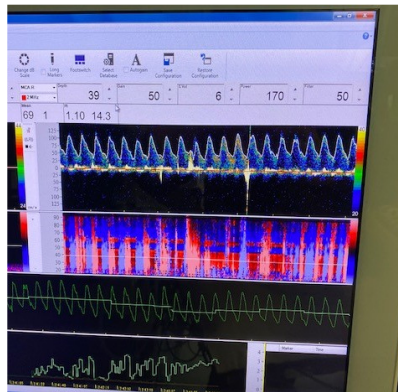
Let op! in de taakbalk (onderaan het TCD scherm) staat de TI waarde vermeld voor beide probes.

De TI waarde dient lager te zijn dan 0,7, en nooit langer dan 30 minuten tussen de 0,7-1,0.

Foto 3



Foto 4



6. Acties en handelingen n.a.v. afwijkende bevindingen tijdens TCD studiemetingen

Dit onderzoek is in opzet een observationele studie van de cerebrale blood flow velocity in de a. cerebri media links en rechts. Tijdens transcraniële dopplermetingen kan een afwijkende flow velocity-patroon worden gedetecteerd.

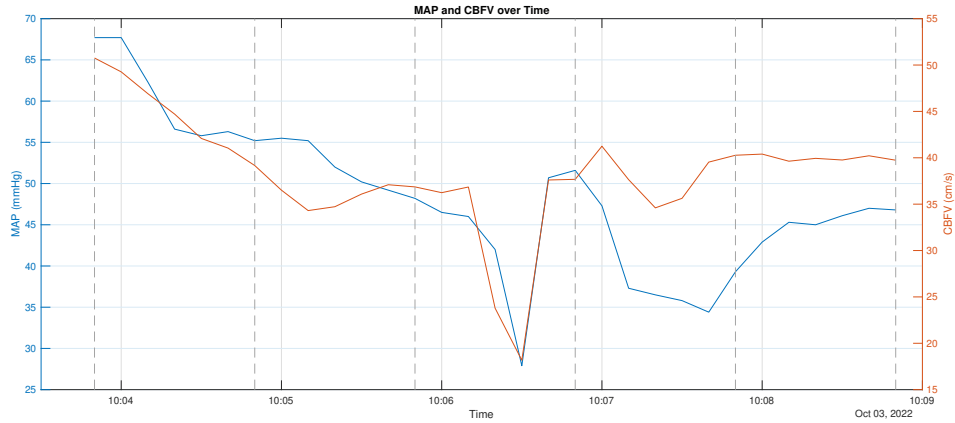
Alleen in de volgende situaties zal de KNF laborant verantwoordelijk voor de TCD studiemetingen melding maken aan het medische team (chirurg / perfusie / anesthesioloog):

1. Grote hoeveelheid achtereenvolgende gasvormige embolieën. Een enkele luchtembolie wordt verwacht en niet gemeld. Emboliën ofwel "High Intensity Transient Signals (HITS)" kunnen ook voorkomen als "shower". Het gaat dan om een dicht opeenvolgende hoeveelheid HITS. Deze laatste categorie wordt direct gemeld aan het behandelteam.
2. Cerebrale Blood Flow- Velocity (CBF-V) = 0 gedurende > 2 minuten.
 - a. *Na detectie van een CBF-V = 0 wordt gecontroleerd op aanwezigheid van technische problemen of een chirurgische verklaring en wordt deze genoteerd.*
 - b. *Indien een afwezige CBF-V langer dan 2 minuten aanhoudt zonder technische verklaring wordt het verantwoordelijke team op de hoogte gesteld van deze bevinding.*
 - c. *Het medisch team (kinderhartchirurgie / anesthesioloog) zijn verantwoordelijk voor de evaluatie en besluitvorming nadien*
3. Afwijkende CBF-V-patronen tijdens aortacaneleplaatsing en positiewisselingen. Alle afwijkingen worden direct gemeld aan de kinderhartchirurg.

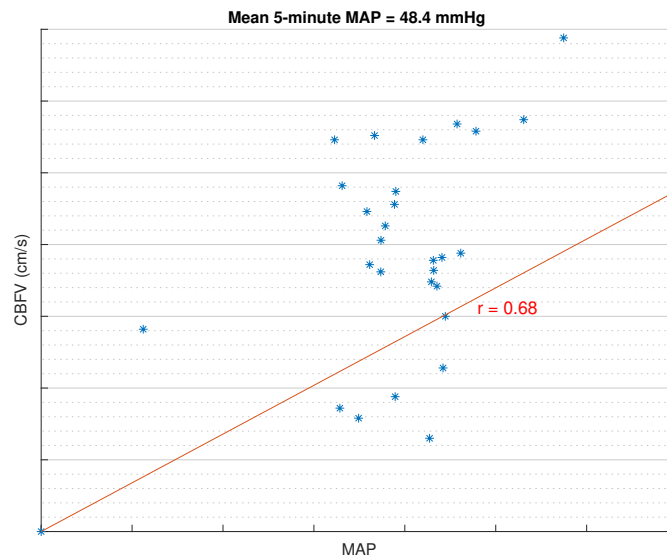
7. Reinigen en desinfecteren van de probes

Probes en fixeerringen worden na toepassing gereinigd middels de bijgeleverde echo desinfectie gevolgd door een eenmalige reiniging met alcoholgaasje. Probes mogen niet worden ongedompeld in alcohol.

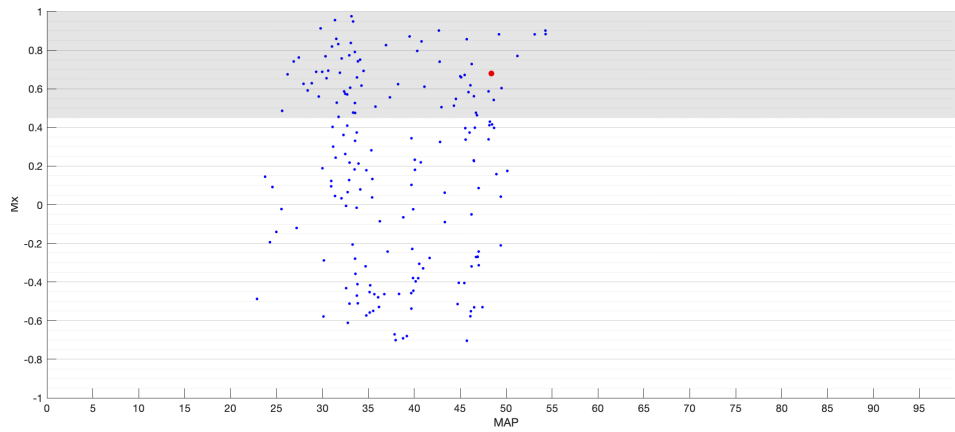
Appendix B Stepwise Delineation CA Curve



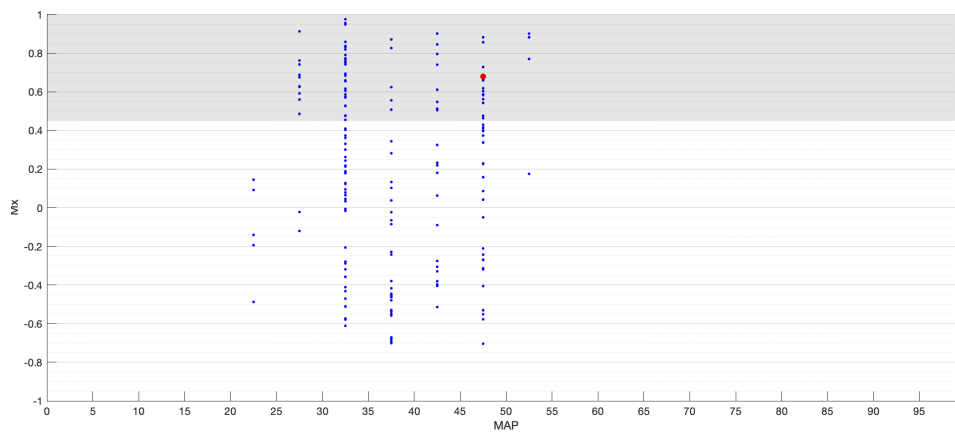
Step 1: A 5-minute period of paired 10-second mean CBFV and MAP values is selected.



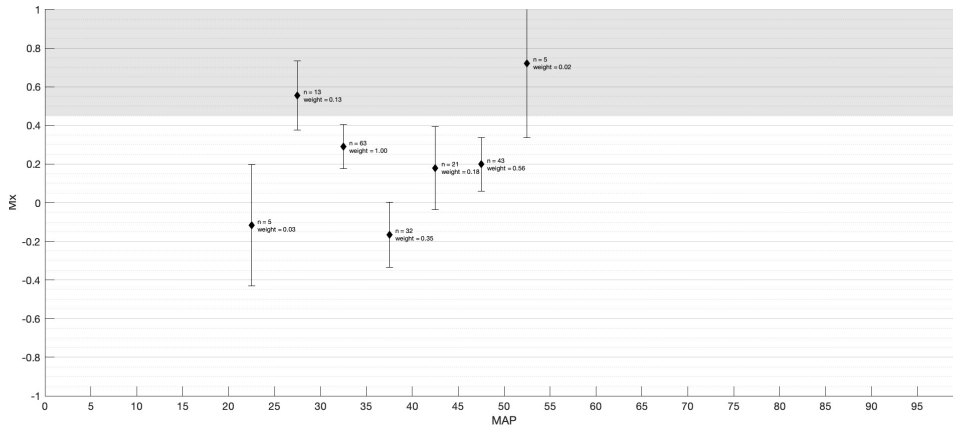
Step 2: The Pearson correlation coefficient ($r = 0.68$) is calculated of the 5-minute period, alongside with the mean of the 10-second mean MAP values (mean 5-minute MAP = 48.8). This is repeated after every 60 seconds, using paired CBFV and MAP 10-second mean values from the preceding 5-minute period. This is continued until the entire surgery period is analyzed.



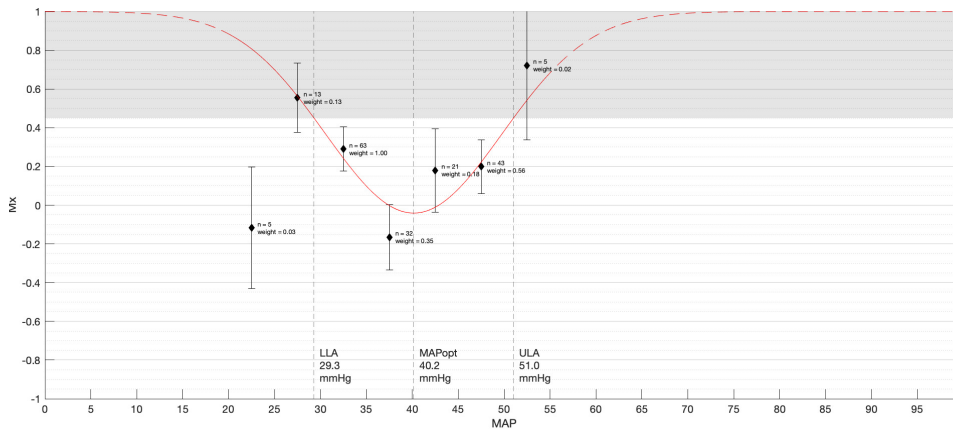
Step 3: The calculated Pearson correlation coefficients are plotted at the corresponding 5-minute mean MAP in a point cloud.



Step 4: The point cloud is grouped into 5 mmHg bins.



Step 5: The mean and 95% confidence interval of all bins are calculated and plotted.



Step 6: The U-shaped curve is fitted to the binned mean CA index values, incorporating a weighting function that considers both the number of Pearson correlation coefficients and the 95% confidence intervals. Subsequently, the LLA and ULA are delineated if the fitted curve crosses the threshold value of the CA index within the observed range of MAP bins. Similarly, the MAPopt is delineated if the minimum of the fitted curve falls within the observed range of MAP.

Appendix C Overview Per Patient Baseline Characteristics

Table 8: Patient characteristics

Patient no.	Birthweight [g]	Weight @ Surgery [g]	Gestational Age [weeks]	Age @ Surgery [days]	Sex [Male/Female]	CHD Diagnosis Group	Surgery Group	CPB Time [min]	Aortic Clamping Time [min]	(S)/ACP Time [min]	Arrest Time [min]	Cooling Temperature [°C]
1	3200	3300	36	7	M	Other (TGA, PA)	Central Shunt +/- Atrial Septectomy	63	0	0	0	35
2	3680	3700	38	5	M	TGA	Arterial switch	190	128	0	0	28
3	2828	2800	39	5	M	TGA	Arterial switch	136	115	0	0	28
4	3758	3700	39	6	F	Other (Truncus Arteriosus)	Other	112	90	0	0	28
5	3465	3500	40	10	M	AoAO (CoA / Hypoplastic AoA)	Aortic arch repair	160	107	68	6	20
6	3200	3050	40	13	M	AoAO (HLHC, CoA / Hypoplastic AoA)	Aortic arch repair	93	56	38	0	25
7	3760	3800	38	4	M	TGA	Arterial switch	124	80	0	0	28
8	3200	3200	39	5	M	Other (Truncus Arteriosus)	Other	147	112	0	0	28
9	3000	3100	38	6	M	AoAO (CoA / Hypoplastic AoA)	CoA repair	109	53	36	0	20
10	3000	3000	39	5	F	AoAO (HLHC, CoA / Hypoplastic AoA)	Aortic arch repair	114	47	34	0	20
11	3128	3100	37	5	M	AoAO (CoA / Hypoplastic AoA)	Aortic arch repair	166	80	39	0	18
12	4620	4700	39	8	F	AoAO (CoA / Hypoplastic AoA)	Aortic arch repair	193	98	65	0	20
13	2880	2800	39	6	M	AoAO (CoA / Hypoplastic AoA)	Aortic arch repair	106	75	0	0	32
14	2050	2100	38	16	F	TGA	Central Shunt +/- Atrial Septectomy	142	93	0	0	28
15	3475	3500	39	4	F	SVP (Other-UVH)	Arterial switch	151	71	57	0	25
16	4260	4200	40	6	M	TGA	Arterial switch	167	121	0	0	28
17*												
18	3165	3400	38	16	M	AoAO (CoA / Hypoplastic AoA)	Aortic arch repair	192	96	82	0	20
19	3500	3600	39	6	F	AoAO (CoA / Hypoplastic AoA)	Aortic arch repair	157	70	46	0	20
20	3500	3400	38	5	M	TGA	Arterial switch	180	122	0	0	28
21	3200	3200	38	9	M	SVP (Other-UVH)	Norwood I	215	127	108	5	20
22	3010	3600	39	5	M	TGA	Arterial switch	175	126	0	0	28
23	3800	3900	39	4	M	TGA	Arterial switch	179	125	0	0	28
24	3738	3700	39	6	M	Other	Central Shunt +/- Atrial Septectomy	56	0	0	0	34
25	4155	4100	38	8	F	SVP (HLHS)	Norwood I	147	102	51	7	20
26	2750	2600	36	8	M	SVP (Other-UVH)	Other	122	79	0	0	28
27	3500	3500	38	4	M	TGA	Arterial switch	147	101	0	0	30
28	3685	3700	38	5	M	TGA	Arterial switch	174	116	0	0	30
29	3000	2900	39	7	M	SVP (Other-UVH)	Central Shunt +/- Atrial Septectomy	59	0	0	0	34
Mean	3396.7	3398.2	38.5	6.9				142.79	95.64 (n = 25)	56.73 (n = 11)	6.0 (n = 3)	26.1
SD	515.9	528.9	1.0	3.3				41.96	24.74 (n = 25)	22.85 (n = 11)	1.0 (n = 3)	5.0

* Patient 17 is excluded from study inclusion but kept in for consistent patient numbering. The mean (SD) for aortic clamping times, (S)/ACP time, and arrest time exclude patients who had no such procedure, and were not taken into account for the calculation of the mean.

Appendix D Results CA Delineation

Table 9: Per patient identified characteristics of cerebral blood flow autoregulation from Transcranial Doppler monitoring.

Patient no.	LLA [mmHg]	MAPopt [mmHg]	ULA [mmHg]	Range [mmHg]	MAPopt - GA [mmHg]
1		42.8			6.8
2	25.4	36.7	48.0	22.6	1.3
3	28.6	42.9	57.2	28.6	3.9
4	31.7	39.1	46.5	14.8	0.1
5*		28.4*			-11.6*
6	34.1	40.3	46.4	12.3	0.3
7	27.6	36.3	45.0	17.4	1.7
8	38.1	53.2			14.2
9					
10					
11	28.0	38.4	48.8	20.8	1.4
12					
13	41.5	50.0	58.4	16.9	11.0
14	33.9	51.4			13.4
15					
16*			39.0*		
(17)					
18					
19	30.2	56.2			17.2
20					
21	19.0	38.6			0.6
22					
23	29.7	41.6	53.6	23.9	2.6
24*		58.4*			19.4*
25	19.0	35.0	51.0	32.0	3.0
26					
27	24.5	34.4	44.3	19.8	3.6
28		35.1	45.8		2.9
29					
n / N = 28	14 (50%)	16 (57%)	11 (39%)	10 (36%)	16 (57%)
Mean	29.4	42.0	49.5	20.9	5.3
SD	6.4	7.0	4.9	6.1	5.6

The delineated CA range values for patient 5*, 16* and patient 24* are considered as errors, delineated values are thus considered false and are excluded from the summary measures.

Appendix E Results TICR and MRI

Table 10: TICR and MRI

Patient no.	Measurement Time [min]	TICR [min]	AUC of TICR [Δ mmHg * sec]	AUC <LLA [Δ mmHg * sec]	AUC >ULA [Δ mmHg * sec]	New WMI 2D Size [mm]
1	132	0	0	0	0	40
2	221	18	5479	361	5118	0
3	210	19	3642	1866	1776	NaN
4	159	75	20996	1400	19596	0
5*	188	0	0	0	0	0
6	148	59	20498	17208	3290	0
7	174	51	19426	4122	15304	2.4
8	226	16	6221	6221	0	0
9	130	0	0	0	0	35.3
10	189	0	0	0	0	0
11	194	29	5676	2579	3097	73.1
12	214	0	0	0	0	NaN
13	233	71	20046	17013	3033	0
14	205	20	3903	3902	0	0
15	220	0	0	0	0	NaN
16*	218	0 (60*)	0 (32340*)	0	0 (32340*)	0
(17)						(11.6)
18	252	0	0	0	0	0
19	242	12	1920	1920	0	0
20	231	0	0	0	0	7.8
21	341	24	9535	9535	0	0
22	233	0	0	0	0	0
23	245	52	2344	4710	18734	6
24*	86	0	0	0	0	Missing
25	187	32	20167	18379	1788	Missing
26	187	0	0	0	0	Missing
27	172	4	1118	375	743	Missing
28	231	30	5040	0	5040	Missing
29	153	0	0	0	0	Missing
n / N =28	28 (100%)	15 (54%)	15 (54%)	14 (50%)	11 (39%)	19 (67.9%)
Mean	200.8	34.1	9734.1	6399.4	7047.2	9.1
SD	48.6	22.1	7936.5	6505.0	7148.4	19.5

The TICR values for patient 5*, 16* and 24* are set to 0. Patient 17 is excluded from analysis due to incomplete CA monitoring data acquisition.

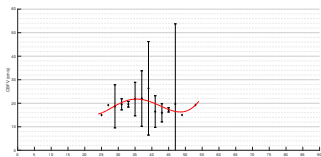
Appendix F Results Imputation CA Characteristics

Table 11: Imputed CA characteristics

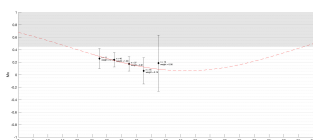
Patient no.	LLA [mmHg]	MAPopt [mmHg]	ULA [mmHg]	Range [mmHg]
1	25.4	42.8	60.2	34.8
2	25.4	36.7	48.0	22.6
3	28.6	42.9	57.2	28.6
4	31.7	39.1	46.5	14.8
5*	33.0	50.6	68.2	35.2
6	34.1	40.3	46.4	12.3
7	27.6	36.3	45.0	17.4
8	38.1	53.2	68.3	30.2
9	31.4	53.3	75.8	43.8
10	36.2	54.5	72.8	36.7
11	28.0	38.4	48.8	20.8
12	20.8	41.2	61.6	40.8
13	41.5	50.0	58.4	16.9
14	33.9	51.4	68.9	35.0
15	30.6	51.9	73.2	42.5
16*	26.7	31.5	36.3	9.6
(17)				
18	24.2	55.4	86.6	62.4
19	30.2	56.2	82.2	52.0
20	26.0	28.4	30.8	4.8
21	19.0	38.6	58.2	39.2
22	28.6	36.9	45.3	16.7
23	29.7	41.6	53.6	23.9
24*	32.6	41.4	50.2	17.6
25	19.0	35.0	51.0	32.0
26	23.1	29.7	36.3	13.2
27	24.5	34.4	44.3	19.8
28	24.4	35.1	45.8	21.4
29	32.9	44.3	55.6	22.7
N = 28				
Mean	28.8	42.6	56.3	27.5
SD	5.5	8.2	14.0	13.5

Notes

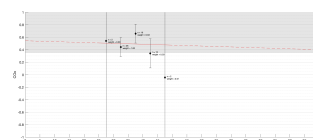
Appendix G All plots



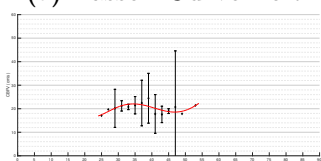
(a) Lassen Curve Left



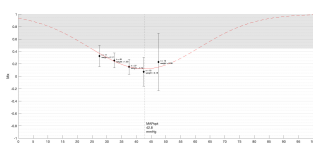
(b) Mx Left



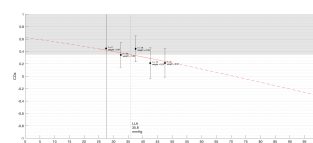
(c) COx Left



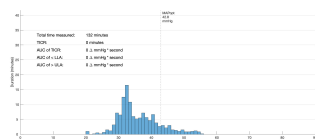
(d) Lassen Curve Right



(e) Mx Right

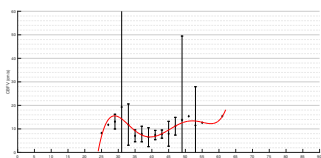


(f) COx Right

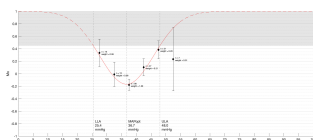


(g) Duration of MAP

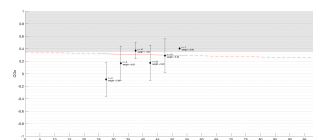
Patient 1



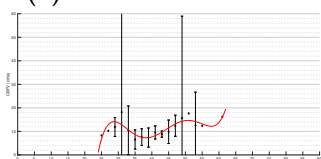
(a) Lassen Curve Left



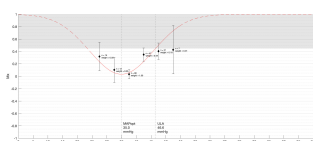
(b) Mx Left



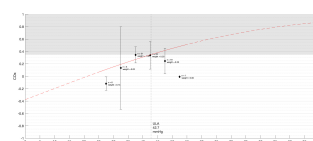
(c) COx Left



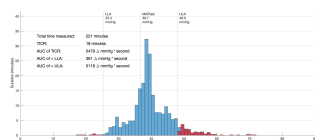
(d) Lassen Curve Right



(e) Mx Right

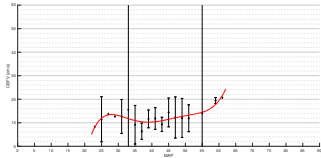


(f) COx Right

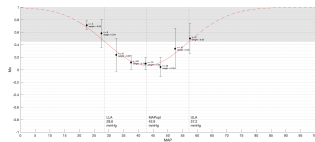


(g) Duration of MAP

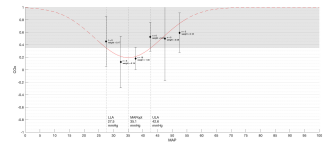
Patient 2



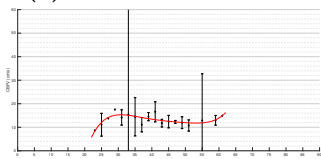
(a) Lassen Curve Left



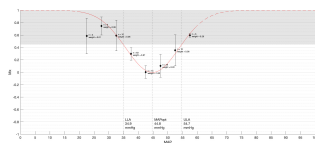
(b) Mx Left



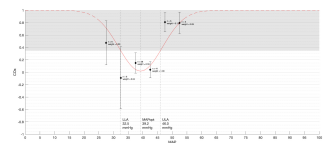
(c) COx Left



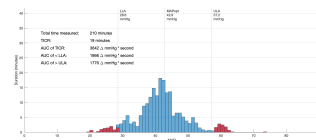
(d) Lassen Curve Right



(e) Mx Right

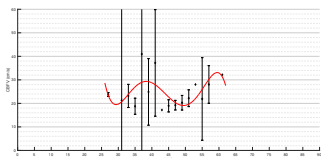


(f) COx Right

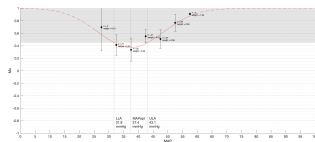


(g) Duration of MAP

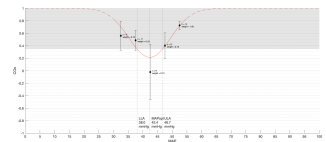
Patient 3



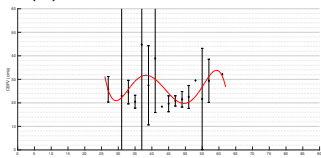
(a) Lassen Curve Left



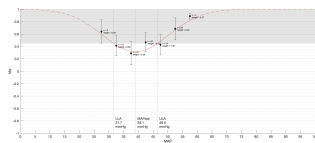
(b) Mx Left



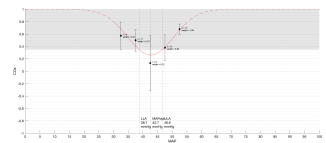
(c) COx Left



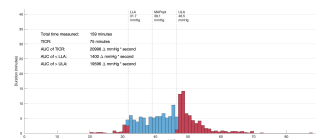
(d) Lassen Curve Right



(e) Mx Right

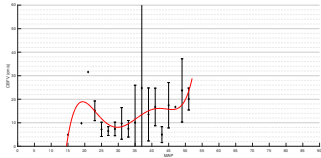


(f) COx Right

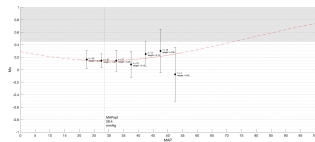


(g) Duration of MAP

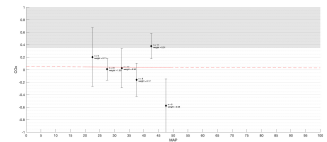
Patient 4



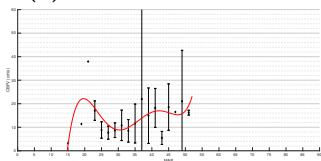
(a) Lassen Curve Left



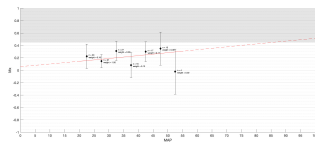
(b) Mx Left



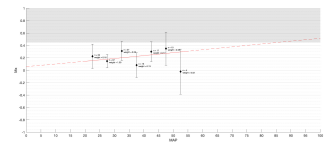
(c) COx Left



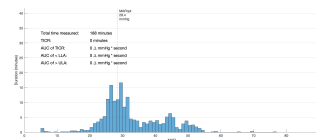
(d) Lassen Curve Right



(e) Mx Right

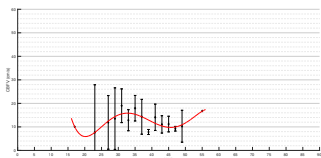


(f) COx Right

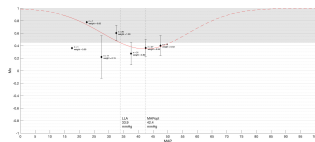


(g) Duration of MAP

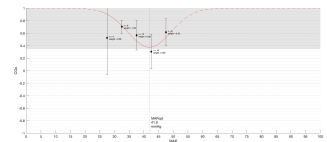
Patient 5



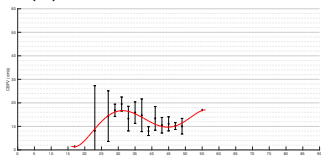
(a) Lassen Curve Left



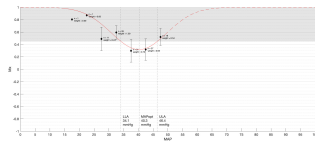
(b) Mx Left



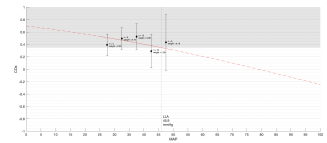
(c) COx Left



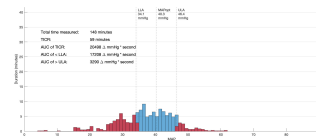
(d) Lassen Curve Right



(e) Mx Right

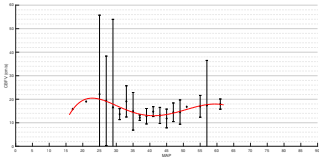


(f) COx Right

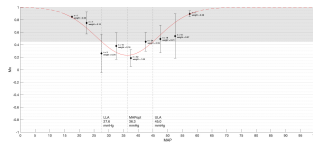


(g) Duration of MAP

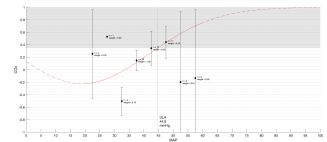
Patient 6



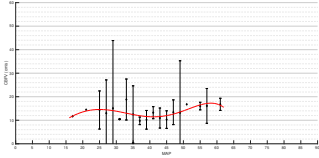
(a) Lassen Curve Left



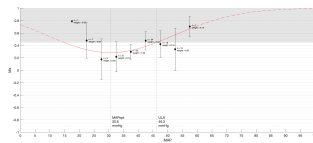
(b) Mx Left



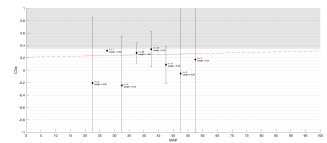
(c) COx Left



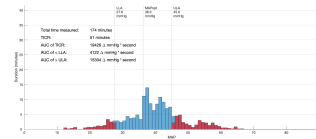
(d) Lassen Curve Right



(e) Mx Right

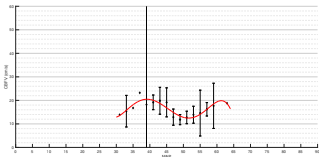


(f) COx Right

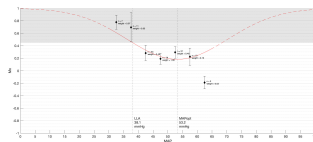


(g) Duration of MAP

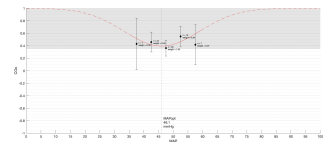
Patient 7



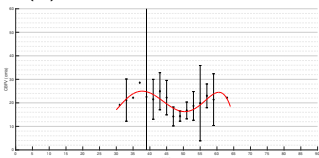
(a) Lassen Curve Left



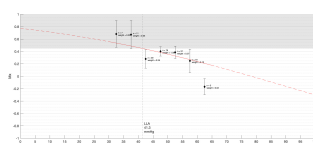
(b) Mx Left



(c) COx Left



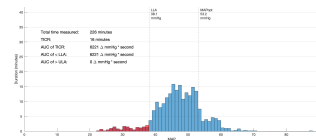
(d) Lassen Curve Right



(e) Mx Right

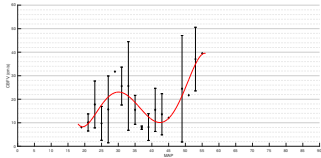


(f) COx Right

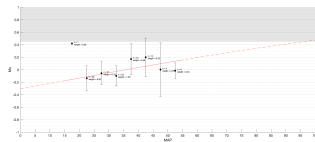


(g) Duration of MAP

Patient 8

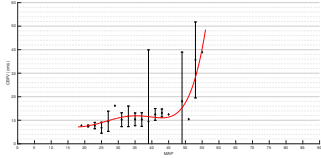


(a) Lassen Curve Left

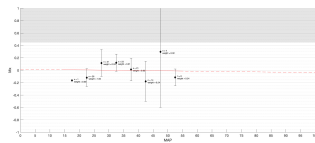


(b) Mx Left

(c) COx Left

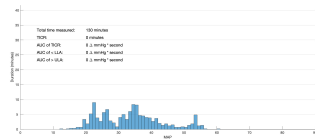


(d) Lassen Curve Right



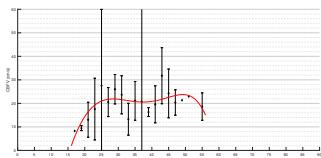
(e) Mx Right

(f) COx Right

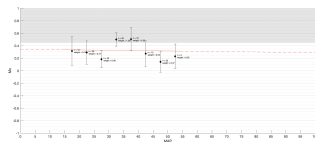


(g) Duration of MAP

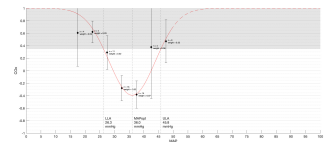
Patient 9



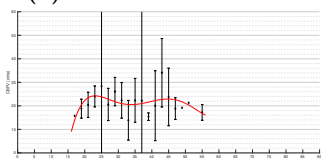
(a) Lassen Curve Left



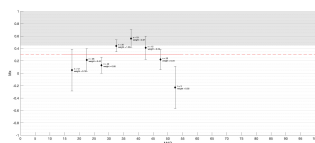
(b) Mx Left



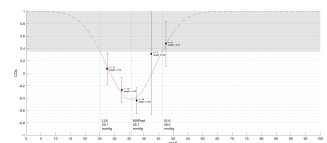
(c) COx Left



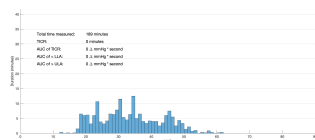
(d) Lassen Curve Right



(e) Mx Right

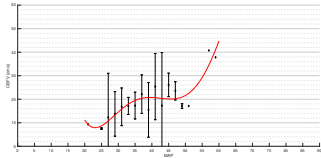


(f) COx Right

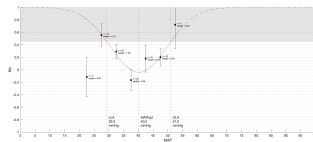


(g) Duration of MAP

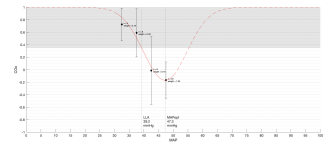
Patient 10



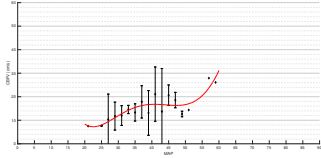
(a) Lassen Curve Left



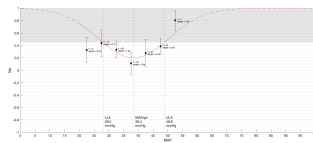
(b) Mx Left



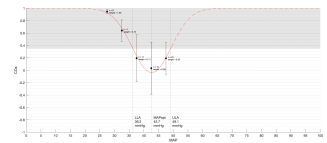
(c) COx Left



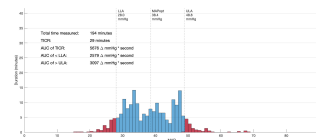
(d) Lassen Curve Right



(e) Mx Right

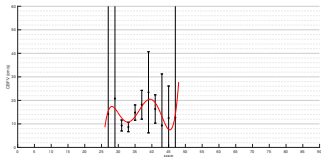


(f) COx Right

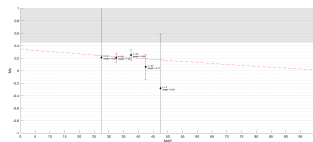


(g) Duration of MAP

Patient 11

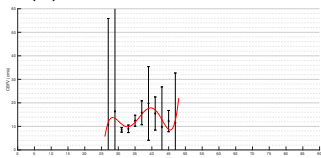


(a) Lassen Curve Left

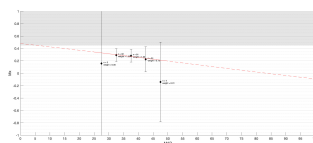


(b) Mx Left

(c) COx Left

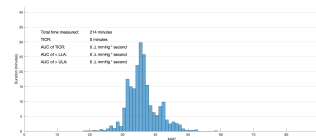


(d) Lassen Curve Right



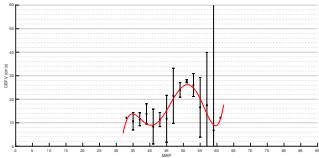
(e) Mx Right

(f) COx Right

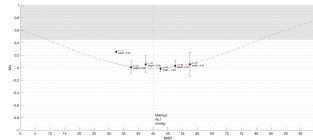


(g) Duration of MAP

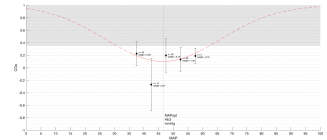
Patient 12



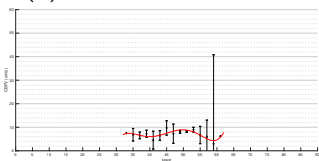
(a) Lassen Curve Left



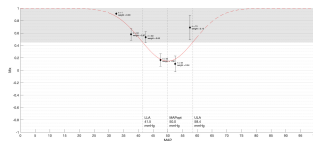
(b) Mx Left



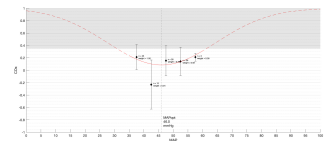
(c) COx Left



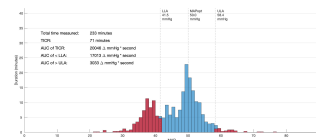
(d) Lassen Curve Right



(e) Mx Right

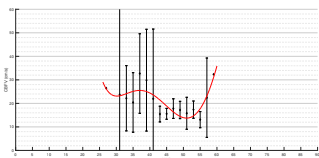


(f) COx Right

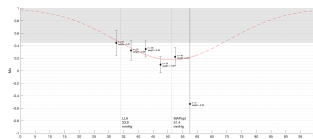


(g) Duration of MAP

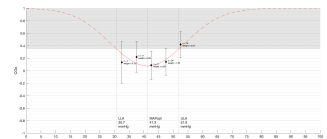
Patient 13



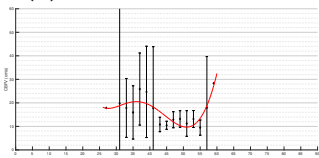
(a) Lassen Curve Left



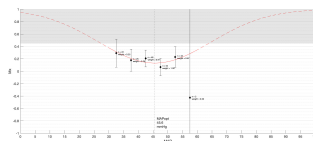
(b) Mx Left



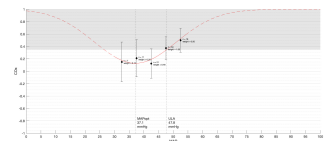
(c) COx Left



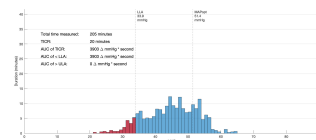
(d) Lassen Curve Right



(e) Mx Right

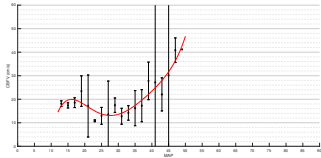


(f) COx Right

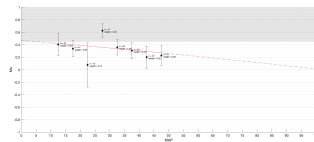


(g) Duration of MAP

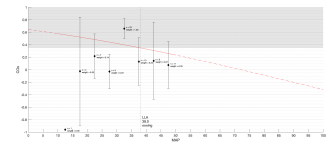
Patient 14



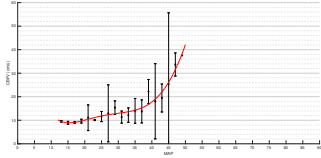
(a) Lassen Curve Left



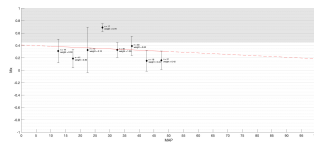
(b) Mx Left



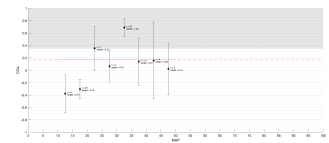
(c) COx Left



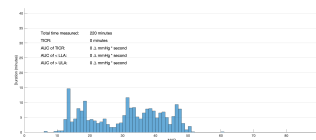
(d) Lassen Curve Right



(e) Mx Right

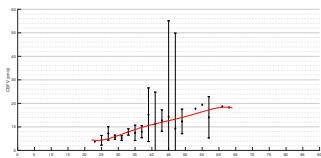


(f) COx Right

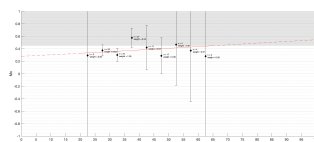


(g) Duration of MAP

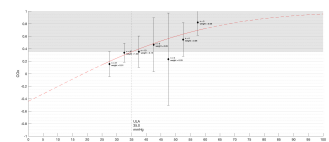
Patient 15



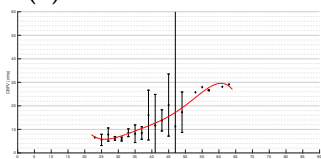
(a) Lassen Curve Left



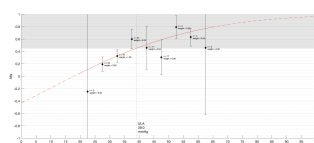
(b) Mx Left



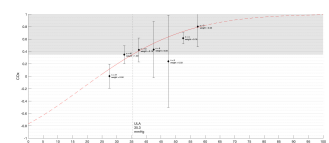
(c) COx Left



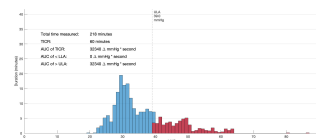
(d) Lassen Curve Right



(e) Mx Right



(f) COx Right

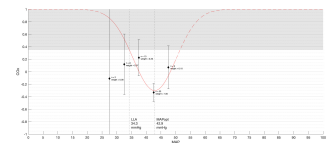


(g) Duration of MAP

Patient 16

(a) Lassen Curve Left

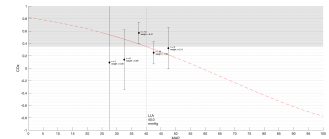
(b) Mx Left



(c) COx Left

(d) Lassen Curve Right

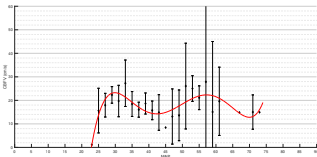
(e) Mx Right



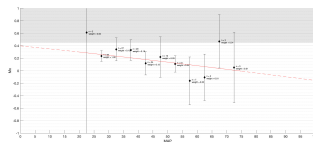
(f) COx Right

(g) Duration of MAP

Patient 17

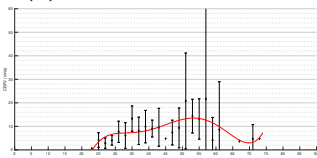


(a) Lassen Curve Left

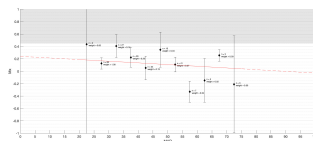


(b) Mx Left

(c) COx Left



(d) Lassen Curve Right

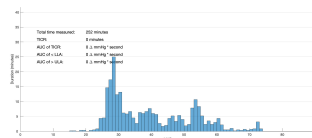


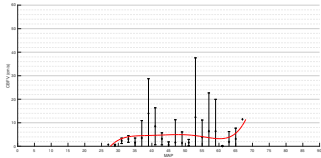
(e) Mx Right

(f) COx Right

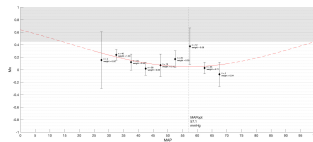
(g) Duration of MAP

Patient 18

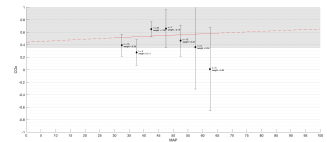




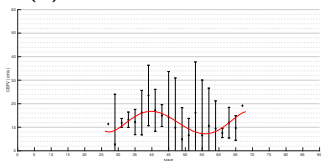
(a) Lassen Curve Left



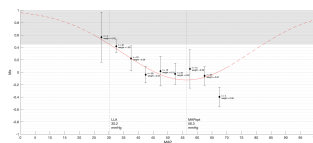
(b) Mx Left



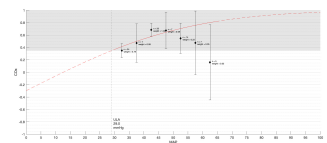
(c) COx Left



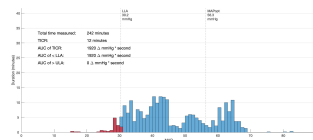
(d) Lassen Curve Right



(e) Mx Right

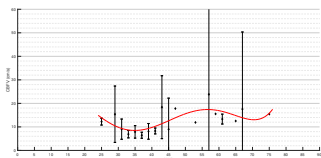


(f) COx Right

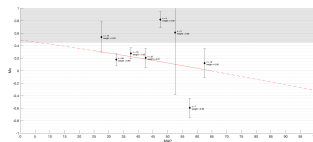


(g) Duration of MAP

Patient 19



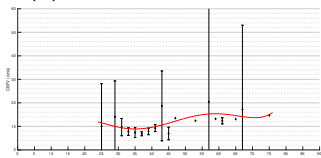
(a) Lassen Curve Left



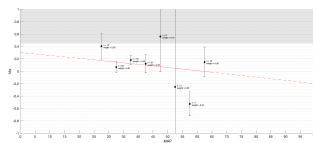
(b) Mx Left



(c) COx Left



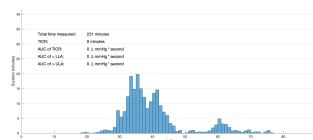
(d) Lassen Curve Right



(e) Mx Right

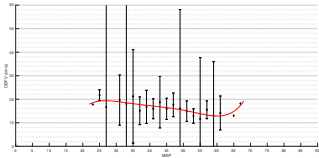


(f) COx Right

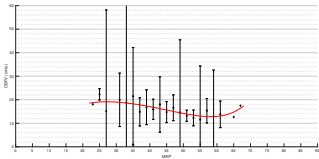


(g) Duration of MAP

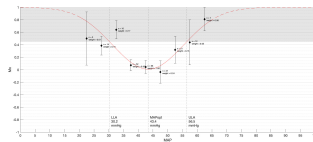
Patient 20



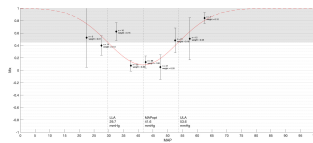
(a) Lassen Curve Left



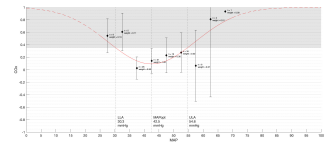
(d) Lassen Curve Right



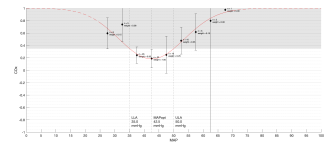
(b) Mx Left



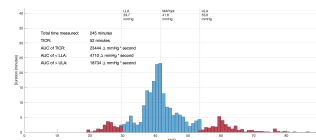
(e) Mx Right



(c) COx Left

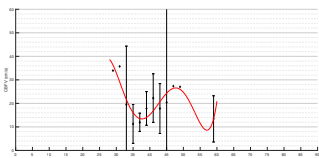


(f) COx Right

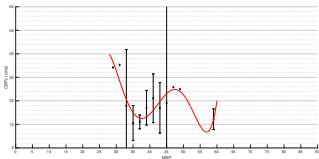


(g) Duration of MAP

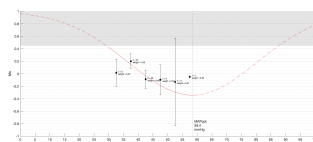
Patient 23



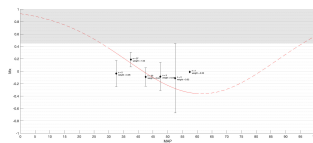
(a) Lassen Curve Left



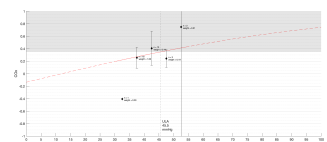
(d) Lassen Curve Right



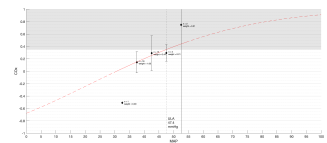
(b) Mx Left



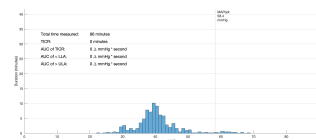
(e) Mx Right



(c) COx Left

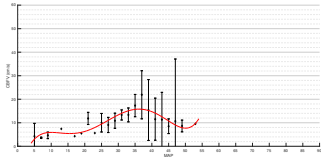


(f) COx Right

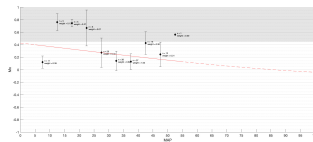


(g) Duration of MAP

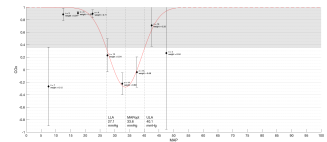
Patient 24



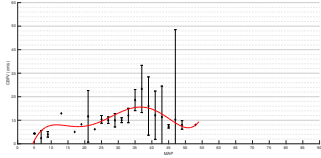
(a) Lassen Curve Left



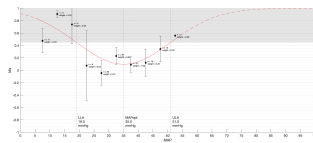
(b) Mx Left



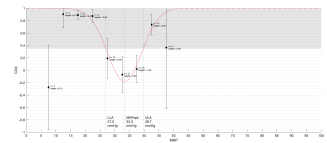
(c) COx Left



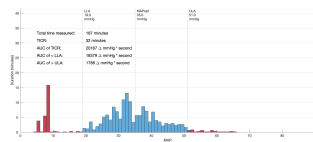
(d) Lassen Curve Right



(e) Mx Right

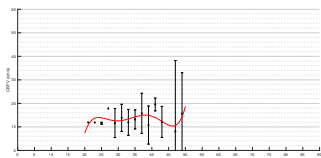


(f) COx Right

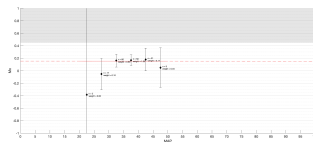


(g) Duration of MAP

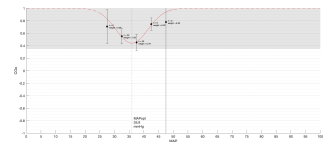
Patient 25



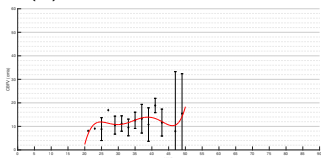
(a) Lassen Curve Left



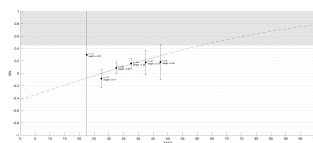
(b) Mx Left



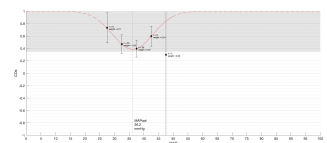
(c) COx Left



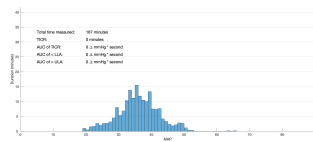
(d) Lassen Curve Right



(e) Mx Right

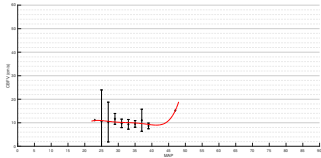


(f) COx Right

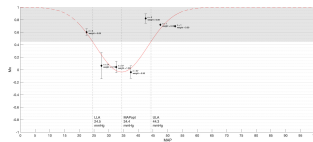


(g) Duration of MAP

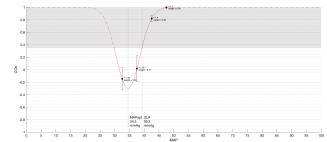
Patient 26



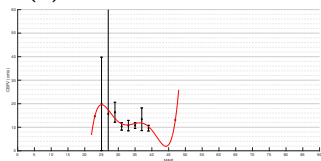
(a) Lassen Curve Left



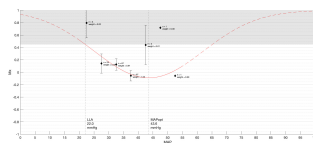
(b) Mx Left



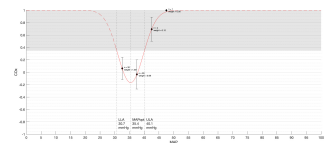
(c) COx Left



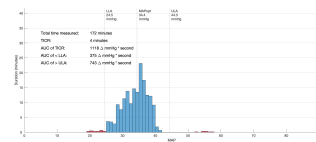
(d) Lassen Curve Right



(e) Mx Right

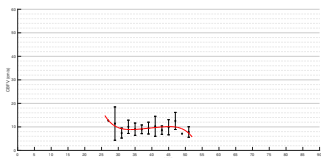


(f) COx Right

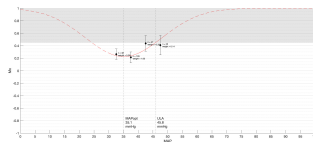


(g) Duration of MAP

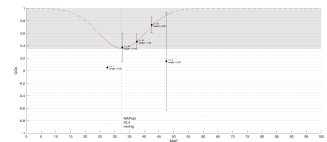
Patient 27



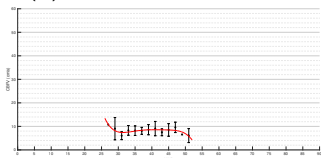
(a) Lassen Curve Left



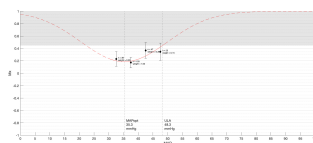
(b) Mx Left



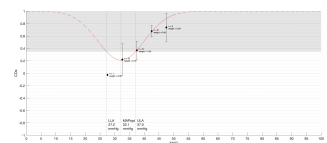
(c) COx Left



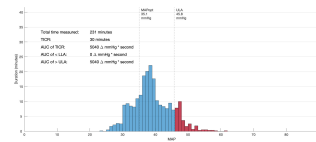
(d) Lassen Curve Right



(e) Mx Right

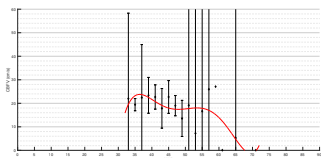


(f) COx Right

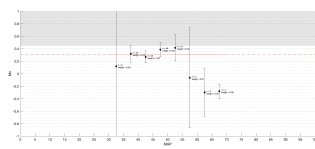


(g) Duration of MAP

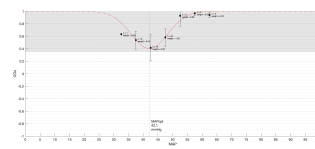
Patient 28



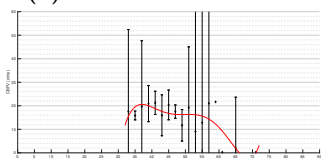
(a) Lassen Curve Left



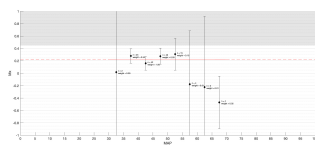
(b) Mx Left



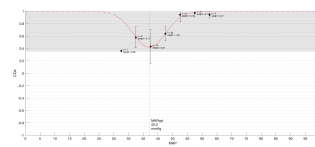
(c) COx Left



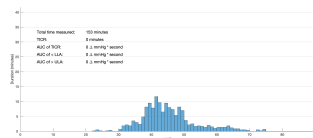
(d) Lassen Curve Right



(e) Mx Right



(f) COx Right



(g) Duration of MAP

Patient 29

Appendix H MatLab Code

main.m

```
% Main script for data analysis FLOWER research project
% Boyd Victor Martherus, boymartherus@gmail.com
clear all
close all
clc

date = datetime("today");
warning('off','all');

%% Check path
directory_list = search_pts;
check_path

%% settings
handle = input('Type handle for filename, e.g. CPB: \n', 's');
type = input('Select interval for analysis; 0 for whole surgery, 1 for CPB, 2 for
manual input, 3 for variable (sternum open, start incisie) to (sluiten, sternum
gesloten, einde ingreep). Enter here: \n'); % 0 for whole operation, 1 for
cpb, 2 for manual
fig_format = 'eps'; % input('Enter figure saveas format i.e.: svg, png, eps (needs
"eps" in saveas function): \n','s');

%% Data Analysis
% Preallocate k
k = [];

% SELECT PATIENTS HERE, FOR SPECIFICS: type 2 for whole procedure copy: k = [2, 5, 9,
12]; for type 0: k = [1, 2, 3, 4, 6, 7, 8, 10, 11 for CPB copy: k = [11];
for k = 1:size(directory_list,2);
    close all
    try
        %% Load all patient data in to datafile (df) of selected patient: k
        rmpath(directory_list{:});
        directory_current = directory_list{k};
        addpath(directory_current)
        fprintf('\n\nCurrent Pt: %s\n',directory_current)

        %% Make 'Figures' folder
        figures_dir = fullfile(directory_current, 'Figures_4');
        if ~exist(figures_dir, 'dir')
            mkdir(figures_dir);
        end

        %% Load df file and signal names.
        df = [];
        csv_files = [];
        tr = [];
        event = [];
        idx_start = [];
        idx_stop = [];

        [df, csv_files, tr, event, idx_start, idx_stop] = process_patient_data
(directory_current, type);

        %% Retime into 10 second averages for Lassen and Mx --> NOTE CHECK FOR ARTEFACTS
AND FOR NAN DATA
        timestep = seconds(10);

        TT10 = retime(df{3,:}, 'regular', 'mean', 'TimeStep', timestep);
        TT10.Properties.VariableNames = {csv_files{:}};
```

```

%% For explaining only; for 110011
% rawCBFV = df{3,6}; % CBFV Links
% rawMAP = df{3,10}; % MAP Rechts

%% Artefact Cleaning for TT10
% Find index for MAP column
map_signal = {'PM_DATA_MEAN_BLOOD_PRESSURE_ARTERIAL.csv'};
contains_map = [];
for i = 1:numel(df(1, :))
    contains_map(i) = contains(df{1, i}, map_signal);
end

column_map = [];
column_map = find(contains_map);

% Calculate the mean MAP of selected period
map_mean = mean(df{3,column_map}.Data, 'omitnan');
map_std = std(df{3,column_map}.Data, 'omitnan');

% Delete all MAP values greater than mean(MAP)+std(MAP)*3
map_cutoff = 3*map_mean;
map_above_idx = find(df{3,column_map}.Data > map_cutoff | df{3,column_map}.Data <=
5)

% make vector for 10 before and after indices where MAP > cutoff MAP
map_above_idx_plus = map_above_idx+10;
map_above_idx_min = map_above_idx-10;

% initialize
map_above_idx_all = [];

for i = 1 : size(map_above_idx,1);
    map_above_idx_all = [map_above_idx_all, map_above_idx_min(i) :<
map_above_idx_plus(i)];
end

map_above_idx_all = unique(map_above_idx_all);
df{3,column_map}.Data(map_above_idx) = NaN;

% Delete 10 sec epoch values in TT10 where >50% of MAP is NaN
for i = 1:(size(TT10,1)-1);
    StartTime = TT10.TimeStamp(i);
    StopTime = TT10.TimeStamp(i+1);
    % find idx in df where
    epoch_idx = find(df{3, column_map}.TimeStamp > StartTime & df{3, column_map}.<
TimeStamp < StopTime);
    nan_prop = mean(isnan(df{3,column_map}.Data(epoch_idx)));

    if nan_prop > 0.5
        TT10.("PM_DATA_MEAN_BLOOD_PRESSURE_ARTERIAL.csv")(i) = NaN;
    end
end

%% plot 10 second averages
k = 888; % Set this to 999 to enable this function
if k == 999
    figure(999);
    set(figure(999),'Units', 'centimeters', 'Position', [0, 12, 40, 16]);%,<
'WindowState', 'minimized');
    yyaxis left; % Left y-axis for MAP
    plot(TT10.TimeStamp(ts_Mx{29}), TT10.("PM_DATA_MEAN_BLOOD_PRESSURE_ARTERIAL.<
csv")(ts_Mx{29}))

```

```

ylabel('MAP (mmHg)')
yyaxis right; % Right y-axis for CBFV
plot(TT10.TimeStamp(ts_Mx{29}), TT10.("MCA_LEFT_ENVELOPE_TOPROBE.csv")(ts_Mx{
{29}))
ylabel('CBFV (cm/s)')
xlabel('Time')
title('MAP and CBFV over Time')

% Add vertical lines every 5 minutes
timeStamps = TT10.TimeStamp(ts_Mx{29});
for i = 1:length(timeStamps)
    if mod(minutes(timeStamps(i) - timeStamps(1)), 1) == 0
        xline(timeStamps(i), '--', 'Color', [0.5, 0.5, 0.5], 'LineWidth', 4
0.5); % Adjust color and line width as needed
    end
end
grid on; % Turn on grid for both axes
end

%% Lassen
% Define left and right CBFV data
cbfv_list = {'MCA_LEFT_ENVELOPE_TOPROBE.csv', 'MCA_RIGHT_ENVELOPE_TOPROBE.csv'};
% cbfv_list = {'MCA_RIGHT_ENVELOPE_TOPROBE.csv'};

% Select interval length and stepsize: 2 min interval, no overlap
interval_length = seconds(120);
step_size = seconds(120);

% Calc_on_interval is used only to select correct interval of CBFV and MAP, not
used for calculation of correlation coefficient
for i = 1:length(cbfv_list)
    try
        % Enter the signal used for calculating the Mx, signal 1 is CBFV, signal 2
is ABP
        signal = {cbfv_list{i}, 'PM_DATA_MEAN_BLOOD_PRESSURE_ARTERIAL.csv'};
        signal = {cbfv_list{i}, 'PM_DATA_END_TIDAL_CO2.csv'};

        % Calculate 10 sec means of CBFV and MAP for Lassen curve, Mx is not used
here.
        [ts_L, MAP, cbfv, Mx] = calc_on_interval(TT10, signal{1}, signal{2},
interval_length, step_size); % Plot is made here

        MAP = MAP';
        cbfv = cbfv';

        % Plot Lassen curves
        bin_width = 2;
        [bin_centers, CBFV_mean_CI] = plot_Lassen(MAP, cbfv, bin_width);

        % Construct the filename using the current date and time
        filename = sprintf('%s_%s_type_%d_Lassen_%s_%s_%s_%s_%s.%s', datestr(now,
'yyyy-mm-dd'), directory_current(end-5:end), type, handle, signal{1}, signal{2},
string(event.(idx_start)), string(event.(idx_stop)), fig_format);

        % Construct the full file path by combining the directory path and
filename
        full_path = fullfile(figures_dir, filename);

        % Save the figure to the specified file path
        saveas(figure(11), full_path, 'eps');

    catch ME_L

```

```

        fprintf('Error processing Lassen analysis for signal %d for patient %d.\n', i, k);
    fprintf('Error message: %s\n', ME_L.message);
    continue % Skip to next analysis
end
end

%% Mean velocity index (Mx)
% Select interval length and stepsize; 5 min interval, 1 min overlap
interval_length = seconds(300);
step_size = seconds(60); % so every 60 seconds Mx is calculated over the last 300
seconds

% Calculate Pearson correlation coefficient between two timetable variables
for i = 1:length(cbfv_list)
    try
        % Enter the signal used for calculating the Mx, signal 1 is CBFV, signal 2
is ABP.
        signal = {cbfv_list{i}, 'PM_DATA_MEAN_BLOOD_PRESSURE_ARTERIAL.csv'};

        % mean MAP, cbfv and Mx is calculated over interval length
        [ts_Mx, MAP, cbfv, Mx] = calc_on_interval(TT10, signal{1}, signal{2},
interval_length, step_size); % Plot is made here
        MAP = MAP';
        cbfv = cbfv';

        % Define the bin edges and plot average Mx with 95CI
        bin_width = 5;

        % Set index name and cutoff here
        index_name = ('Mx');
        index_cutoff = 0.45;
        CArange = {[], [], []};
        [bin_centers, Mx_mean_CI, CArange] = plot_index_CI(MAP, Mx, bin_width,
index_name, index_cutoff);

        % Construct the filename using the current date and time
        filename = sprintf('%s_%s_type_%d_Mx_%s_%s_%s_CAR_%s_%s_%s_%s', datestr
(now, 'yyyy-mm-dd'), directory_current(end-5:end), type, handle, signal{1}, signal{2},
num2str(CArange(1), '%.1f'), num2str(CArange(2), '%.1f'), num2str(CArange(3), '%.1f'),
fig_format);

        % Construct the full file path by combining the directory path and
filename
        full_path = fullfile(figures_dir, filename);

        % Save the figure to the specified file path
        saveas(figure(10), full_path, 'epsc');

    catch ME_Mx
        fprintf('Error processing Mx analysis for signal %d for patient %d.\n', i,
k);
        fprintf('Error message: %s\n', ME_Mx.message);
        continue % Skip to next analysis
    end
end

%% Retime into 60 second averages for NIRS
timestep = seconds(60);
TT60 = retime(df{3,:}, 'regular', 'mean', 'TimeStep', timestep);
TT60.Properties.VariableNames = {csv_files{:}};
% Define left and right NIRS data

```

```

nirs_list = {'AD_NIRS-Left.csv', 'AD_NIRS-Right.csv'};
% nirs_list = {'AD_NIRS-Left.csv'};

%% Artefact Cleaning for TT60
% Delete 60 sec epoch values in TT60 where >50% of MAP is NaN
for i = 1:(size(TT60,1)-1);
    StartTime = TT60.TimeStamp(i);
    StopTime = TT60.TimeStamp(i+1);
    % find idx in df where
    epoch_idx = find(df{3, column_map}.TimeStamp > StartTime & df{3, column_map}.
TimeStamp < StopTime);
    nan_prop = mean(isnan(df{3, column_map}.Data(epoch_idx)));

    if nan_prop > 0.5
        TT60.("PM_DATA_MEAN_BLOOD_PRESSURE_ARTERIAL.csv")(i) = NaN;
    end
end

%% Hemoglobin volume index (Cox)
% Select interval length and stepsize: 10 min interval, 2 min overlap
interval_length = seconds(600);
step_size = seconds(120);

% Calculate Pearson correlation coefficient between two timetable variables
for i = 1:length(nirs_list)
    try
        % Enter the signal used for calculating the Mx, signal 1 is nirs, signal 2
is ABP.
        signal = {nirs_list{i}, 'PM_DATA_MEAN_BLOOD_PRESSURE_ARTERIAL.csv'};

        % mean MAP, nirs and Mx is calculated over interval length
        [ts_Cox, MAP, nirs, Cox] = calc_on_interval(TT60, signal{1}, signal{2},
interval_length, step_size); % Plot is made here
        MAP = MAP';
        nirs = nirs';

        % Define the bin edges and plot average Cox with 95CI
        bin_width = 5;

        % Set index name and cutoff here
        index_name = ('Cox');
        index_cutoff = 0.35;
        CArange = {[], [], []];
        [bin_centers, Cox_mean_CI, CArange] = plot_index_CI(MAP, Cox, bin_width,
index_name, index_cutoff);

        % Construct the filename using the current date and time
        filename = sprintf('%s_%s_type_%d_Cox_%s_%s_%s_CAR_%s_%s_%s_%s', datestr
(now, 'yyyy-mm-dd'), directory_current(end-5:end), type, handle, signal{1}, signal{2},
num2str(CArange(1), '%.1f'), num2str(CArange(2), '%.1f'), num2str(CArange(3), '%.1f'),
fig_format);

        % Construct the full file path by combining the directory path and
filename
        full_path = fullfile(figures_dir, filename);

        % Save the figure to the specified file path
        saveas(figure(10), full_path, 'epsc');

    catch ME_Cox
        fprintf('Error processing Cox analysis for signal %d for patient %d.\n',
i, k);
    end
end

```

```

        fprintf('Error message: %s\n', ME_COx.message);
        continue % Skip to next analysis
    end
end

%% TICR and AUC TICR
Calculate Time In Critical Region and Area under the curve of TICR
for i = 1;
    try
        [total_time, TICR, AUC] = timebelowthreshold(TT10, type, handle, \
directory_current, figures_dir, fig_format);

        catch ME4
            fprintf('Error processing TICR & AUC TICR analysis for signal %d for \
patient %d.\n', i, k);
            fprintf('Error message: %s\n', ME4.message);
            continue % Skip to next analysis
        end
    end

    %% Final Catch
    catch ME_final
        fprintf('Error processing type %d for patient %d. Skipping to next patient. \
\n', type, k);
        fprintf('Error message: %s\n', ME_final.message);
        continue % Skip to next patient
    end
end
end

```

search_pts.m

```
function directory_list = search_pts()

    main_directory = '2_ResearchData/1_ResearchData_Cardio';
    % main_directory = '2_ResearchData/2_ResearchData_Non_Cardio';

    %% Get a list of all directories in the main directory
    directories = dir(main_directory)
    directory_list=[]

    %% Loop over each directory
    for i = 1:length(directories)

        % Ignore directories that are not actually directories
        if ~directories(i).isdir || strcmp(directories(i).name, '.') || strcmp(
(directories(i).name, '..')
            continue;
        end

        % Construct the full path to the directory
        directory_path = fullfile(main_directory, directories(i).name);

        % Display a message indicating the search is complete for this directory
        fprintf('Search complete for directory: %s\n', directory_path);

        directory_list{end+1} = directory_path;
    end
    fprintf('Total patients found: %d\n', size(directory_list,2))
end
```

check_path.m

```
function path_check()

% Define paths
currentpath = pwd;
correctpath = '/Users/Boyd/Documents/MATLAB/FLOWER';

% Check if current path is correct
if ~strcmp(currentpath, correctpath)
    error('MATLAB is not in the correct path.');
```

else

disp('MATLAB is in the correct path.');

end

end

process_patient_data.m

```
function [df, csv_files, tr, event, idx_start, idx_stop] = process_patient_data(
directory_current, type)
% Check for .csv files
csv_files = search_csv_files(directory_current); % looks into results map

% Load data into datafile
data = cell(1, size(csv_files,2));
for i = 1:size(csv_files,2)
    filename = append(directory_current, '/Results/', csv_files{i});
    temp = load_data(filename);
    data{:,i} = table2timetable(temp);
end

% Append csv and data
temp = csv_files;
for i = 1:length(csv_files)
    temp{2,i} = data{1,i};
end
df = temp;
clear temp;

% Load and detect events in eventlist.txt
filename = append(directory_current, '/Results/', 'eventlist.txt');
[event, event_times] = detect_events(filename);
event = cell2table(event)

% Select interval and save into df{3,:} --> Note df{2,:} is whole measurement
% Find index for interval defined in type; 0 whole, 1 CPB, 2 manual
[df, tr, idx_start, idx_stop] = find_idx(df, type, event, event_times);
end
```

search_csv_files.m

```
function csvFiles = search_csv_files(directory)
% This function finds all .csv files in a directory and returns a cell array of file
names

% Get a list of all files in the directory
files = dir(append(directory, '/Results'));

% Preallocate a cell array to store the file names
csvFiles = cell(1, numel(files));

% Loop through all files and check if they have the .csv extension
for i = 1:numel(files)
    [~, ~, ext] = fileparts(files(i).name);
    if strcmpi(ext, '.csv')
        % This is a .csv file, so store its name in the output cell array
        csvFiles{i} = files(i).name;
    end
end

% Remove any empty cells from the output array
csvFiles(cellfun(@isempty, csvFiles)) = [];
end
```

detect_events.m

```
function [events, event_times] = detect_events(logfile)
% DETECT_EVENTS detects events in a logfile
% [EVENTS, EVENT_TIMES] = DETECT_EVENTS(LOGFILE) detects
% events in a logfile and returns the events, and event
% times as output arguments.
%
% Example usage:
% [events, event_types, event_times] = detect_events('logfile.txt');

% Read in the logfile as a table
filename = logfile;
logdata = readtable(logfile, 'Delimiter', 'tab', 'ReadVariableNames', false);

% Define event keywords and corresponding types
keywords = {'begin anesthesie:', 'start (incisie):', 'ao-canule:', 'start bypass', 'ao-
klem:', 'cardioplegie', 'ao-klem los *:', 'stop bypass', 'einde ingreep', 'sluiten',
'sternum', 'einde anesthesie'};

% Initialize variables
events = {};
event_times = datetime.empty;

% Loop through each row in the logfile
for i = 1:height(logdata)
% Get the log message for the current row
message = logdata{i, 6};

% Check if the message contains any of the event keywords
for j = 1:length(keywords)
if contains(message, keywords{j})
% Add the event and event type to the corresponding variables
events{end+1} = message;
% Keep only the time part of the date-time information
event_times(end+1) = datetime(logdata{i, 5}, 'InputFormat', 'dd-MM-yyyy HH:
mm:ss', 'Format', 'HH:mm:ss');
break;
end
end
end
fprintf('Events detected from %s\n', filename)
```

find_idx.m

```
function [df, tr, idx_start, idx_stop] = find_idx(df,type,event,event_times)
%FIND_IDX Summary of this function goes here
% Detailed explanation goes here
tr = [];
idx_start = [];
idx_stop = [];

if type == 2;
    fprintf('Missing event for selected type, please enter start- and stop- event
manually from event list.\n')
    % Ask for the first input
    input1 = input('Enter the first input: \n');
    % Ask for the second input
    input2 = input('Enter the second input: \n');
end

for i = 1:length(df)
    signal = df{2,i};
    if type == 0 % operatie tijd
        idx_start = find(contains(event{1, :}, 'start (incisie)'));
        start_time = event_times(idx_start);

        idx_stop = find(contains(event{1, :}, 'sluiten:'));
        stop_time = event_times(idx_stop);

    elseif type == 1 % cpb tijd
        idx_start = find(contains(event{1, :}, 'start bypass'));
        start_time = event_times(idx_start);

        idx_stop = find(contains(event{1, :}, 'stop bypass'));
        stop_time = event_times(idx_stop);

    elseif type == 2
        idx_start = input1;
        start_time = event_times(idx_start);

        idx_stop = input2;
        stop_time = event_times(idx_stop);

    elseif type == 3
        % find start time
        idx_start = find(contains(event{1, :}, 'sternum open'));
        if isempty(idx_start) % If 'sternum open' is not found
            idx_start = find(contains(event{1, :}, 'start (incisie)'));
        end

        idx_start = idx_start(1);
        start_time = event_times(idx_start);

        % find stop time
        idx_stop = find(contains(event{1, :}, 'sluiten:'));
        if isempty(idx_stop) % If 'sternum gesloten' is not found
            idx_stop = find(contains(event{1, :}, 'stop bypass'));
        end
        if isempty(idx_stop) % If 'sternum gesloten' is not found
            idx_stop = find(contains(event{1, :}, 'sternum gesloten:'));
        end
        if isempty(idx_stop) % If 'sternum gesloten' is not found
            idx_stop = find(contains(event{1, :}, 'einde ingreep:'));
        end
        if isempty(idx_stop)
            idx_stop = find(contains(event{1, :}, 'einde anesthesie:'));
        end
    end
end
```

```

        end
        idx_stop = idx_stop(end);
        stop_time = event_times(idx_stop);
    else
        fprintf('Invalid input, please run again.')
    end
    end
    tr{i} = timerange(start_time,stop_time); % takes the last stop time incase of
double event
    newsignal = signal(tr{i},:);
    df{3,i} = newsignal;
end
% Display the inputs
    fprintf('The start time is: %s, of event: "%s". \n', start_time, char(event{:},
idx_start));
    fprintf('The stop time is: %s, of event "%s". \n', stop_time(end), char(event{:},
idx_stop(end)));
end

```

calc_on_interval.m

```
function [ts, MAP, signal, r] = calc_on_interval(T, x_col, y_col, interval_length, step_size)
% Extract columns x_col and y_col from T
X = T.(x_col);
Y = T.(y_col);

% Calculate total duration of data
total_duration = seconds(T.TimeStamp(end) - T.TimeStamp(1));

% Calculate number of intervals and allocate memory for results
num_intervals = ceil(total_duration/seconds(step_size));
r = zeros(num_intervals, 1);
R = [];

% Loop over intervals with overlap
for i = 1:num_intervals
    % Define interval start and end times
    interval_start = T.TimeStamp(1) + (i-1)*step_size;
    interval_end = interval_start + interval_length;

    % Get data for current interval
    current_interval = timerange(interval_start, interval_end, 'closed');
    T_current = T(current_interval,:);
    X_current = T_current.(x_col);
    Y_current = T_current.(y_col);

    % Calculate correlation coefficient using corrcoef
    R = corrcoef(X_current, Y_current, 'Rows', 'complete'); % Reject this interval if
    % at least one NaN is present, set pairwise to just omit the NaN values
    MAP(i) = mean(Y_current);
    signal(i) = mean(X_current);
    r(i) = R(1, 2);
    ts{i} = current_interval;

    if i == 9999 % CHANGE THIS TO PLOT PEARSON (for 110011 use i == 29)
        % Plot the data points
        figure(99)
        % Set figure size for a square plot
        figureSize = [12, 12, 16, 16];
        hold on
        plot(X_current-min(X_current), Y_current-min(Y_current), '*')

        % Plot the line with the slope of the correlation coefficient
        xLine = [0, 90];
        slope = R(1,2);
        yLine = slope * xLine;
        plot(xLine, yLine)

        % Display the slope value alongside the line
        text(23+1, slope * 23, ['r = ' num2str(slope, '%.2f')], 'Color', 'red',
        'FontSize', 12);

        xlabel('MAP')
        ylabel('CBFV (cm/s)')
        xlim([0, 35])
        ylim([0, 35])
        title(['Mean 5-minute MAP = ' num2str(MAP(i), '%.1f') ' mmHg'])

        ax = gca;
        ax.GridAlpha = 0.2;
        ax.GridColor = 'k';
    end
end
```

```
ax.GridLineStyle = '-';
ax.YGrid = 'on';
ax.YMinorGrid = 'on';

% Set ticks based on the range of the data
xticks([0:5:35])
xticklabels({})
yticks([0:5:35])
yticklabels({})

hold off
end
end

end
```

plot_Lassen.m

```
function [bin_centers, Lassen] = plot_Lassen(MAP, cbfv, bin_width)
close all
% Define the figure size
figure(11)
set(figure(11), 'Units', 'centimeters', 'Position', [12, 12, 36, 16], 'WindowState', 'minimized');

% Define the bin edges
bin_edges = [];
bin_edges = (floor(min(MAP)/bin_width)*bin_width : bin_width : ceil(max(MAP)/bin_width)*bin_width);
bin_edges = bin_edges';

% Remove NaN values from CBFV and MAP
not_nan_idx = ~isnan(cbfv) & ~isnan(MAP);
% not_nan_idx = ~isnan(MAP);
CBFV_clean = cbfv(not_nan_idx);
MAP_clean = MAP(not_nan_idx);

% Discretize the MAP values into the bins
bin_idx = discretize(MAP_clean, bin_edges);

% Calculate the mean and standard deviation of cbfv for each bin
Lassen_mean = accumarray(bin_idx, CBFV_clean, [length(bin_edges)-1, 1], @(x) mean(x, 'omitnan'));
Lassen_std = accumarray(bin_idx, CBFV_clean, [length(bin_edges)-1, 1], @(x) std(x, 'omitnan'));
% Lassen_mean = accumarray(bin_idx, CBFV_clean, [], @(x) mean(x, 'omitnan'));
% Lassen_std = accumarray(bin_idx, CBFV_clean, [], @(x) std(x, 'omitnan'));

% Calculate the standard error of the mean and t-value for a 95% confidence interval
N = [];
N = histcounts(MAP_clean, bin_edges(1:end));
SEM = Lassen_std./sqrt(N);

df = N - 1;
df(find(N == -1)) = 0;
t = tinvcdf(0.975, df);
% orig: t = tinvcdf(0.975, length(N)-1);

% Calculate the confidence interval for each bin
CI = t'.*SEM;

% Calculate the single mean and confidence interval value for each bin
Lassen = [Lassen_mean, CI];

% Calculate the bin centers
bin_centers = bin_edges(1:end-1)+bin_width/2;

% Calculate the number of cbfv values in each bin
Lassen_count = accumarray(bin_idx, 1, [], @(x) sum(x, 'omitnan'));

% Replace the corresponding elements in x3 with new values
value_index = find(Lassen_count ~= 0); % Replace with the desired new values

% Plot the binned data
hold on
scatter(bin_centers(value_index), Lassen_mean(value_index), 'kd', 'filled')
errorbar(bin_centers, Lassen(:,1), Lassen(:,2), 'k', 'LineStyle', 'none');
% for i = 1:numel(Lassen_count)
%     text(bin_centers(i) + .75, Lassen_mean(i), sprintf('n = %d\nmean = %.2f\nCI = %.',
```

```

2f', Lassen_count(i), Lassen(i,1), Lassen(i,2)), 'HorizontalAlignment', 'left');
% end
xlabel('MAP')
ylabel('CBFV (cm/s)')
xlim([0, 90])
xticks(0:5:90)
ylim([0 60])

% fit polyfit 5th order
% x = MAP_clean;
x = bin_centers(value_index);
% y = CBFV_clean;
y = Lassen_mean(value_index);
[p, S] = polyfit(x,y,5);
xlin = bin_edges(1):0.01:bin_edges(end);
[ly_fit, delta] = polyval(p,xlin, S);

% plot(MAP_clean, CBFV_clean, '*')
plot(xlin,y_fit,'r-')
% plot(xlin,y_fit+2*delta,'m--',xlin,y_fit-2*delta,'m--')

% Set the grid alpha to 0.2 for y-axis above 0.4
ax = gca;
ax.GridAlpha = 0.2;
ax.GridColor = 'k';
ax.GridLineStyle = '-';
ax.YGrid = 'on';
ax.YMinorGrid = 'on';

yLimit = get(gca, 'YLim');
hold off;
% fill between the grid lines and the upper limit
% patch([bin_edges(1),bin_edges(end)+bin_width,bin_edges(end)+bin_width,bin_edges(1)],
[lyLimit(2),yLimit(2),0.45,0.45], 'k', 'EdgeColor', 'none', 'FaceAlpha', 0.1);

end

```

plot_index_CI.m

```
function [bin_centers, index_mean_CI, CArange] = plot_index_CI(MAP, index, bin_width, index_name, index_cutoff)
% This function plots the correlation coefficient on binned MAP with
% selected bin_width. Enter index name for the y-axis, index_cutoff is used
% to plot and calculate the limits of CA.

close all
% Define the figure size [left, bottom, width, height]
figure(10)
set(figure(10), 'Units', 'centimeters', 'Position', [0, 12, 40, 16]); % 'WindowState', 'minimized');

% Remove NaN values from index and MAP
not_nan_idx = ~isnan(index) & ~isnan(MAP);
index_clean = index(not_nan_idx);
MAP_clean = MAP(not_nan_idx);

% Define the bin edges
bin_edges = (floor(min(MAP_clean)/bin_width)*bin_width : bin_width : ceil(max(MAP_clean)/bin_width)*bin_width);
bin_edges = bin_edges';

% Plot point cloud %%% Optional %%%
% hold on
% plot(MAP_clean, index_clean, 'b')
% plot(MAP_clean(23), index_clean(23), 'r', 'MarkerSize', 15)
% hold off

% Discretize the MAP values into the bins
bin_idx = discretize(MAP_clean, bin_edges);

% Calculate the mean and standard deviation of index for each bin
index_mean = accumarray(bin_idx, index_clean, [], @(x) mean(x, 'omitnan'));
index_std = accumarray(bin_idx, index_clean, [], @(x) std(x, 'omitnan'));

% Calculate the standard error of the mean and t-value for a 95% confidence interval
N = histcounts(MAP_clean, bin_edges(1:end));
SEM = index_std./sqrt(N); % original SEM = index_std./sqrt(N);

df = N - 1;
df(find(N == -1)) = 0;
t = tinv(0.975, df);
% orig: t = tinv(0.975, length(N)-1);

% Calculate the confidence interval for each bin
CI = t'.*SEM;

% Calculate the single mean and confidence interval value for each bin
index_mean_CI = [index_mean, CI];

% Calculate the bin centers
bin_centers = bin_edges(1:end-1)+bin_width/2;

% Plot binned Index values
%hold on
%plot(bin_centers(bin_idx), index_clean, 'b')
%plot(bin_centers(bin_idx(23)), index_clean(23), 'r', 'MarkerSize', 15)
%hold off

% Calculate the number of index values in each bin
index_count = accumarray(bin_idx, 1, [], @(x) sum(x, 'omitnan'));
```

```

% Weights for fitting
weights_CI = (1./CI);
weights_CI(isnan(weights_CI)) = 0;
weights_CI = weights_CI/max(weights_CI)

weights_N = N/max(N)

weights = (2*weights_N .* weights_CI');
weights = weights/max(weights)

%% clear x3 where y3 = 0
% Replace the corresponding elements in x3 with new values
value_index = find(index_count ~= 0); % Replace with the desired new values

% Plot the binned data
hold on
% TEMP CHANGED
scatter(bin_centers(value_index),index_mean(value_index),'kd', 'filled')
errorbar(bin_centers,index_mean_CI(:,1),index_mean_CI(:,2),'k', 'LineStyle', 'none');
for i = 1:numel(value_index);
    j = value_index(i);
    % text(bin_centers(j) + 0.65, index_mean(j), sprintf('n = %d \nmean = %.2f \nCI = %
%.2f \nweight = %.2f', index_count(j), index_mean_CI(j,1), index_mean_CI(j,2), weights
(j)), 'HorizontalAlignment', 'left', 'FontSize', 6, 'FontWeight', 'normal');
    text(bin_centers(j) + 0.65, index_mean(j), sprintf('n = %d \nweight = %.2f',
index_count(j), weights(j)), 'HorizontalAlignment', 'left', 'FontSize', 6,
'FontWeight', 'normal');
end
xlabel('MAP')
ylabel(index_name)
xlim([0 100])
xticks(0:5:100)
ylim([-1 1])

%% Quartic curve fitting on point cloud -- blue dashed
x = MAP_clean;
y = index_clean;
[p, S] = polyfit(x,y,2);
xlin = bin_edges(1):0.0001:bin_edges(end);
[ly_fit, delta] = polyval(p,xlin, S);

% extend fit outside bins -- blue dashed
xlin2 = 0:0.1:100;
[ly2_fit, delta2] = polyval(p,xlin2, S);
% plot(xlin2, y2_fit, '--b')

% plot this later so its in foreground
% plot(xlin, y_fit, 'r')

% first derivative
k = polyder(p);
k_fit = polyval(k,xlin2);
% plot(xlin2, k_fit)

% second derivative
k2 = polyder(k);
k2_fit = polyval(k2,xlin2);
% plot(xlin2, k2_fit)

%% Quadratic fit curve on means
x3 = bin_centers;
y3 = index_mean;

```

```

%%
% [p3, S3] = polyfit(x3,y3,2);

% [y3_fit, delta3] = polyval(p3,xlin2, S3);

% Respectively, this plots the quadratic fit on the means, quadratic fit on
% point cloud plotted over [0 100], and quadratic fit on measured bins.
% plot(xlin2,y3_fit,'--','Color','#D95319')
% plot(xlin2,y2_fit,'b:')
% plot(xlin,y_fit,'r-') % xlin, y_fit-delta, 'r--', xlin, y_fit+delta, 'r--')

%% Find MAPopt, LLA, and ULA with quadratic curve
clear MAPopt
% find map opt through 1st derivative = 0 and 2nd derivative > 0
% MAPopt = mean(xlin2(find(k_fit < 0.001 & k_fit > -0.001 & k2_fit > 0)))

clear LLA
clear ULA
% find LLA & ULA range
% LLA = mean(xlin2(find(y2_fit < index_cutoff & xlin2 < MAPopt & k2_fit > 0, 1, \
'first')))
% ULA = mean(xlin2(find(y2_fit < index_cutoff & xlin2 > MAPopt & k2_fit > 0, 1, \
'last')))

%% Fit gaussian on 10sec CBFV ans MAP points, a*exp^-(x-b).^2/(2c^2)
% a = height peak, b = translation minimum, c = width (inverse, d = upper limit
% a = 1/(sigma*sqrt(2pi)), b = median mu, c = standard deviation sigma, d = upper limit

% Legacy
% [g] = fit(x, y, @(a, b, c, d, x) d-a.*exp(-((x-b)./c).^2), 'StartPoint', [1, 40, 10, \
1], 'Lower', [-Inf 15 5 1], 'Upper', [Inf 65 50 1]);

% New 'correct'
% [graw] = fit(x, y, @(a, b, c, d, x) d-a.*exp(-((x-b).^2 ./ 2*c.^2)), \
'StartPoint', [1, 40, 10, 1], 'Lower', [0 0 0 1], 'Upper', [2 Inf Inf 1]);
% [graw, gof_graw] = fit(x, y, @(a, b, c, d, x) d-a.*exp(-((x-b)./c).^2), 'StartPoint', \
[1, 40, 1, 1], 'Lower', [0 0 0 1], 'Upper', [2 Inf Inf 1])

% [g] = fit(x3, y3, @(a, b, c, d, x) d-a.*exp(-((x-b).^2./2*c.^2)), 'StartPoint', [1, \
40, 10, 1], 'Lower', [0 0 0 1], 'Upper', [Inf Inf Inf 1]);
% [g, gof_g] = fit(x3, y3, @(a, b, c, d, x) d-a.*exp(-((x-b)./c).^2), 'StartPoint', [1, \
40, 1, 1], 'Lower', [0 -Inf 0 1], 'Upper', [2 Inf Inf 1], 'weights', weights)

gc = coeffvalues(g)
MAPopt = gc(2);

% Find crossover gaussian and cutoff value
[g2] = @(x) g(x)-index_cutoff;
LLA = fzero(@(x) g2(x), MAPopt-10);
ULA = fzero(@(x) g2(x), MAPopt+10);

% inside
grawfit = feval(graw, xlin);
gfit = feval(g, xlin);
% plot(xlin, gfit, '-r', xlin, grawfit, '-b');
% plot(xlin, gfit, '-r');

% extrapolate
grawfit2 = feval(graw, xlin2);
gfit2 = feval(g, xlin2);

```

```

% plot(xlin2, gfit2, '--b',xlin2, grawfit2, '--r');
% plot(xlin2, gfit2, '--r');

%% Delete Inputs if outside xlin
if (LLA < xlin(1) == 1 | LLA > MAPopt)
    LLA = NaN;
    llaxl = [];
end

if (ULA > xlin(end) == 1 | ULA < MAPopt | ULA < 0)
    ULA = NaN;
    ulaxl = [];
end

if MAPopt < xlin(1) | MAPopt > xlin(end) == 1
    MAPopt = NaN;
    mapoptxl = [];
end

%% display CA range TEMP CHANGED
if MAPopt < xlin(1) | MAPopt > xlin(end) == 0
    % mapoptxl = xline(MAPopt,'--', 'Alpha', 0.5,'DisplayName', 'MAPopt',
'Label', ...
    % {'MAPopt ', sprintf('%.1f', MAPopt), 'mmHg' []},
'LabelOrientation','horizontal', ...
    % 'LabelVerticalAlignment', 'bottom');
end

if LLA < xlin(1) == 0 | LLA > MAPopt
    %llaxl = xline(LLA,'--', 'Alpha', 0.5,'DisplayName', 'LLA', 'Label', ...
    %{'LLA ', sprintf('%.1f', LLA), 'mmHg' []},
'LabelOrientation','horizontal', ...
    %'LabelVerticalAlignment', 'bottom');
end

if ULA > xlin(end) == 0 | ULA < MAPopt
    %ulaxl = xline(ULA,'--', 'Alpha', 0.5,'DisplayName', 'ULA', 'Label', ...
    %{'ULA ' sprintf('%.1f', ULA) 'mmHg' []}, 'LabelOrientation','horizontal',
...
    %'LabelVerticalAlignment', 'bottom');
end

%% Plot settings
% Set the grid alpha to 0.2 for y-axis above index_cutoff
ax = gca;
ax.GridAlpha = 0.2;
ax.GridColor = 'k';
ax.GridLineStyle = '-';
ax.YGrid = 'on';
ax.YMinorGrid = 'on';

yLimit = get(gca,'YLim');
hold off;
% fill between the grid lines and the upper limit
patch([0,100,100,0],[yLimit(2),yLimit(2),index_cutoff,
index_cutoff],'k','EdgeColor','none','FaceAlpha',0.1);

CRange = [LLA, MAPopt, ULA];

end

```

timebelowthreshold.m

```
function [total_time, TICR, AUC] = timebelowthreshold(timetable, type, handle,
directory_current, figures_dir, fig_format)
%UNTITLED Summary of this function goes here
close all

%% Load LLA MAPopt ULA
%% Create a dialog window for entering variable values
% prompt = {'LLA:', 'MAPopt:', 'ULA:'};
% dlgtitle = 'Variable Selection';
% dims = [1 35];
% defaultInput = {'', '', ''};
% input = inputdlg(prompt, dlgtitle, dims, defaultInput);

% Call the selectOption function with your options
[selected, LLA_value, MAPopt_value, ULA_value] = selectOptionFromFolder(figures_dir,
type, handle);

% Extract the entered values
LLA = str2double(LLA_value);
MAPopt = str2double(MAPopt_value);
ULA = str2double(ULA_value);

% Create a dialog window for selecting the limit variable. Remove comments below to
choose limits used
% checkboxOptions = {'< LLA', '< MAPopt', '> ULA', '< LLA & > ULA'};
% [selectedOption, isSelected] = listdlg('ListString', checkboxOptions,
'SelectionMode', 'single', 'PromptString', 'Select the limit variable:');
selectedOption = 4;

% Check if a limit variable is selected
if isempty(selectedOption)
    error('No limit variable selected.');
```

```
end

% Determine the selected limit
switch selectedOption
    case 1
        limit = LLA;
    case 2
        limit = MAPopt;
    case 3
        limit = ULA;
    case 4
        limit = [LLA, ULA];
end

% set figure size
figure(12)
set(figure(12), 'Units', 'centimeters', 'Position', [0, 12, 40, 16]);
hold on

%% Function code
% calculate stepsize for the 10 or 60 seconds means --> should be
% either 10 or 60
stepsize = seconds(diff(timetable.TimeStamp(1:2)));

% Extract the MAP column from the timetable
map = timetable('PM_DATA_MEAN_BLOOD_PRESSURE_ARTERIAL.csv');

% Total time of interval i.e. whole procedure, CPB, or manual
total_time = 0;
```

```

total_time = minutes(seconds(size(map,1)*stepsize));

if size(limit,2) > 1
    % Find the indices where MAP is below the threshold
    below_threshold_indices = find(map < limit(1));
    above_threshold_indices = find(map > limit(2));
    threshold_indices = [below_threshold_indices; above_threshold_indices];

    % Convert segment durations to numeric values in seconds
    map_diff = [abs(limit(1)-map(below_threshold_indices)); abs(map(
above_threshold_indices)-limit(2))];
    AUC = sum(map_diff.*stepsize);

    map_diff_below = abs(limit(1)-map(below_threshold_indices));
    AUC_below = sum(map_diff_below.*stepsize);
    map_diff_above = abs(map(above_threshold_indices)-limit(2));
    AUC_above = sum(map_diff_above.*stepsize);

    text(5, 155, sprintf('AUC of < LLA:'), 'FontSize', 12);
    text(20, 155, sprintf('%.0f \Delta mmHg * second', AUC_below), 'FontSize', 12);
    text(5, 140, sprintf('AUC of > ULA:'), 'FontSize', 12);
    text(20, 140, sprintf('%.0f \Delta mmHg * second', AUC_above), 'FontSize', 12);

elseif size(limit,2) == 1
    % Find the indices where MAP is below the threshold
    threshold_indices = find(map <= limit(1));
    % Convert segment durations to numeric values in seconds
    map_diff = limit-map(threshold_indices);
    AUC = sum(map_diff.*stepsize);
end

% Calculate the total time duration below the threshold
TICR = minutes(seconds(size(map(threshold_indices),1)*stepsize));

% Create a histogram plot with colored bars
h = histogram(map, 'BinWidth', 1);
h2 = histogram(map(threshold_indices), 'BinWidth', 1);
h2.FaceColor = "red";
xlabel('MAP');
ylabel('Duration (minutes)');

% Set the y-axis limits to match the total time range
xlim([0 90]);
ylim([0, 250]);

%% display CA range
mapoptxl = xline(MAPopt,'--', 'Alpha', 0.5,'DisplayName', 'MAPopt', 'Label', ...
{'MAPopt ', sprintf('%.1f', MAPopt), 'mmHg' []},\
'LabelOrientation','horizontal', ...
'LabelVerticalAlignment', 'top');
llaxl = xline(LLA,'--', 'Alpha', 0.5,'DisplayName', 'LLA', 'Label', ...
{'LLA ', sprintf('%.1f', LLA), 'mmHg' []},\
'LabelOrientation','horizontal', ...
'LabelVerticalAlignment', 'top');
ulaxl = xline(ULA,'--', 'Alpha', 0.5,'DisplayName', 'ULA', 'Label', ...
{'ULA ', sprintf('%.1f', ULA), 'mmHg' []}, 'LabelOrientation','horizontal',\
...
'LabelVerticalAlignment', 'top');

%% Plot settings
% Set the grid alpha to 0.2 for y-axis above index_cutoff
ax = gca;

```

```

ax.GridAlpha = 0.2;
ax.GridColor = 'k';
ax.GridLineStyle = '-';
ax.YGrid = 'on';
ax.YTick = linspace(0, 360, 13);
ax.YTickLabel = (0:5:60);
ax.YMinorGrid = 'off';

%% ADD TICR values
% Add variable values as text annotations
text(5, 200, sprintf('Total time measured:'), 'FontSize', 12);
text(20, 200, sprintf('%.0f minutes', total_time), 'FontSize', 12);
text(5, 185, sprintf('TICR:'), 'FontSize', 12);
text(20, 185, sprintf('%.0f minutes', TICR), 'FontSize', 12);
text(5, 170, sprintf('AUC of TICR:'), 'FontSize', 12);
text(20, 170, sprintf('%.0f \Delta mmHg * second', AUC), 'FontSize', 12);

hold off
% fill between the grid lines and the upper limit
% patch([0,100,100,0],[yLimit(2),yLimit(2),index_cutoff,↵
index_cutoff],'k','EdgeColor','none','FaceAlpha',0.1);

%% Save figure
% Construct the filename using the current date and time
filename = sprintf('%s_%s_type_%d_Hist_%s_%s_%s_%s.%s', datestr(now, 'yyyy-mm-dd'),↵
directory_current(end-5:end), type, handle, LLA_value, MAPopt_value, ULA_value,↵
fig_format);

% Construct the full file path by combining the directory path and filename
full_path = fullfile(figures_dir, filename);

% Save the figure to the specified file path
saveas(figure(12), full_path, 'eps');

end

```

selectOptionFromFolder.m

```
function [selectedOption, LLA, MAPopt, ULA] = selectOptionFromFolder(directory, type, handle)
% Get a list of files in the specified directory
files = dir(directory);
filenames = {files.name};

% Filter filenames to include only those containing "Mx" or "Cox"
options = filenames(contains(filenames, 'Mx') & contains(filenames, sprintf('type_%d', type)) & contains(filenames, sprintf('type_%d', type)));

% Create the popup dialog
[choice, ~] = listdlg('PromptString', 'Select an option:', 'SelectionMode', 'single', 'ListString', options, 'ListSize', [900 200]);

% Process the selected option
if ~isempty(choice)
    selectedOption = options{choice};
    % Check if "CA" is present in the selected option
    if contains(selectedOption, 'CA')
        % Extract LLA, MAPopt, and ULA from the selected choice
        values = strsplit(selectedOption, '_');
        LLA = values{end-3};
        MAPopt = values{end-2};
        ULA = values{end-1};
    else
        error('CA range is not found.');
```

Bilateral Transcranial Doppler (TCD) monitoring during neonatal cardiac surgery: a feasible addition?

B.V. Martherus^{1,3}, E.M.R. Fonteyn², D. J. van Vriesland², J. Ceelie¹, K. van Loon¹
 1 Department of Anesthesiology, Wilhelmina Children's Hospital, University Medical Centre Utrecht, Utrecht, The Netherlands
 2 Department of Neurology and Neurosurgery, UMC Utrecht Brain Center, University Medical Centre Utrecht, Utrecht, The Netherlands
 3 Technical Medicine, University of Twente, Enschede, The Netherlands
 Funding: Wilhelmina Research Fund, Janivo Stichting



FLOWER – Cerebral blood flow in neonates during cardiac- and major noncardiac surgery

The FLOWER project aims to investigate the feasibility and potential added value of TCD monitoring in neonates scheduled for cardiac- and major non-cardiac surgery within 6 weeks after birth.

PI: K. van Loon MD, PhD
 Presenter: B.V. Martherus BSc



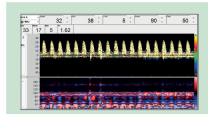
Introduction

While survival rates of neonates with critical congenital heart disease (CCHD) improved, the challenge of reducing white matter injury, likely attributable to insufficient blood flow to the brain, remains urgent. There is a growing focus on optimizing neurodevelopmental outcomes throughout the field. Evidence-based blood pressure (BP) and circulatory management strategies in CCHD patients are desirable. Cerebral autoregulation (CA) monitoring offers a promising avenue for setting individualized BP goals.

We aimed to study whether CA monitoring with transcranial Doppler (TCD) during neonatal cardiac surgery is feasible to optimize our neuromonitoring strategy.

Methods

We employed bilateral insonation of the middle cerebral arteries (MCA) using 2 MHz probes (DWL, Compumedics) via the temporal window fixed with commercially available adhesives. In addition to near infrared spectroscopy (NIRS) and cerebral function monitoring (CFM) monitoring, we recorded real-time cerebral blood flow velocity (CBFV), and arterial blood pressure curves including mean arterial pressure (MAP). Signals were averaged into 10-second means. To delineate the CA range, we calculated the mean velocity index (Mx) every 60 seconds, as a 5-minute Pearson's correlation coefficient between the CBFV and MAP 10-second means. Automatic curve fitting techniques were applied to determine the limits of CA. A cutoff value for Mx of 0.45 was used to determine the state of CA.

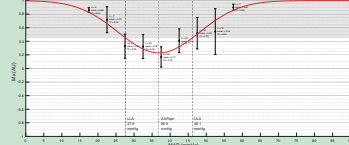


Playback of a recording of CBFV in the right MCA during cardiac surgery.

Positioning of the ultrasound probe on the temporal window with mounting ring and adhesive.



CA curve from TCD monitoring during Arterial Switch procedure



Mx values, grouped into 5 minute bins, are averaged and graphed with velocity counts (n) and a 95% confidence interval (CI). Impaired autoregulation (Mx > 0.45) is highlighted in gray. The measurement time: 179 minutes, CPB: 124 minutes, aortic clamping: 80 minutes. Subject details: gestational age 28 weeks, age at surgery 4 days.

Results

CA was monitored during 14 neonatal cardiac surgeries, all performed within 16 days after birth. Mean patient gestational age was 36.5 weeks (range 36 - 40), and mean birth weight was 3435 grams (range 2050 - 4520). Satisfactory insonation of the bilateral MCA was achieved with low power (90 mW/cm²) in all neonates at an insonation depth ranging from 30 to 39 mm. Repositioning of probes during the procedure was not necessary. Mean TCD measuring time was 208 minutes (range 132 - 287). In our post hoc analysis limits of CA were apparent in 9 out of 14 (64%) neonates.

Our method facilitates delineation of the CA curve during neonatal cardiac surgery without the need for constant vigilance and repositioning of probes.

This approach holds the potential to optimize cerebral perfusion monitoring and ultimately improve neurodevelopmental outcomes.

Contact:
 K. van Loon k.vanloon@umcutrecht.nl
 B.V. Martherus b.v.martherus@gmail.com

Appendix I WCPCCS Poster